

TALLINN UNIVERSITY OF TECHNOLOGY
DOCTORAL THESIS
4/2018

**Laser Scanning of Built Environment and
Landforms with Spatial Modelling
Applications**

KALEV JULGE



TALLINN UNIVERSITY OF TECHNOLOGY
School of Engineering
Department of Civil Engineering and Architecture
Road Engineering and Geodesy Research Group

This dissertation was accepted for the defence of the degree of Doctor of Philosophy in Civil Engineering on December 19, 2017.

Supervisor: Prof. Artu Ellmann
Department of Civil Engineering and Architecture, Tallinn
University of Technology

Opponents: Dr. Antero Kukko
Department of Remote Sensing and Photogrammetry, Finnish
Geospatial Research Institute, National Land Survey of Finland
Department of Built Environment, Aalto University

Assoc. Prof. Milan Horemuž
Department of Urban Planning and Environment
KTH Royal Institute of Technology

Defence of the thesis: January 19, 2018 at 14:00 in room NRG-226.

Declaration:

Hereby I declare that this doctoral thesis, my original investigation and achievement, submitted for the doctoral degree at Tallinn University of Technology has not earlier been submitted for any academic degree.

Kalev Julge



European Union
European Social Fund



Investing in your future

Copyright: Kalev Julge, 2017

ISSN 2585-6898 (publication)

ISBN 978-9949-83-203-3 (publication)

ISSN 2585-6901 (PDF)

ISBN 978-9949-83-204-0 (PDF)

TALLINNA TEHNIKAÜLIKOOL
DOKTORITÖÖ
4/2018

Laserskaneerimine ehitiste ja looduslike pinnavormide mõõdistamisel ning tulemuste modelleerimine

KALEV JULGE

CONTENTS

List of Publications.....	7
Author's contribution	9
Acronyms	10
1. Introduction	11
1.1. Laser scanning technologies and review on earlier studies	11
1.2. Objectives	15
1.3. Outline.....	15
2. Laser Scanning principles	17
2.1. Georeferencing.....	17
2.2. Calibration of MLS and ALS systems	20
2.3. Trajectory processing of a moving platform.....	20
2.4. Ground filtering	23
2.5. Combining laser scanning technologies.....	23
3. Used Sensors and Methods.....	25
3.1. Prototype MLS system.....	27
3.1.1. Sensor synchronization and trajectory post-processing.....	29
3.1.2. MLS system calibration.....	30
3.2. Ground filtering	33
3.3. Aligning ALS, MLS and TLS point clouds	35
3.4. Accuracy assessment.....	36
4. Results	37
4.1. Mobile Laser Scanning	37
4.2. Ground Filtering.....	42
4.3. Combining Airborne and Terrestrial Laser Scanning results.....	45
4.3.1. Surveying complex structures.....	46
4.3.2. Monitoring coastal processes.....	48
5. Conclusions	51
6. Future research	53
List of references.....	54
Acknowledgements	61

Abstract	62
Kokkuvõte	63
Publication I	65
Publication II	91
Publication III.....	99
Publication IV	117
Publication V	127
Curriculum Vitae.....	139
Elulookirjeldus	144

LIST OF PUBLICATIONS

The following peer reviewed papers (indexed either by the Scopus or Web of Science database or both), presented here to fulfil the requirements for the PhD degree of Tallinn University of Technology, are an inseparable part of this thesis:

- I Julge, K., Vajakas, T., Ellmann, A., (2017). Performance analysis of a compact and low-cost mapping-grade mobile laser scanning system. *Journal of Applied Remote Sensing*, 11(4), 044003, doi:10.1117/1.JRS.11.044003.
- II Julge, K., Ellmann, A., Vajakas, T., Kolka, R. (2016). Initial tests and accuracy assessment of a compact mobile laser scanning system. In: *The International Archives of the Photogrammetry, Remote Sensing and Spatial Information Sciences* (633–638). XXIII ISPRS Congress, 12–19 July 2016, Prague, Czech Republic: Copernicus publications. (ISPRS Commission I, ICWG I/Va). doi:10.5194/isprsarchives-XLI-B1-633-2016.
- III Julge, K., Ellmann, A., Gruno, A. (2014). Performance analysis of freeware filtering algorithms for determining ground surface from airborne laser scanning data. *Journal of Applied Remote Sensing*, 8(1), doi:083573-1–083573-15.10.1117/1.JRS.8.083573.
- IV Julge, K., Ellmann, A. (2014). Combining Airborne and Terrestrial Laser Scanning technologies for measuring complex structures. Cygas, D. *Selected papers of the 9th International Conference on Environmental Engineering*, Vilnius, Lithuania, 22-23, May, 2014. (1–7). Vilnius: Vilnius Gediminas Technical University Press "Technika". doi:10.3846/enviro.2014.213.
- V Julge, K., Eelsalu, M., Grünthal, E., Talvik, S., Ellmann, A., Soomere, T., Tõnisson, H. (2014). Combining airborne and terrestrial laser scanning to monitor coastal processes. 2014 IEEE/OES Baltic International Symposium, May 26.-29.2014, Tallinn, Estonia: 2014 *IEEE/OES Baltic International Symposium "Measuring and Modeling of Multi-Scale Interactions in the Marine Environment"*: Tallinn, Estonia, May 26-29, 2014. IEEE, 1–10. (IEEE Conference Proceedings). doi:10.1109/BALTIC.2014.6887874.

Relevant presentations in international conferences:

- Julge, K., Ellmann, A., Vajakas, T., Kolka, R. (2016) Initial tests and accuracy assessment of a compact mobile laser scanning system. *XXIII International Society for Photogrammetry and Remote Sensing Congress*, Prague, Czech Republic.
- Julge, K., Eelsalu, M., Grünthal, E., Talvik, S., Ellmann, A., Soomere, T., Tõnisson, H. (2014) Combining airborne and terrestrial laser scanning to monitor coastal processes. *IEEE/OES Baltic Symposium 2014*, Tallinn, Estonia.
- Julge, K., Ellmann, A. (2014) Combining Airborne and Terrestrial Laser Scanning technologies for measuring complex structures. *9th International Conference “Environmental Engineering”*, Vilnius, Lithuania.

Additional relevant publications associated with the subject of the thesis are listed in the Curriculum Vitae.

AUTHOR'S CONTRIBUTION

I am the main author of all the studies in this dissertation with contributions from all the co-authors.

- **Paper I.** Designing the research plan, selecting the equipment, integrating and synchronizing the sensors, carrying out field measurements, measuring the lever arms, empirically determining the calibration parameters, data processing, assessment of the results were carried out by the author. The algorithms and software for calculating the point cloud and boresight calibration were developed by MSc. Toivo Vajakas. The publication was written by the author and improved in cooperation with all co-authors.
- **Paper II.** The research plan was designed in co-operation with all the co-authors. Selecting the equipment, integrating and synchronizing the sensors, carrying out field measurements were done by the author and Mr. Riivo Kolka. The software for calculating the MLS point cloud was developed by MSc. Toivo Vajakas. Data processing and assessment of the results were carried out by the author. The publication was written by the author and improved in cooperation with the supervisor Prof. Artu Ellmann.
- **Paper III.** The idea for evaluating ground filtering algorithms was proposed by MSc. Anti Gruno. Designing the research plan, selection of the algorithms, empirically determining the suitable parameters, data processing, assessment and analysis of the results were carried out by the author. The reference data were provided by MSc. Anti Gruno and the Estonian Land Board. The publication was written by the author and improved in cooperation with the supervisor Prof. Artu Ellmann.
- **Paper IV.** Designing the research plan, carrying out field measurements; aligning ALS and TLS point clouds, data processing, assessment of the results were carried out by the author. The publication was written by the author and improved in cooperation with the supervisor Prof. Artu Ellmann.
- **Paper V.** The research plan was designed in co-operation with all the co-authors. Field measurements were performed by the author with help from MSc. Maris Eelsalu, Dr. Silja Märdla and Dr. Hannes Tõnisson. Aligning ALS and TLS point clouds was carried out by the author. Data processing was performed by the author and MSc. Erkkö Grünthal. The part of the manuscript regarding laser scanning technology, field work and data processing was written by the author and improved in cooperation with the supervisor Prof. Artu Ellmann. The part of the manuscript regarding the analysis of coastal processes was written by MSc. Maris Eelsalu, Prof. Tarmo Soomere and Dr. Hannes Tõnisson.

ACRONYMS

1D	one-dimensional
2D	two-dimensional
3D	three-dimensional
ALDPAT	Airborne LIDAR Data Processing and Analysis Tools
ALS	Airborne Laser Scanning
ATIN	Adaptive TIN
ATV	All-Terrain Vehicle
BIM	Building Information Modelling
BOBYQA	Bound Optimization BY Quadratic Approximation
CORS	Continuously Operating Reference Station
DEM	Digital Elevation Model
ELB	Estonian Land Board
ETEW	Elevation Threshold with Expand Window
GNSS	Global Navigation Satellite System
GPS	Global Positioning System
FOV	Field of view
IMU	Inertial Measurement Unit
INS	Inertial Navigation System
ISPRS	International Society for Photogrammetry and Remote Sensing
KF	Kalman Filter
LIDAR	Light Detection and Ranging
LP	Linear Prediction
LS	Laser Scanning
MCC	Multiscale Curvature
MEMS	Micro Electro Mechanical System
MLS	Mobile Laser Scanning
MXS	Maximum Local Slope
NMEA	National Marine Electronics Association
PM	Progressive Morphology 2D
PPS	Pulse-per-second
PPK	Post-Processed Kinematic
RMSE	Root Mean Square Error
RTK	Real-Time Kinematic
TIN	Triangulated Irregular Network
TLS	Terrestrial Laser Scanning
UTM	Universal Transverse Mercator
WGS84	World Geodetic System 1984

1. INTRODUCTION

1.1. Laser scanning technologies and review on earlier studies

This study attempts to analyse different Laser Scanning (LS) technologies and applications relevant to the surveying and civil engineering industries, as well as their advantages and limitations. Therefore, a general overview of LS technologies is presented to understand the context and relevance of this thesis.

LS is a remote sensing method, which utilizes Light Detection and Ranging (LIDAR) technology. It uses laser pulses to measure distances to objects. Based on these distances (and the angles of laser beams with respect to certain reference axis/planes) the 3D coordinates of measured points are calculated. The LIDAR device can be mounted on a static tripod (terrestrial laser scanning – TLS) or moving platforms. The latter ones comprise of either an aircraft (airborne laser scanning – ALS) or a mobile ground platform (mobile laser scanning – MLS).

LS is a relatively modern technology. Although, the first experiments were conducted in the 1960's, it was only in the 1990's that the technology became usable in engineering tasks. Nowadays, LS is a well established surveying method. Therefore, most of the research is concentrated on data processing, finding new applications and making the technology more accessible (e.g. manufacturing cheaper and smaller sensors).

A large amount of LS studies have been conducted and reported in the past two decades. Wehr and Lohr (1999) presented a thorough overview on ALS principles. A review of ALS and TLS technology can be found in Vosselman and Maas (2014). ALS methodology for extracting forest inventory data can be found in e.g. Hyypä et al. (2008). A description of the surveying methodology, scanning principles, coverage and patterns of TLS can be found in e.g. Reshetyuk (2009), Petrie and Toth (2008). Recently, Telling et al. (2017) have reviewed the use of TLS for Earth Sciences research and Mukupa et al. (2016) for deformation monitoring of structures. Some practical examples of using TLS for deformation monitoring of engineering structures include Mill et al. (2014, 2015) and Löhmus et al. (2017).

TLS is used to gather high-resolution and accurate spatial data about objects such as buildings, bridges, statues, road surfaces or other structures. It is especially useful in situations where the traditional point-wise surveying techniques are not suited in providing enough accuracy or details, e.g. complicated facades, curved objects, etc. With TLS it is possible to gather data with an accuracy of cm or even more (Dorninger et al. 2011) and at a resolution of up to a few mm. However, in order to save time and to prevent unreasonable increase of the data file sizes, the point cloud resolution is usually set at a few cm depending on the complexity of the measured object.

TLS point clouds measured from different surveying stations need to be registered, which is a spatial transformation that aligns different point clouds by using common targets or overlapping surfaces. The coordinates in a point cloud may be calculated in some known coordinate system or in some project specific relative coordinate system. In the former case, existing geodetic reference points are used. In the latter case, either local construction site reference marks are used or one of the point clouds is used as a base and the other point clouds are transformed to the coordinate system of that point cloud.

With ALS and MLS, the calculation of a point cloud is more complicated. In order to determine the position and orientation of the moving platform at any moment, a Global Navigation Satellite System (GNSS) receiver and an Inertial Navigation System (INS) are used. GNSS receiver measures the 3D position and INS records the pitch, roll and heading (along with accelerations, both the vector and magnitude components) of the platform. GNSS and INS data need to be combined to calculate the trajectory of the platform either in real-time (by using real-time-kinematic (RTK) corrections) or from post-processing. Since the GNSS coordinates refer to the global geodetic system, then the resulting point cloud may need to be transformed to a local coordinate system.

In ALS surveys the LIDAR device is placed on an aircraft: e.g. plane, helicopter. ALS is used in applications with a need to quickly measure large areas or elongated corridors, for example ground surfaces for compilation of Digital Elevation Models (DEM), infrastructure objects, etc., or areas otherwise inaccessible, such as deserts or glaciers. ALS is cost effective if used to cover very large areas, using ALS in small projects is usually impractical.

In many countries nation-wide ALS surveys have been conducted as a part of the national mapping activities. Examples in Europe include Germany, Netherlands, Austria (Mandlbürger et al. 2011), Switzerland (Artuso et al. 2003), Finland (Ahokas et al. 2008) and Estonia (**Paper III**). Such surveys make ALS much more accessible for many specific applications, including planning of civil and road engineering projects.

Generally, due to mapping flight elevations reaching several kilometres, ALS point cloud is much less dense than a TLS point cloud and varies usually from 0.1...20 points per m². Acquisition of more high-resolution data requires lowering flight elevation and, therefore, more time, flight hours and more funds. The accuracy of ALS is less than that of TLS, estimated at 15 cm in favorable conditions (Huising and Gomes Pereira 1998; Gruno et al. 2013).

The main goals of LS data processing include determination of the ground points from the point cloud and forming DEM-s. Since the point cloud initially contains points from all sorts of different features (buildings, vegetation, etc.) then determining ground points is not always an easy task. The correct classification of ground/non-ground points is crucial to the accuracy of subsequent ground surface models and to large variety of spatial analyses based on them. Several algorithms (see, e.g. a comprehensive review by Meng et al. (2010)) for filtering ground points have been developed based on elevation differences, slope angles, etc. Different freeware algorithms are compared to

each other in order to identify the most optimum for varying landscapes. This is also one of the goals of the present study (and that of **Paper III**).

Different filtering algorithms have previously been compared, e.g. by Zhang and Whitman (2005); Sithole and Vosselman (2004); Tinkham et al. (2011); Goncalves and Pereira (2010) and Sulaiman et al. (2010). These contributions compare and evaluate various ground filtering algorithms (both implemented in freeware and commercial software) on different data sets including urban areas, high and low vegetation and mountainous terrains in areas ranging from a few hectares to a few km². The “ground truth” data are either gathered from separate ground measurements or generated by another ground filtering software and/or by manual classification. The number of correctly and incorrectly classified points are used for statistical analysis.

MLS survey principles are similar to that of ALS. Usually a car, ATV, snowmobile, boat, backpack, etc has been used as a MLS platform. The usability and performance of multiplatform MLS was analyzed by Kukko et al. (2012). Puente et al. (2012) reviewed land based MLS systems. Geometric validation of a ground-based MLS system is presented in Barber et al. (2008). Sensor inter-calibration (e.g. the integration and time synchronization of the sensors) related to ALS and MLS systems has been discussed by El-Sheimy and Schwarz (1998), Yadav et al. (2014) and Madeira et al. (2012).

MLS uses less powerful LIDAR than ALS. Therefore, it can be safely operated near people. However, in contrast to the ALS surveys, the trajectory calculations of MLS surveys are influenced by GNSS obstructions (e.g. trees, buildings, tunnels, etc). The MLS range to targets is much smaller than in ALS. Therefore, it is less affected by errors caused by laser beam divergence and measuring the range and angles. MLS systems can vary in accuracy based on the quality and robustness of the used sensors. The achievable MLS accuracy remains generally somewhere between that of the TLS and ALS. In this thesis, the terms “mapping-grade” and “survey-grade” accuracy are used, as defined by Olsen et al. (2013). A mapping-grade MLS system yields three dimensional (3D) point accuracy of 5–20 cm (2σ), whereas a survey-grade system yields accuracy of better than 5 cm (2σ).

Numerous studies have been performed to evaluate the accuracy of MLS systems. A rigorous 3D error analysis to calculate the theoretical achievable accuracy of MLS systems was performed by Glennie (2007). Glennie (2009) also used control points measured with GNSS, tachymetry and levelling to evaluate MLS accuracy. Barber et al. (2008) compared MLS point clouds with control points measured with RTK and static GNSS surveys. The planar accuracy was determined to be 10 cm, while the vertical accuracy of 4 cm was achieved. Haala et al. (2008) compared planar patches from MLS point clouds with existing models and determined an agreement within a few cm. Puente et al. (2013) compared multiple passes of the same MLS system and found that the relative accuracy remained within a couple of cm. Hauser et al. (2016) analyzed the accuracy of a mapping-grade MLS system with respect to TLS. These and

other similar studies have proved that the MLS data accuracy is sufficient to be used in many mapping and surveying applications

MLS is widely used for surveying traffic corridors, road engineering structures (roads, tunnels, bridges, traffic signs, etc.), buildings, monitoring deformations, etc. (Olsen et al. 2013) In these surveys MLS is a faster and cost-effective alternative to static TLS, even though there is a slight tradeoff in accuracy. MLS data have also been used in geomorphological studies to detect landslides and sinkholes (Carter et al. 2001), monitoring rock-falls (Lato et al. 2009), detecting faults and measuring their size (Carter et al. 2007), evaluating the extent of topographical changes (Vaaja et al. 2011). MLS has been implemented in forestry studies, e.g. mapping large forest plots (Liang et al. 2014) and extracting tree and pole features (Jaakkola et al. 2010), as well as in archaeology (Zlot et al. 2014) and assessing solar potential (Jochem et al. 2011). Therefore, MLS has many uses in various multi-disciplinary fields, beyond surveying and mapping.

In the past decade, numerous commercial MLS systems have been constructed by different manufacturers. Generally, these systems are expensive, large in size, and sometimes difficult to operate. A commercially manufactured MLS system is often used on a specially designed platform. Due to non-standardized platforms, the installation to the non-designated platforms can be impractical, cumbersome and time-consuming, also useless in car-inaccessible areas. Therefore, MLS systems consisting of small light-weight LIDAR and GNSS/INS sensors have previously been self-assembled to overcome these shortcomings: e.g. Jaakkola et al. (2010), Wallace et al. (2012), Brooks et al. (2013), Glennie et al. (2013), Jozkow et al. (2016). However, some of these use LIDAR profilers so the density of the point cloud is reduced, whereas the achieved accuracy was not sufficient. To complement the existing MLS solutions, a new prototype MLS system, which is generally smaller, less expensive, conveniently transportable, easy-to-use and slightly more accurate, is constructed within frames of the present study (also reported in **Papers I and II**). The sensor inter-calibration, data processing and the achieved results are presented. The goal is to assemble a mapping-grade MLS system, which can be transported overseas in hand-luggage, easily mounted and calibrated.

Sometimes different LS methods need to be used in conjunction with one another, e.g. using TLS or MLS for ground-based surveying the facades and ALS for roof-tops. The applications for the combined use of different LS technologies has not been researched much. Holopainen et al. (2013) explored the use of ALS, TLS and MLS for tree mapping in a heterogeneous urban forest. Combining ALS and TLS for quantifying erosion and deposition by a landslide is described in Bremer and Sass (2012).

It is important to take into account the aspect of varying data resolution and accuracy of the methods. Also, the point clouds require careful alignment based on common reference marks and surfaces. Two case studies are presented on combining ALS and TLS: for surveying complex structures and monitoring coastal erosion zones. See a more extended discussion in **Papers IV and V**.

1.2. Objectives

The main objective of this study is to analyze the use of LS technologies for surveying built environment, landforms and engineering structures. This includes assembling a prototype MLS system, analyzing the effectiveness of ground filtering algorithms and the possibility of using different LS technologies in conjunction with one another.

The subobjectives can be defined as follows:

- 1) To construct a compact, easy-to-use, conveniently transportable and low-cost mapping-grade MLS system.
- 2) To develop and describe the methodology for sensor inter-calibration, i.e. time synchronization and boresight calibration.
- 3) To verify the accuracy of the developed MLS system with precise TLS reference data.
- 4) To assess the 3D, vertical, horizontal and relative accuracy of the developed MLS system.
- 5) To determine the optimum freeware ground filtering algorithm with an application to ALS surveys over different types of landscape.
- 6) To consider the determined optimum ground filtering algorithm on other ALS, TLS and MLS data.
- 7) To develop a robust methodology for combined use of different LS technologies for surveys of engineering structures and coastal erosion areas.

1.3. Outline

The Introduction (Chapter I) with the literature review provides a brief overview of the current state of LS technology and outlines the objectives of the dissertation. The rest of the thesis is structured as follows. Chapter 2 describes some of the relevant theoretical principles of LS, including georeferencing, calibration, trajectory processing, ground filtering and combining different LS methods. Chapter 3 presents an overview of equipment, data and methodologies used in the studies conducted. Chapter 4 summarizes the results published in **Papers I-V**. For the readers' convenience, the studies will be introduced and discussed in the logical sequence they might come up in practical tasks. Finally, the conclusions and discussion on further research conclude the thesis.

2. LASER SCANNING PRINCIPLES

In this section, relevant LS principles used in the present thesis are presented. These include the georeferencing of point cloud data, calibration of moving LS systems, trajectory processing, ground filtering and combining LS technologies. The principles of LIDAR measurements (e.g. measuring the distance travelled by the laser beam) are not discussed here as they have been thoroughly covered in a number of previous works, e.g. Wehr and Lohr (1999).

2.1. Georeferencing

The initial point cloud (for all LS methods) is calculated based on the distance and horizontal/vertical angles (i.e. polar coordinates) measured with a LIDAR sensor. Generally, the 3D position of a point P_s (expressed via coordinates x , y , z) in local scanner frame for a time instant t – can be calculated by

$$P_s(t) = \begin{bmatrix} r(t) \cdot \cos \beta(t) \cdot \sin \alpha(t) \\ r(t) \cdot \cos \beta(t) \cdot \cos \alpha(t) \\ r(t) \cdot \sin \beta(t) \end{bmatrix} \quad (1)$$

where:

P_s – 3D position of an individual LIDAR point in the scanner's coordinate frame;

r is the range (slope distance) from scanner to survey point;

β is the vertical angle reckoned from horizontal plane defined by the x , y axis of the scanner;

α is the horizontal angle reckoned from either the x or y axis of the scanner.

An example of the interrelations between spherical polar coordinates and x , y , z coordinates in the local scanner frame (based on Velodyne VLP-16 LIDAR) is illustrated on Fig. 1.

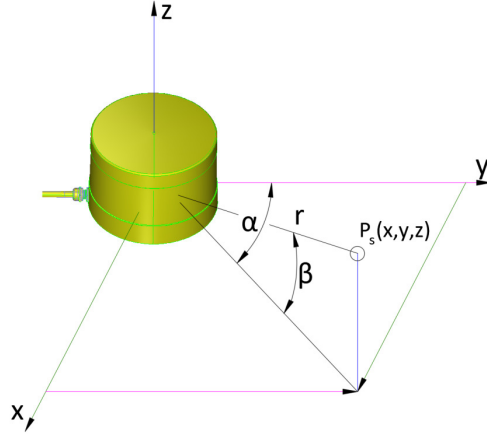


Fig. 1 The interrelations between spherical polar coordinates (α , β , r) of VLP-16 to x , y , z coordinates. (**Paper II**)

The initial point cloud given in the scanner frame can be transformed into other (global) coordinate frames. In TLS this is achieved by using at least three (two if the z -axis of both frames coincide) georeferenced points clearly identifiable in the point cloud. These are used to shift and rotate the point cloud into the selected geodetic frame. Transforming a point cloud into a global, national or local (construction site) coordinate system is required to determine the location of the measured object with respect to other structures and landforms.

In MLS and ALS, it is necessary to take into account the position and attitude measured with a GNSS/INS system. GNSS/INS data, as well as the determined boresight angles and lever arms, are used for direct georeferencing, i.e. transforming point coordinates from the scanner frame to geodetic frame. Direct georeferencing equation for each time instant t is given as

$$P_G(t) = P_{GNSS}(t) + R_l^G(t) \cdot R_b^l(t) \cdot (R_s^b \cdot P_s(t) + L^b) \quad (2)$$

where:

P_G – 3D position of the measured LIDAR point in global frame;

P_{GNSS} – position of the navigation sensor in global frame;

R_l^G – transformation (includes shift and rotation) between the global and the local horizontal frame;

R_b^l – rotation matrix from the body (INS) frame to the local horizontal frame defined by roll, pitch and heading;

R_s^b – boresight rotation matrix, i.e. rotation from scanner's frame to the body (INS) frame;

L^b – location of the scanner in the body frame, i.e. the lever arms between the scanner and the navigation sensor center.

The general interrelations between different coordinate frames in Eq. 2 are depicted on Fig. 2. Evidently the calibration values, i.e. the boresight rotation matrix and the lever arm offsets, are necessary to accurately transform the point cloud from the scanner coordinate system into a global coordinate system. Boresight and lever arm values are determined during the calibration of a MLS system.

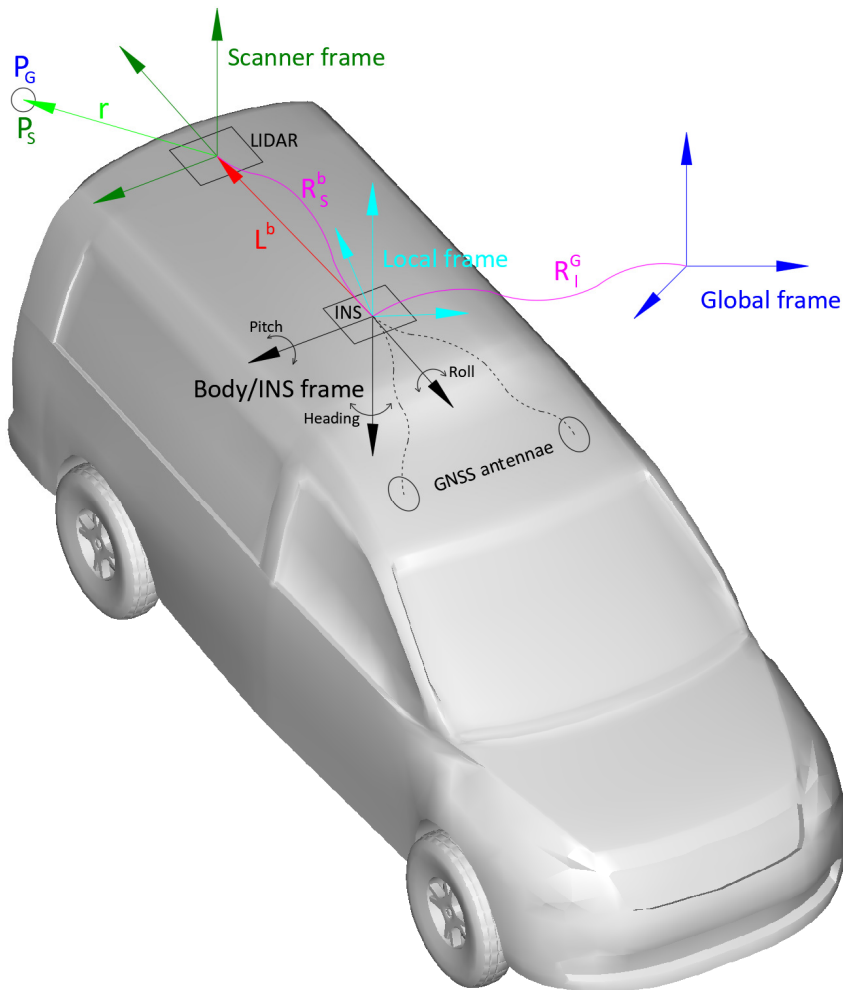


Fig. 2 Coordinate frames of a typical MLS system, where P is a measured LIDAR point, whereas subscript s denotes coordinates in the scanner frame and G in the global frame. r is the range. P_G is the same point in the global frame. L^b - the lever arms (offset) between the INS and LIDAR sensors measured in the body/INS frame. R_s^b is the boresight rotation matrix, i.e. the rotation between the LIDAR and body/INS frame. The rotation matrix (R_b^l) between body/INS and the local frame is defined by the heading, roll and pitch of the platform (the origin of the frames generally coincide). R_l^G is the transformation between the local and global frame. The exact configuration and the direction of all the frame axis' depends on the used sensors and calculation methods. Therefore, it varies among different MLS systems.

2.2. Calibration of MLS and ALS systems

Calibration of LS systems involves determining the lever arms and the boresight calibration matrix (see Fig. 2). Ideally, the calibration could be performed in laboratory conditions by measuring the offset and orientation of the scanner in relation to the INS. However, direct measurement can only be achieved for the lever arms and not for boresight angles because any small mistake in calibration amplifies errors in the field measurements. Boresight calibration in a laboratory is therefore impractical and very rarely (if ever) used. In practice, the boresight calibration is performed by analyzing the point cloud data gathered with the MLS or ALS system. This analysis can be performed manually or using a statistical adjustment.

Manual calibration involves changing the boresight and sub-sequently reprocessing the data, until the point cloud is “visually correct”. This method is used by e.g. Kukko (2013) and Jaakkola et al. (2010). However, manual calibration is subjective and relies heavily on the skills and experience of the operator. Therefore, in most cases, some kind of calculation method is used. Various methods can be used for determining calibration parameters (e.g. Rieger et al. 2010; Leslar et al. 2016; **Paper I**). Usually, planar patches are aligned with control measurements. The alignment outcome is evaluated by least-squares method or other adjustment algorithms (e.g. Skaloud and Lichti 2006). The parameters, which result in the best alignment (e.g. yielding the smallest least-squares residuals), are considered as the optimized boresight values.

It is beneficial to be able to conduct the boresight calibration quickly and without the need for additional reference data. If a time-consuming rigorous calibration can be avoided, then the MLS system becomes easy-to-use in surveying campaigns overseas where it has to be mounted on a new platform.

2.3. Trajectory processing of a moving platform

Due to obstructions it may happen that the GNSS reception is temporarily lost. During the non-reception of GNSS signals the INS can be used to determine the motion in the platform position and orientation. Although INS is more accurate in the short-term, the INS-induced positioning errors accumulate over time, which leads to a rapid decrease in the accuracy of the subsequent position estimation. Therefore, GNSS and INS results need to be combined into a coherent spatial solution.

To estimate the most likely trajectory of a moving system, i.e. the periodic position and orientation, a Kalman Filter (KF) (Kalman 1960) can be used. This has been customarily implemented in trajectory processing algorithms. A simplified explanation of KF can be expressed as (Bishop and Welch 2001):

$$\hat{E}(t) = K(t) \cdot M(t) + (1 - K(t)) \cdot \hat{E}(t - 1) \quad (3)$$

where:

$\hat{E}(t)$ is the current position and attitude estimation at a time-moment t ;

$K(t)$ is “Kalman Gain”;

$M(t)$ is the measured value;

$\hat{E}(t - 1)$ is the previous position and attitude estimation.

KF is a recursive process that determines the current estimate of a value, e.g. the coordinates and attitude of a MLS system, at a time-instant t , by taking into account the available measurements from the present and from previous time epochs (Maybeck 1979). KF is used to minimize the errors caused by incorrect measurements. The only unknown component in Eq. 3 is the Kalman gain $K(t)$, which is calculated for each consequent time epoch. KF estimates the optimum averaging factor for each consequent time frame by analyzing the data from the previous states.

This is a short and primitive description of the KF to explain the main principles and necessity of KF in trajectory processing. More detailed information about the KF general principles can be found in the original publication (Kalman 1960). KF application for trajectory calculation is explicitly discussed in Mohamed and Schwarz (1999). Note that the intention of the present study is not to elaborate KF methodology, instead the existing KF algorithms will be used for calculating the trajectory and attitude of the MLS system.

KF can also be used for trajectory smoothing. Smoothing is necessary since during GNSS signal outages the trajectory will drift and as a result an illogical position estimate can be obtained. If the MLS trajectory is calculated during post-processing, then both forwards and backwards KF smoothing is used (Fig. 3).

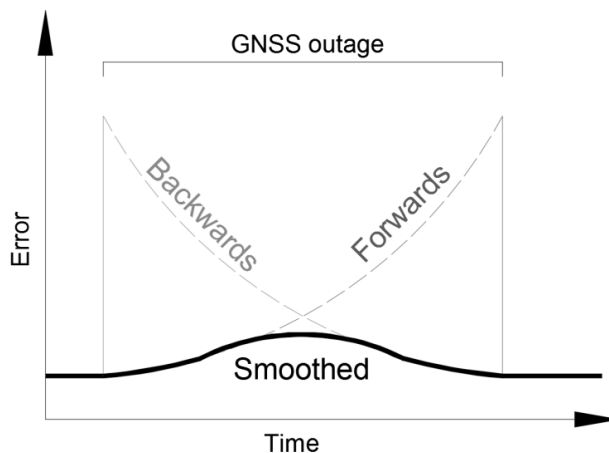


Fig. 3 Forwards and backwards smoothing of MLS trajectory with a Kalman Filter (modified from Groves (2015))

Therefore, a post-processed trajectory is more accurate than a real-time trajectory, which is based on RTK GNSS data and utilizes a real-time KF. In real-time positioning the “future” data is unknown. Therefore, processing forwards and backwards is not applicable. With good GNSS reception the performance of RTK and post-processed-kinematic (PPK) trajectories are comparable. However, relying on real-time data in areas with poor or non-existent GNSS reception may lead to large discrepancies as is illustrated on Fig. 4.

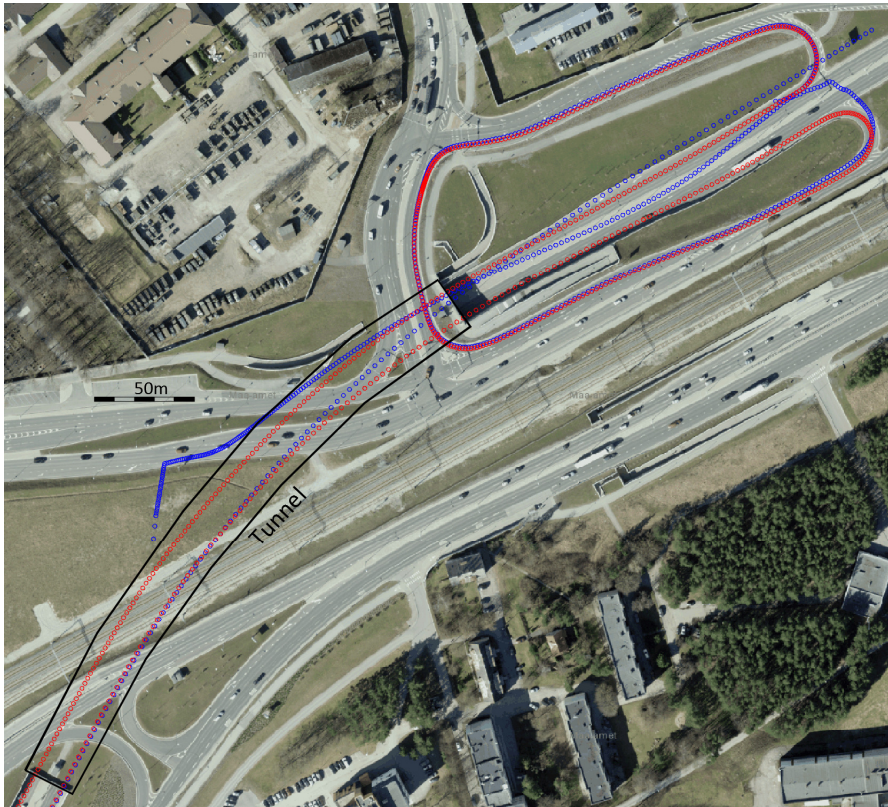


Fig. 4 Difference between real-time and post-processed trajectory while driving through a tunnel (denoted by the black contour). Blue dots – real-time-kinematic (erratic) trajectory, red dots – post-processed realistic trajectory.

2.4. Ground filtering

By combining the trajectory with LIDAR measurements, a georeferenced point cloud is calculated (Eq. 2). Among these points there is usually a number of ground points. Separating ground points from non-ground points automatically can be achieved with ground filtering algorithms.

Ground filtering algorithms are based on the assumption that the correlation between neighboring ground points is stronger than between non-ground points or between ground and non-ground points. Using a threshold value limiting the allowed elevation difference or slope between points, it is possible to identify backscattered signals either as ground or non-ground points. As the laser pulse returns with the lowest elevation are more likely to be ground points then these are considered as starting points for the methods described below.

There are several basic ground classification methods. The first method considers elevation difference between neighbouring points. If the elevation difference is larger than a pre-set threshold, then the higher point is considered to be non-ground. The second method calculates the slope between two neighbouring points. If the slope value is steeper than the threshold, then the higher point is classified as non-ground. Both of these methods can fail on landscapes with near vertical landforms such as sheer cliff faces.

A more advanced way to filter point clouds is to generate a preliminary surface model from either raw point cloud data or the points with the minimum elevation in smaller cells. Then it is possible to compare the vertical distance of each individual point to this coarse ground surface. The points lower than the surface or within the threshold value are identified as ground points. This method is usually implemented iteratively, where all the points that are classified as ground in the iteration are used to calculate a new surface for the next iteration. The non-ground points are discarded from further iterations. (Zhang 2007)

All the aforementioned methods can be applied on their own or combined with each other, as an iterative process or as a single step. Filtering algorithms that automatically classify points as ground/non-ground are usually developed with some specific terrain type in mind, thus their efficiency is largely dependent on the type of landscape to be tested. In order to determine the all-round best ground classification algorithms, they all need to be tested on a variety of terrains and the results compared with some sort of “ground truth” (**Paper III**).

2.5. Combining laser scanning technologies

In some cases, combining LS technologies can be useful – in applications where it is not possible to cover the entire object with only one method or in projects where for different steps of the process different methods are better suited. For example, in generating 3D models of buildings, structures or built environment as a whole. With TLS and MLS, it is possible to gather high-resolution data

about building facades but the rooftops are most likely not visible and often not accessible. Contrastingly, in ALS data the roof-tops are captured well, whereas there is only little usable data about the facades. (**Paper IV**)

Another use would be monitoring the volume of earthworks at large sites. ALS could be used to generate the initial model of the whole area, whereas TLS could be used to monitor the cut and fill volumes. It would also be possible to monitor coastal processes by using ALS to detect whether there are significant volume changes and in case there are, to use TLS to accurately specify the extent of the changes (**Paper V**). Another example would be combining ALS and TLS to monitor the extent of landslides or debris flows by using existing ALS data to reconstruct a pre-event surface and TLS to measure and create a post-event surface (Bremer and Sass 2012). These are just a few possible examples.

Although combining different LS methods obviously has potential, there are some complicating issues. ALS data are much sparser and less accurate than that of TLS or MLS. Therefore, ALS cannot be used in applications, which require high resolution and accurate data. Also given the relatively large differences in spatial resolution, the methods for data processing have to be adapted to best suit the data in hand. This is especially pronounced while using automatic filtering, segmenting, or modelling algorithms that require the use of different parameters depending on the point cloud density.

Additionally, combining different LS methods raises a few accuracy-related problems. The main issue is how to ensure that the datasets are aligned to each other, i.e. there are no systematic errors present between them. TLS could adopt an arbitrary coordinate system where the x , y , z coordinates as well as the orientation are random. This saves time from coordinating reference points and is usually done if the location of the object in the global or national coordinate system is not required. ALS and MLS results usually refer to global or national geodetic reference frames.

Even if the point clouds are using the same coordinate system, there is still a possibility that systematic errors would occur. This is caused by the fact that the measurements are done by using different reference marks. For example, the TLS is done by using geodetic points on the ground and ALS or MLS uses data from GNSS systems and INS to calculate the position and orientation. The methodology for aligning different point clouds is discussed further in Section 3.3.

3. USED SENSORS AND METHODS

As discussed in Section 1.2., the objectives of the present thesis include the analysis of different LS technologies for surveying structures and landforms. To achieve this goal, several sensors are combined to construct a MLS system and a number of instruments are used for gathering test and reference data. In addition, different study areas, calculation algorithms and methods for statistical evaluation of the quality of the results are implemented.

To give an overview of the used methodology and sensors, a summary of the objectives, used equipment, study areas, reference data and methods for evaluating the results are presented in Table 1. The details of each case study are presented in corresponding publications.

The methodology used for constructing the prototype MLS system and techniques for synchronizing the sensors as well as the calibration process are discussed at length in Section 3.1. This is followed with a description of the ground filtering algorithms and the methodology for acquiring the necessary reference data in Section 3.2. Methods for aligning different LS point clouds are discussed in Section 3.3. Finally, the general methodology for evaluating the accuracy of achieved results is presented in Section 3.4.

Table 1. A summary of the objectives and equipment, data, study areas and methods used.

Paper	Main objective	Equipment / data to be tested	Study areas	Reference data	Evaluation method and applied statistical criteria
I	Construct a low-cost portable MLS system and evaluate its accuracy.	Point cloud gathered with MLS system consisting of Velodyne VLP-16 LIDAR and SBG Systems Ellipse-D GNSS/INS.	Road, parking lot, underpass, tunnel, beach.	Point clouds gathered with Leica C10 TLS and Riegl VMZ/VZ-400 MLS.	Vertical, horizontal, relative accuracy. Min, max, median, RMSE.
II	Present the initial results obtained with the MLS system.	Point cloud gathered with MLS system consisting of Velodyne VLP-16 LIDAR and Advanced Navigation Spatial Dual GNSS/INS.	Parking lot.	Point cloud gathered with Leica C10 TLS.	Vertical, horizontal accuracy. RMSE.
III	Evaluate freeware ground filtering algorithms.	6 freeware ground filtering algorithms applied to a ALS point cloud gathered with Leica ALS-50II.	4 different landscapes areas covering in total 24 km ² .	ALS point cloud gathered with Leica ALS-50II. Ground filtering with Terrascan software and visual checking.	Vertical accuracy. Min, max, median, RMSE.
IV	Use different LS technologies in conjunction for surveying complex structures.	TLS point cloud gathered with Leica C10 and ALS point cloud gathered with Leica ALS-50II.	Historic water tower.	Control points measured with robotic total station Trimble S6.	Vertical comparison. RMSE.
V	Use different LS technologies in conjunction for monitoring erosion zones.	TLS point cloud gathered with Leica C10 and ALS point cloud gathered with Leica ALS-50II.	An eroding beach.	Control points measured with robotic total station Trimble S6.	Vertical comparison. RMSE.

3.1. Prototype MLS system

The developed portable MLS system is based on Velodyne VLP-16 LIDAR and SBG Systems Ellipse-D¹ dual antenna GNSS/INS system. The sensors are mounted on a specially designed rigid frame so that their relative position is fixed. The INS and LIDAR are mounted close to each other to improve the accuracy of determining the lever arms and boresight angles. The GNSS antennas, which are used for the dual-antenna heading measurement, are mounted to the sides in order to avoid obstruction of LIDAR measurements and for easier mounting on different platforms. The primary GNSS antenna is placed on the left-hand side, whereas the inter-antenna distance is set to 90 cm. The LIDAR sensor is pitched at a 45° angle.

The origins and the axis of the coordinate frames used in this study are as follows:

- Scanner's frame – the origin is located in the geometrical center of the VLP-16, the orthogonal axis of the horizontally aligned device are as follows: x – right (with respect to the y -axis), y – forward, z – up (i.e. a right-handed system); the scanner's frame is rotated with respect to the INS frame by the boresight angles and the origin is offset by the lever arms.
- INS (body) frame - the origin is the INS center and is marked on the Ellipse-D; the orthogonal axis of the horizontally aligned device are as follows: x – forward, y – right (with respect to the x -axis), z – down (right-handed system); the INS frame is aligned with the frame of the platform (e.g. car).
- Local frame – Earth-tangential reference system (ETRS) (Hofton et al. 2000) where the origin is located at the INS center; x – north, y – east, z – down (right-handed system); the local frame is rotated with respect to the INS frame by roll, pitch and heading values measured with the INS.
- Global frame – the coordinates are initially recorded in WGS84, which are transformed into some specific 2D Cartesian coordinate system (e.g. Lambert-EST or UTM map projections, whereas the heights are reckoned from the ellipsoid or geoid) before using in the georeferencing formula.

The MLS system can be mounted on a suitable platform with adjustable suction cups or bolted to a horizontal surface. Thus, it can be placed on different types of cars, all-terrain-vehicles, backpacks, snowmobiles, trains, boats, etc. Fig. 5 depicts examples of the system mounted to a car with suction cups and bolted to a backpack frame. The technical characteristics of the used sensors are outlined in Appendix A of **Paper I**.

¹ Note that a preceding study stage (as reported in **Paper II**) exploited a GNSS/INS system Advanced Navigation Spatial Dual, which has comparable performance with the SBG Ellipse-D.



Fig. 5 MLS sensors on a purpose-built frame mounted on car's rear-side (above) and a backpack (below). The car-mounted LIDAR device is in the center, on top of the GNSS/INS unit, dual GNSS antennae are located on the sides. **(Paper I)**

Over the past few years a number of prototype MLS systems consisting of small, light-weight LIDAR and GNSS/INS sensors have been constructed. A comparison between these and the MLS assembled in this study is presented in Table 2. As can be seen, other similar MLS systems are either more expensive or less accurate than the one proposed in this study.

Table 2. Summary of prototype MLS systems

Paper authors	Systems/sensors used	Cost* of the LIDAR sensor	Accuracy
Jaakkola et al. (2010)	Ibeo Lux profile LIDAR Novatel SPAN-CPT GNSS/INS	~18 000 USD	Horizontal 22 cm Vertical 9.2 cm
Wallace et al. (2012)	Ibeo Lux profile LIDAR MEMS IMU - microstrain 3DM-GX3 35 GPS receiver (Novatel OEMV1-df) (HD video camera)	~18 000 USD	Horizontal 32 cm Vertical 14 cm
Glennie et al. (2013)	Velodyne HDL-32E LIDAR Oxford Technical Services Inertial+2 INS Novatel dual-frequency GPS antennae and receivers	~30 000 USD	Horizontal 16 cm Vertical ~4 cm
Jozkow et al. (2016)	Velodyne HDL-32E or Velodyne VLP-16 LIDAR Novatel GNSS receiver Epson M-G362PDC1 or MicroStrain 3DM-GX3-35 IMU	~30 000 USD or ~8 000 USD	Vertical 49 cm (initial estimate)
Paper I	Velodyne VLP-16 LIDAR SBG Systems Ellipse-D GNSS/INS	~8 000 USD	Horizontal 15 cm Vertical 8 cm Relative 3 cm

* The total cost of the MLS systems is difficult to approximate, since this information is usually not listed in the publications (nor all the exact models of the sensors). Also the cost of the GNSS/INS systems is generally not public and varies among different distributors. Therefore, only the approximate cost of the LIDAR scanners is presented.

3.1.1. Sensor synchronization and trajectory post-processing

The SBG Ellipse-D is a unit that combines GNSS and INS sensors. Therefore, these are already synchronized by the device itself. The VLP-16 LIDAR and the Ellipse-D data are synchronized by pulse-per-second (PPS) signals generated with the GNSS. The Ellipse-D output port and VLP-16 interface box are interconnected with a cable.

Ellipse-D GNSS/INS device issues a PPS synchronization pulse in conjunction with a once-per-second NMEA RMC sentence, which are issued sequentially. The PPS length is not critical, whereas the RMC sentence must be issued between 50...500 milliseconds after the falling edge of the PPS pulse.

The synchronization is tested by introducing an incremental (positive and negative) time delay to the LIDAR data. With the artificial time delays, the results deteriorated. Therefore, no constant time-delay is detected.

Raw data from all sensors (GNSS, INS, LIDAR) are logged into a laptop computer onboard the measurement platform. The raw GNSS observations from the Antcom G5 dual antennas (5 Hz data rate) are combined with Continuously Operating Reference Station (CORS) GNSS base station data to determine a

precise kinematic trajectory for the platform using the Waypoint/Novatel Inertial Explorer software package. In addition to the GNSS trajectory, 200 Hz raw inertial measurements are used in a tightly-coupled KF with forward and backward processing. As a result, a best-fit estimate of the platform position and attitude is obtained.

3.1.2. MLS system calibration

The lever-arm dimensions are estimated using the engineering drawings of the components and the frame. It is assumed that the accuracy of direct mechanical measurement of the lever arms can be performed within a couple of mm accuracy since all the sensors are located close together and attached to the same rigid metallic frame.

For the developed system an optimization algorithm is implemented to determine the boresight angles. The calibration needs to be performed once after changing the mounting platform. The optimization is performed with point cloud data gathered without prior rigorous calibration of the MLS system. The optimization algorithm is based on Bound Optimization BY Quadratic Approximation (BOBYQA) (Powell 2009). **(Paper I)**

BOBYQA is a numerical optimization algorithm that does not require calculating derivatives of the objective function in order to solve bound constrained optimization problems. It uses a trust region method by forming quadratic models with interpolation. In each iteration, a new point is calculated, either by solving a trust region sub-problem subject to the bound constraints, or by choosing a point to replace an interpolation point in order to achieve linear independence in the interpolation conditions. (Powell 2009)

The objective function g to be optimized is constructed to minimize “fuzziness” of the point cloud on selected objects (subsets in point cloud) by means of principal components analysis (PCA) (Pearson 1901). PCA gives approximation of test points as ellipsoid. Ellipsoid axes lengths can be calculated as eigenvalues $\lambda_1, \lambda_2, \lambda_3$ of covariance matrix for 3D point coordinates data.

Two following types (T_k) of calibration objects K (clusters) are used:

- flat 2D areas (e.g. road surface, vertical wall). Objective function g is to reach a “flat” ellipsoid, i.e. to minimize the thickness of ellipsoid in surface normal direction.
- straight and thin 1D objects (e.g. traffic sign poles, lamp posts). Objective function g is to minimize cross-section diameter of ellipse.

Description of the algorithm to find improved parameter vector P'' from original estimate P' , i.e. to optimize the boresight angles and lever arm offsets, is as follows:

Inputs:

- Initial parameter vector P'
- Measured data D in the LIDAR local coordinates (not georeferenced)

Defined functions:

- Coordinate transform $f(P,D)$ to convert measured data to Cartesian point cloud C
- Goal function $g(P)$ for parameter P , using calibration objects $D_{1..K}$
 - For each calibration object $k = 1..K$ calculate value g_k
 - Calculate the eigenvalues $\lambda_1, \lambda_2, \lambda_3$ of correlation matrix of coordinates of $f(P,D_k)$
 - Calculate depending on type T_k :
 - if $T_k = 1D$ then $g_k = \sqrt{(\lambda_2^2 + \lambda_3^2)}$
 - if $T_k = 2D$ then $g_k = \lambda_3$
 - Calculate total goal function $g = \text{sum}(g_k)$ where $k = 1..K$

Algorithm:

- Determine manually or semi-automatically from the initial point cloud $C(P',D)=f(P',D)$ the K calibration objects (clusters) as subsets of measured data $D_k \subset D$. For each $k = 1..K$ define type of subset T_k , where T_k can be 1D (for linear objects) or 2D (for flat surface objects).
- Find optimal vector of parameter values P'' that minimizes the goal function g using BOBYQA optimization
- Compute georeferenced point cloud with adjusted parameters $C'' = f(D,P'')$

Results:

- Optimal vector of parameter values P'' , i.e. the boresight calibration angles
- Georeferenced point cloud C'' that takes into account the calibration results (an example of a point cloud before and after optimization is depicted in Fig. 6).

If original test objects are not fully correct due to errors in initial parameters P' then the process is repeated with P'' value used as initial P' . The objective function is calculated for each test object separately and thereafter summed to determine the total objective function used in BOBYQA optimization.

The optimization process does not require additional reference data. However, for reliable calibration it is important that at least some of the test objects are measured while the pitch, roll and heading of vehicle are intensely changing. This can be achieved by selecting test objects where the vehicle is performing turns. Otherwise, objective function does not have well-defined minimum for all calibration parameters (Plasencia et al. 2014).

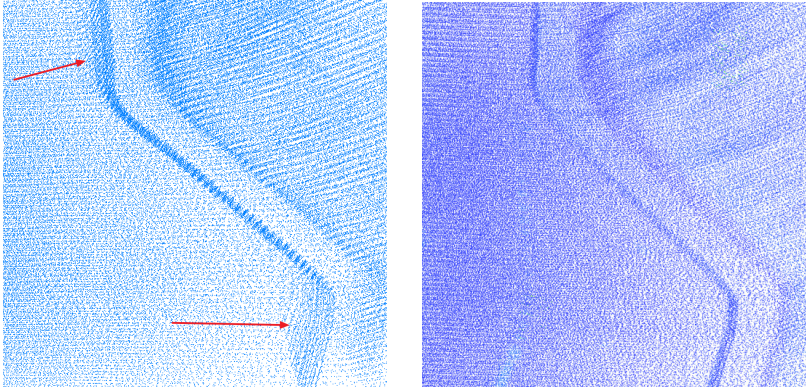


Fig. 6 Example of a point cloud before (left) and after (right) the optimization of the boresight angles with BOBYQA algorithm. Red arrows indicate areas on a curbstone that are unrealistically “fuzzy” due to the boresight misalignment. The same areas are “crisp” after the optimization.

The data used in the optimization of boresight angles are acquired in a parking lot located next to a building facade and surrounded with street light poles. The MLS is mounted on a car, which drove parallel to the facade forwards and backwards and with slight (and intentional) swerving. Heading and pitch can be optimized while moving only in a straight line, provided that there are also vertical objects in the point cloud. However, the movement in both directions and while turning is important for determining the roll value. On a straight road, roll misalignment does not blur the “sharpness” of the point cloud. The vehicle is moving at around 15 km/h. Therefore, the point cloud is dense due to significant overlap of subsequent measurements. At higher velocities, the overlap between consecutive point sub-sets reduce. This causes difficulties in optimizing the boresight pitch value.

Optimization is performed by selecting 20 clusters – 12 on the road surface, 5 on the building facade and 3 around lamp poles (Fig. 7). The radius for including points in the calculation of the total goal function g is defined as 2 m for the clusters on the road surface and lamp poles and 1 m for the clusters on the facade. The reasoning for such a limited radius on the facade is to exclude reflections from windows, which is an excessively noisy area of the point cloud. The clusters on the road and lamp posts are given an equal weight of 1. The clusters on the building facade are given a weight of 0.75 since these are further away from the LIDAR sensor and a longer range decreases the accuracy of a MLS system.

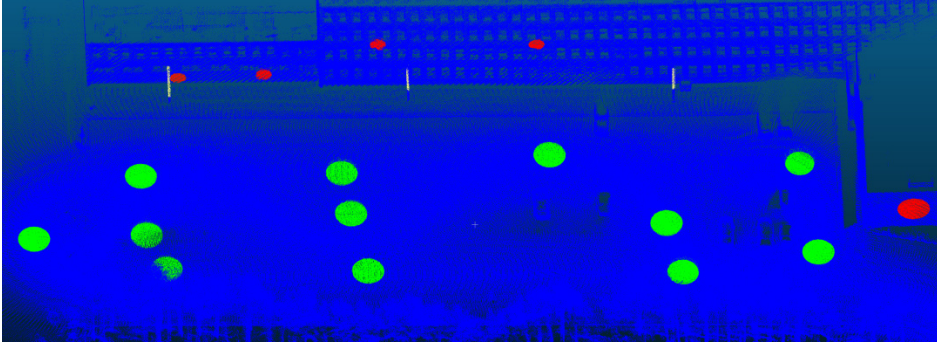


Fig. 7 User-defined clusters used in the BOBYQA optimization process (green – clusters on the road, red – clusters on the facade, yellow vertical bars - clusters around lamp poles). (**Paper I**)

The optimization is performed in four iterations. The initial boresight values are derived from the mechanical drawings of the frame and the sensors (0° for heading and roll, -45° for pitch). In the next cases the values that are calculated in the previous iteration are used. The optimization process is finished after the meaningful digits of g value for the user defined clusters did not change. The results are shown in Table 3.

Table 3. Optimization of boresight angles

Iteration no.	Heading, $^\circ$	Pitch, $^\circ$	Roll, $^\circ$	g , unitless
1	1.3367	-45.1973	-0.5983	0.1071
2	1.3932	-45.2742	-0.6038	0.1011
3	1.4105	-45.2732	-0.5963	0.1010
4	1.4091	-45.2734	-0.5982	0.1010

Overall, the relatively low accuracy of the used sensors yields a situation where the calculated point cloud is still somewhat noisy. This makes the rigorous calibration of the MLS system challenging. After a successful calibration, a georeferenced point cloud can be calculated from as discussed in Section 2.1.

3.2. Ground filtering

One of the main point cloud processing tasks is to separate the ground points from the rest of the points. Ground points can be used to form DEM-s of landforms or models of the road surface. In order to automatically classify ground points, ground filtering algorithms are used.

The ground filtering algorithms tested during the studies are as follows (**Paper III**):

- Adaptive TIN (ATIN) (Axelsson 2000);
- Elevation Threshold with Expand Window (ETEW) (Zhang and Whitman 2005);
- Maximum Local Slope (MXS) (Vosselman 2000);
- Progressive Morphology 2D (PM) (Zhang et al. 2003);
- Multiscale Curvature (MCC) (Evans and Hudak 2007);
- Linear Prediction (LP) (Kraus and Pfeifer 1998).

The first four of these (ATIN, ETEW, MXS and PM) are implemented in ALDPAT 1.0 (Zhang 2007), MCC in MCC-Lidar 1.0 (Evans and Hudak 2007) and LP in FUSION Metrics 0.85.0 (McGaughey 2011) software. Out of these ALDPAT has a graphical user interface while MCC-Lidar and FUSION make use of the command prompt. The tested algorithms have changeable parameters (usually 6-8, except MCC that only has 2) e.g. the thresholds for elevation differences or slopes, number of iterations, etc. Finding the most suitable combination of parameter values (presented in **Paper III**) for each tested algorithm is essential for the correct classification of ground points.

The ALS data used for testing ground filtering algorithms are provided by the Estonian Land Board (ELB), which performs the ALS mapping in Estonia using the Leica ALS50-II airborne laser scanner. The ALS flight altitude 2400 m resulted in a point cloud with the average point density of 0.45 points/m². The algorithms are tested on 4 diverse test areas ranging from 4 to 8 km² in size. The areas are selected in a way that they include a variety of terrains e.g. high and low vegetation, urban areas, high and low landforms, artificial landscape, etc. or a mixture of all these.

The reference data are generated by combining an algorithm with manual classification. This is proceeded by first applying a widely used algorithm (ATIN in the Terrasolid Terrascan software (Soininen 2012)) to the point cloud. Since more than 50% of Estonia is covered with forests or underwood, then the parameters for automatic filtering with the Terrascan software are set in ELB in a way to best remove vegetation. However, this may yield errors on steeper slopes. The removal of these errors is accomplished by visual verification. Within these DEM (formed of points initially classified as ground by the Terrascan software) areas, obvious mistakes are easily identifiable because summits of slopes appear to be “cut off”. In these suspicious locations several cross-sections of both the DEM and the point cloud are inspected. If the ground surface is identifiable in the point cloud, i.e. there is a row of points with small height discrepancies, then these are manually classified as the ground surface. This process is iteratively repeated until the ground classifications appear to be correct. In questionable cases complementary data sources, such as large scale orthophotos, are used for additional verification. The ground points classified with this methodology are used to verify the results of this study.

This means that the reference data cover the entire test areas, large majority of blunders have been corrected and the remaining relatively small errors have only a little weight because the entire data set is very large. With this method, the ALS positioning errors do not influence the results because the source for both the reference and test data are the same, i.e. possible ALS positioning errors are equal in both datasets (as opposed to using terrestrial measurements for “ground truth” where the ALS error would affect the differences between reference and ALS data). Therefore, all the detected height discrepancies are most likely caused by classification errors solely.

DEM-s are formed from the ground points classified with the tested algorithms and from the reference data. The elevations of these DEM-s are compared and the differences are used for statistical analysis to evaluate the performance of each ground filtering algorithm. For more details, see **Paper III**.

3.3. Aligning ALS, MLS and TLS point clouds

When surveying complex structures or objects with limited accessibility, it is not always possible to complete the survey with only one LS technology. Therefore, sometimes different LS techniques are implemented to measure separate parts of the surveyed object or at different time epochs (e.g. Holopainen et al. (2013), Bremer and Sass (2012)). These datasets need to be properly aligned before using them together for further modeling and analysis.

The problem of aligning ALS, MLS and TLS point clouds could be easily solved by finding distinguishable points in both point clouds and manually moving one of the clouds to the correct location. Unfortunately, ALS data are usually not dense enough to accurately determine the coordinates of individual points. Therefore, it is necessary to find the value of the systematic errors by other means.

The systematic error of elevation can be determined by identifying horizontal surfaces (e.g. a nearby parking lot) that are present on both point clouds. By comparing the elevation differences between the same surface measured by different LS methods, the extent of the systematic error should become evident. Points near the edge of the surface should be discarded to minimize the errors caused by shifts at the x, y plane and the large size of the ALS laser beam footprint on the ground caused by divergence. For example, a part of the ALS pulse might reflect from a curbstone instead of the pavement. The larger the surface area the better because a larger sample amount reduces the influence of inaccurate points. (**Papers IV and V**)

Eliminating systematic errors in planar coordinates can be slightly more complicated. As mentioned earlier, ALS point clouds tend to be too sparse for accurate determination of certain points or edges. For this the ALS data need to be processed first. The aim is to find planar surfaces, e.g. facets of a pitched roof, that intersect and form an edge. Although the edge is generally not clearly defined in the point cloud, the points belonging to the surfaces can be used to construct planes and the line of intersection between these planes is the sought

edge. If there are three intersecting planes, then this results in a single corner point. (**Paper IV**)

Using these common edges or points, it is possible to match the location in different datasets and register the point clouds. Obviously, this method can be proceeded only in urban areas where there are clearly defined artificial sharp edges. Finding such features on landforms in non-built areas is unlikely. Also since these roof-edges and -points are most likely present in ALS data, then there is no guarantee that they are visible in TLS and MLS point clouds.

3.4. Accuracy assessment

In the present studies, the quality of the achieved results is generally assessed by comparing the results with some form of reference data. Below the principles of most commonly used methods for assessing the accuracy are presented:

- Vertical accuracy is generally evaluated by comparing DEM or TIN models along the z-axis.
- Horizontal accuracy is evaluated by comparing the planar coordinates of objects detected in both the measured and reference data.
- Relative accuracy is evaluated by measuring distances between clearly identifiable objects in both datasets.
- 3D accuracy is evaluated by measuring the shortest distance from a surveyed point to the interpolated surface of the reference point cloud.

The discrepancies between the investigated results and the reference data are determined by using:

$$\theta_i = h_{ref} - h_{test} \quad (4)$$

where θ_i is the i -th discrepancy from reference data; h_{ref} is the reference value and h_{test} is the investigated value.

These discrepancies are used in statistical analysis to find maximum, minimum and median differences, as well as to calculate the root mean square errors (RMSE) within each test area as follows:

$$RMSE = \sqrt{\frac{\sum_{i=1}^n \theta_i^2}{n}} \quad (5)$$

where n is the number of observations and $i = 1, 2, \dots, n$.

These standard statistical values have often been used in previous studies to evaluate the accuracy of LS point clouds.

4. RESULTS

4.1. Mobile Laser Scanning

The main research objective of the studies is to construct a relatively low-cost MLS system, which is light-weight and easy-to-use, can be rapidly mounted on several platforms and meets the mapping-grade accuracy requirement of 20 cm. The accuracy is evaluated by comparisons with high-accuracy TLS and survey-grade MLS systems.

The prototype MLS system consists of relatively cheap, small and light-weight sensors, which can be easily synchronized and placed on any selected platform. The construction, synchronization and calibration of the MLS system are described in Section 3.1.

In **Paper I** the self-assembled MLS is tested in a car-mounted and a backpack mode. The point cloud is georeferenced without independently coordinated reference points in order to test the MLS system accuracy before further alignment. An optimization algorithm based on Bound Optimization BY Quadratic Approximation (BOBYQA) by Powell (2009) is implemented to determine the boresight angles. The prototype mapping-grade MLS data are compared against the terrestrial and survey-grade MLS reference data in areas with varying land cover and GNSS reception.

Both theoretical and experimental accuracy are determined. Also the errors are separated by scan angle and range. As expected, the accuracy is highly dependent on the range from LIDAR to the surveyed object. This is found in both theoretical and experimental accuracy assessment. Scan angle does not influence the theoretical 3D accuracy but it significantly affects the horizontal and vertical accuracy components. However, in practical experiments the influence of scan angle is difficult to evaluate and is not as clear as the correlation with range. For more details, see **Paper I**.

Generally, the scan angle affects the incidence angle. In particular, at extreme incidence angles the accuracy of the measurement decreases. However, often in engineering surveying coarse-grained or uneven surfaces (e.g. historic structures, rough concrete elements or roads) are measured. A laser beam with a large incidence angle (i.e. nearly parallel to the surface) can reflect back from these coarse surfaces. (Mill and Ellmann 2017)

In MLS the objects near nadir (e.g. road surface) are much closer than objects at 90 degrees (e.g. facades). Therefore, these are not influenced as much by beam divergence, ranging, etc. and the accuracy near nadir is better than the expected theoretical accuracy.

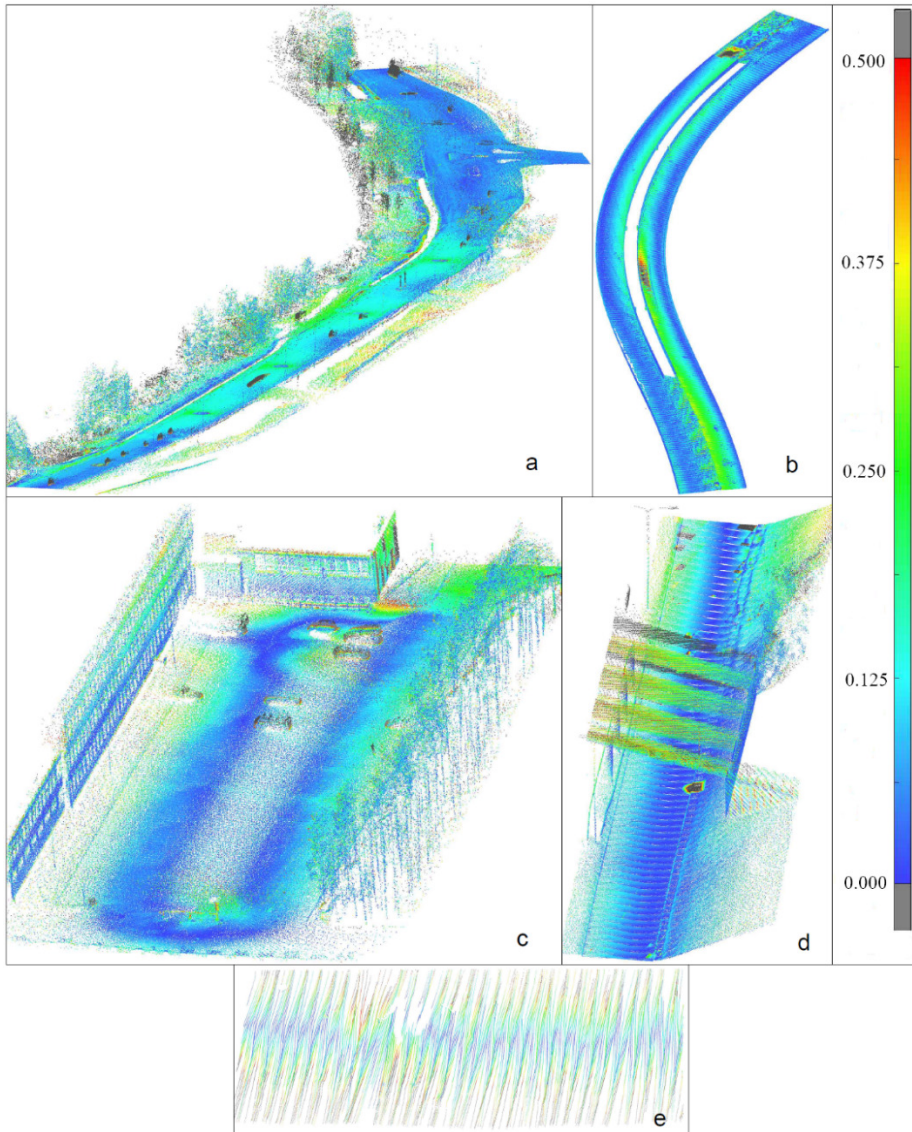


Fig. 8 3D comparison between MLS point clouds and reference data at study areas: a) “road”, b) “tunnel”, c) “parking lot”, d) “underpass”, e) “beach” The vertical bar colour denote discrepancies. The units are meters. (**Paper I**)

Fig. 8 presents 3D comparison between MLS point clouds and reference data. However, simple 3D differences are affected by the different densities and noise levels of point clouds, as well as from the fact that instable points (e.g. vegetation) are taken into consideration. Also 3D differences do not give an overview of the vertical, horizontal and relative accuracy components. Therefore, these components are evaluated separately.

To evaluate the vertical accuracy of the prototype MLS system, triangulated irregular network (TIN) models are calculated based on the point clouds of only the road surface (the ground surface for the “beach” study area). The surface points are automatically extracted with MCC algorithm (Evans and Hudak 2007), which achieved the best performance in a comparison of ground filtering algorithms presented in **Paper III**. The surface models are compared to the reference TIN models along the vertical z -axis. Statistics of the vertical accuracy assessment for all sites are presented in Table 4.

Table 4. Vertical comparison (along the z -coordinate) between MLS point clouds and reference data. MLS minus reference. Units in meters.

Study area	Min	Max	Mean	RMSE
Road	-0.350	0.412	0.029	0.072
Parking lot	-0.253	0.384	0.013	0.061
Underpass	-0.202	0.264	-0.015	0.064
Tunnel	-0.347	0.269	-0.034	0.089
Beach	-0.376	0.520	0.041	0.128
Average	-0.306	0.370	0.007	0.083

The results in Table 4 indicate that the reference data and mapping-grade MLS data agree in average at approximately 6-9 cm vertically. The beach data gathered with backpack platform show slightly worse agreement, at approximately 13 cm. This is due to the unpredictable and jerky motion of the backpack platform during the walking of the operator. Such irregular motion makes it difficult to maintain an accurate trajectory, as well as determine the accurate values for roll, pitch and heading. The mean offsets between MLS and reference data are both positive and negative. This indicates that these offsets are not caused by systematic errors in determining the lever arms and boresight angles. A more likely cause is the inaccuracy of the vertical component of GNSS positioning.

The horizontal accuracy of the MLS system is assessed by comparing the 2D coordinates of clearly identifiable features in MLS and reference point clouds. These are the edges of road markings (white coating on the paved surface) measured very close to the LIDAR sensor. The edges of road markings measured further from the nadir of the scanner were not clearly identifiable. To evaluate horizontal accuracy further from nadir, vertical surfaces on the facade and the wall of the underpass are used. Small sections of point clouds (approximately 1m x 1m) of the same vertical surface in both MLS and reference data are used to calculate a least squares best-fit plane for each point cloud independently.

The along-normal distance between the planes is measured from the center of the modelled MLS data plane. Overall, 30 road markings and 10 best-fit planes are used. Horizontal accuracy is not evaluated on the beach area since there are no clearly identifiable features nor vertical surfaces.

Table 5. Planar comparison between MLS point clouds and reference data. Units in meters.

Study area	Min	Max	Mean	RMSE
Road	0.021	0.345	0.143	0.152
Parking lot	0.015	0.274	0.125	0.147
Underpass	0.019	0.257	0.153	0.136
Tunnel	0.052	0.372	0.162	0.185
Average	0.027	0.312	0.146	0.155

The results in Table 5 show that in average the horizontal accuracy of the MLS data is approximately 15 cm. Generally, the horizontal error is slightly smaller near nadir. This is to be expected because points further away suffer more from the errors in attitude determination by the INS. Overall the horizontal accuracy is clearly worse than vertical accuracy but is still within the requirements for mapping-grade MLS systems (20 cm).

Vertical and planar evaluations are performed to assess the absolute accuracy of the MLS. However, in many occasions the absolute accuracy of the point cloud is not as crucial as the relative accuracy. To test the ability of the MLS point cloud to provide accurate relative measurements, several relevant dimensions are measured within the MLS data and the reference data. These measurements included road width, length of road markings, curb heights, facade dimensions and height of lamp poles. Measurements are taken several times and averaged. Relative accuracy is not evaluated on the sandy beach area because there are no clearly identifiable features. The measurements of the MLS and reference data generally agree within 3 cm, and the MLS measurements are nominally within 5% of the actual values, see Table 6.

Table 6. Relative comparison between MLS point clouds and reference data. Units in meters.

Study area	Absolute min	Absolute max	Mean	RMSE
Road	0.015	0.040	0.030	0.028
Parking lot	0.010	0.045	0.030	0.031
Underpass	0.020	0.050	0.035	0.034
Tunnel	0.010	0.030	0.020	0.019
Average	0.014	0.041	0.029	0.028

However, it can be concluded that the relative accuracy of the point cloud is significantly better than the absolute accuracy. Therefore, taking measurements on the road surface, building facades, etc. can be performed with an accuracy of a couple of centimeters.

Considering the achieved vertical accuracy of 8 cm, horizontal accuracy of 15 cm, and the relative accuracy of 3 cm, the MLS system satisfies the objective of mapping-grade accuracy (RMSE better than 20 cm). The developed MLS can be easily deployed on different platforms as demonstrated by testing it on a car and a backpack. Mapping-grade accuracy is achievable without frequent control points, which allows faster data collection and processing.

The analysis demonstrates that the developed mapping-grade MLS system can be used to acquire point cloud data about terrain, roads and buildings. With proper measurement techniques, the system can provide data that can be used effectively to model objects, such as building walls, flat surfaces from bridges and other structures, poles, tree trunks, curbs, etc. Basic engineering, structural, and architectural measurements can also be made with the MLS data, e.g. measuring road width, curb heights, dimensions of a building, etc. This makes the MLS system usable in situations, which do not require survey-grade accuracy.

As the test results are promising, then this encouraged us to start a research and development project with our surveying industry partner Reach-U AS to combine the MLS system with their mobile mapping system centered around a LadyBug 5 panoramic camera. The VLP-16 LIDAR is added to the system and synchronized with the Advanced Navigation Spatial Dual GNSS/INS device as described in **Paper II**. The methodology for sensor inter-calibration and data processing is conducted as described in this study. The integrated system has been successfully implemented for mobile mapping missions in Vietnam and Kenya (Fig. 9).



Fig. 9 The MLS system combined with Ladybug 5 panoramic camera of Reach-U during 2016-2017 field surveys in Hanoi, Vietnam (above) and Nairobi, Kenya (below).

4.2. Ground Filtering

This study describes the performance of freeware ground filtering algorithms listed in Section 3.2. Commercial software are usually expensive and generally used only in large companies or state owned enterprises, which perform large amount of ALS data processing. Thus, a non-associated researcher or enthusiast would not have access to such commercial software. Hence, this paper focuses on practical testing of six common filtering algorithms embedded in three freeware programs.

The analysis of the filtering results reveals that all the tested algorithms cause classification errors to a larger or lesser extent. As expected, the errors are more pronounced in areas with more diverse landscape. The most common errors are commission errors, i.e. errors where non-ground points are erratically classified as ground, e.g. vegetation and buildings; and omission errors, i.e. errors where ground points are classified as non-ground, e.g. on steeper slopes. When comparing DEM-s based on test and reference data, then the best results are achieved with MCC (see Table 7) with an average RMSE of 0.35 meters. Also determining the MCC parameter combinations is the easiest since MCC has only two variables as opposed to 6-8 in other algorithms.

Table 7. The RMSE values of ground filtering results within the test areas. Units in meters.

Algorithm	Root mean square error				
	Kiviõli „mixed“	Neeruti „esker-1“	Purtse „river-valley“	Viitna „esker-2“	Average
ATIN	0.882	0.921	0.298	0.457	0.640
ETEW	3.410	1.481	0.628	0.315	1.459
LP	0.991	0.457	0.289	0.256	0.498
MCC	0.510	0.387	0.238	0.249	0.346
MXS	0.706	0.469	0.259	0.275	0.427
PM	1.117	0.735	0.384	0.340	0.644
Average	1.269	0.742	0.349	0.315	

None of the tested algorithms are able to classify the most challenging areas (e.g. steep-slope hills and buildings) flawlessly. This is illustrated by the “mixed” test area (Fig. 10) where it is very challenging to correctly classify steep slopes and buildings with the same set of parameters. The green parts illustrate the areas where the discrepancies between reference and test data sets are negligible (less than a centimetre). The red represents the steep slopes and hilltops that are erratically removed (omission error) from ground points. The purple and blue colours show the buildings and vegetation respectively that are not removed (commission error) from ground points.

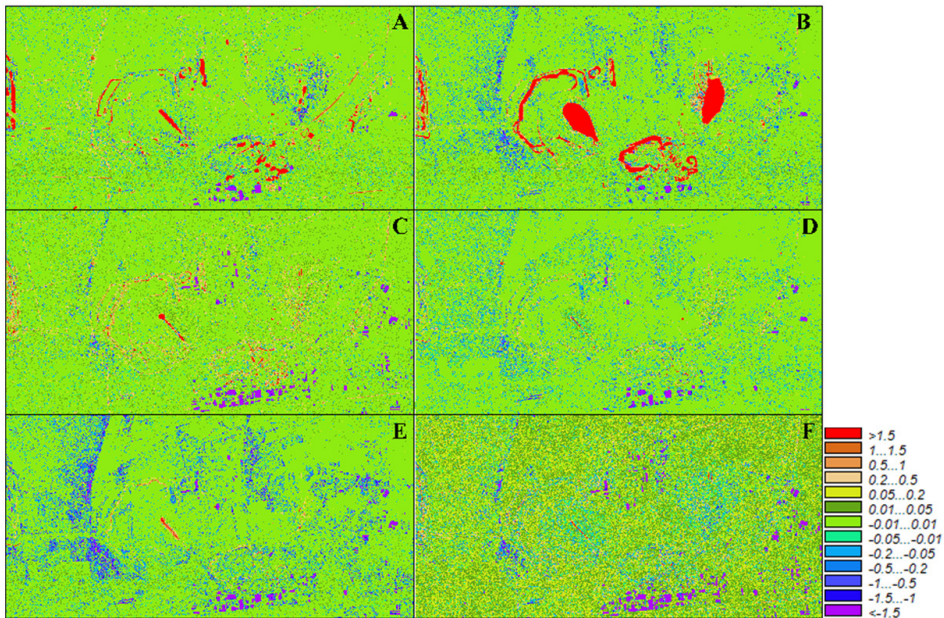


Fig. 10 Detected discrepancies between tested ground filtering algorithm results and the reference data in the „mixed“ test area (8 km²). A – ATIN, B – ETEW, C – LP, D – MCC, E – MXS, F – PM. The units are meters. (**Paper III**)

The ATIN omission errors appear on hilltops and commission errors on larger buildings. Areas covered with vegetation and smaller buildings are classified more or less correctly (Fig. 10A). ETEW yields very large omission errors on hilltops (resulting in a very large RMSE of 3.4 m, see Table 7) and quite large commission errors in forested areas (Fig. 10B). LP yields numerous commission errors on buildings and some omission errors on the steepest slopes, but the ground classification in forested areas is quite reasonable (Fig. 10C). The MCC commission errors are practically absent, however, some omission errors are detected on buildings and forested areas (Fig. 10D). This results in the smallest RMSE of 0.5 m in the “mixed” area, see Table 7. The MXS related large omission errors are associated with the vegetation and buildings. Commission errors are present only on the steepest hills (Fig. 10E). The PM related omission errors are due to buildings and, to some extent, vegetation. Hardly any PM related commission errors are detected (Fig. 10F). However, it is clear that the large RMSE values are mostly caused by gross errors, which are localized at certain landscape features (such as steep slopes). The error distribution analysis reveals that most of the errors are insignificant (less than 1 cm), in “mixed” test area as much as 75 %, see Fig. 11.

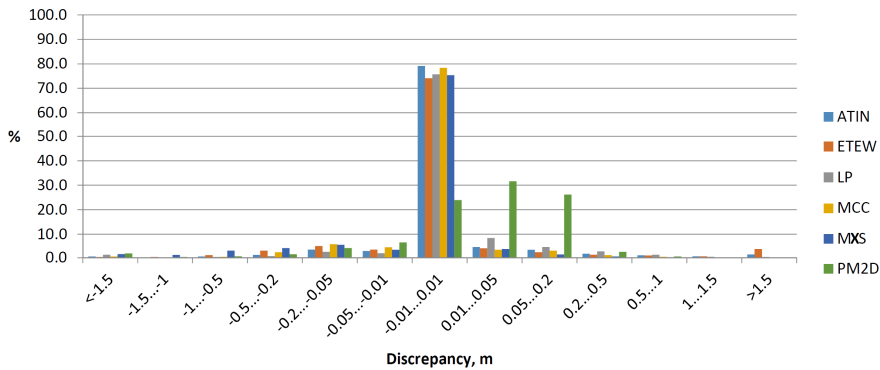


Fig. 11 The distribution of discrepancies between the ground filtering results and the reference data in the “mixed” test area. (**Paper III**)

Within the mixed area (urban, steep hills, low and high vegetation) it is almost impossible to achieve good results with only one combination of parameters or only one algorithm. The area should be divided into sub-areas containing more or less similar features and thereafter applying the algorithm more suitable for the situation. For example, in urban areas that are otherwise relatively flat the best algorithm is ATIN but since it tends to remove points from the tops of hills it cannot be used on complex terrain with the same parameter combinations. MCC on the other hand is efficient in wooded areas.

For all the algorithms some general rules for choosing the values of parameters are identified. On a relatively flat and open landscape where all of the pulse returns are ground points with similar elevations the choice of the values is not of upmost importance because practically the same results can be achieved with every reasonable (e.g. the allowed elevation difference threshold should never be set to 0) parameter combinations. The optimum parameter combinations are more important in areas where the landscape is inclined (e.g. hills). In that case, it should be noted that the elevation and slope thresholds need to be set large enough so that ground points would not be classified as non-ground.

In diverse situation regions, the selection of a suitable parameter set is more difficult, e.g. steep slopes that need to be classified as ground, and on the other hand buildings and vegetation that need to be classified as non-ground. Hence, a compromise is necessary to minimize the classification errors as an errorless classification is usually impossible. MCC algorithm is used in **Papers I** and **V** to extract road and beach surfaces from MLS and TLS data.

4.3. Combining Airborne and Terrestrial Laser Scanning results

So far MLS systems, using TLS as accurate reference data and applying ground filtering algorithms on ALS have been discussed in this thesis. Sometimes it is necessary to use some or all of these LS technologies together, which raises the question of their compatibility and alignment. In this section, two case studies for combining ALS and TLS data are presented.

4.3.1. Surveying complex structures

Using LS to capture a point cloud of complex engineering structures enables surveying the exact geometry of the object. This is difficult with traditional surveying methods (e.g. tachymetry) as it is difficult to determine individual points that need to be measured. LS point clouds are useful for creating accurate models for designing reconstruction plans and for Building Information Modelling (BIM).

This study tackles a TLS survey of a 30 m tall historic water tower (Fig. 12a). In this case, the scanning of the rooftop is impossible because the cone shaped pitched roof of the high-rise water tower is not visible from the ground and it is impossible to place the scanner tripod on it. Also the surrounding buildings are lower than the water tower, thus it is not beneficial to place the scanner on a balcony or a roof of a neighboring building. Therefore, the only possibility is to use ALS data to complete the point cloud of the water tower (Fig. 12b).

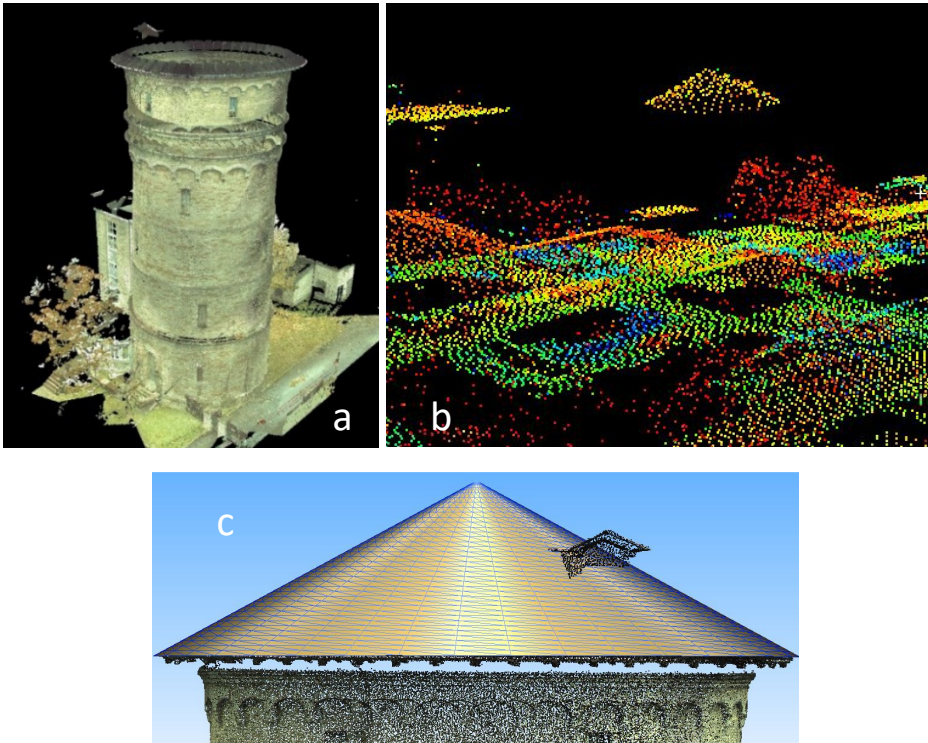


Fig. 12 (a) Point cloud of ground surveyed TLS data where the roof-top is missing. (b) Point cloud of ALS data where the cone shaped roof is clearly visible. (c) The cone-shaped model of the roof constructed from ALS data along with the TLS point cloud of the facade. **(Paper IV)**

The TLS facade survey is conducted with a pulse-based Leica ScanStation C10. The ALS data are received from the Estonian Land Board, which uses a Leica ALS50-II airborne laser scanner. One of the ALS campaigns is flown at a height of 1500 m and the point density is 1.2 points/m². The other campaigns have a flight height of 2400 m with resulting point density of 0.3...0.4 points/m².

In order to take into account the possible systematic errors in elevation, three horizontal reference surfaces near the water tower are selected. These horizontal surfaces have remained unchanged (no roadwork, etc.) since the ALS flights. The reference surfaces are measured with a total station using the same initial points that are used for the TLS orientation.

In order to determine the systematic errors in elevation, the three surfaces are separated from the rest of the ALS point cloud and obvious measurement blunders are removed. Based on these cleaned point clouds TIN models are formed. TIN models derived from ALS data are compared to reference TIN models derived from total station measurements in TLS coordinate system.

It is found that the detected discrepancies between the sparse ALS data and reference surfaces appear to be inadmissible. Therefore, only the denser ALS data are used for modeling the shape of the roof-top. A systematic bias of 0.051 m is detected. This 1D bias is removed from the ALS point cloud for it to conform with the TLS data. The resulting average standard deviation between the two datasets is 2.3 cm.

Based on this case study, it can be presumed that a point density of at least 1 point/m² is required to properly register different point clouds. If this is the case, then determining a systematic error is possible. Otherwise the data are too sparse or too big an area is needed to distinguish a clear trend with any certainty.

The tower and the roof are aligned in the horizontal x, y plane by matching the centers of the tower and that of the roof. The planar coordinates of the tower's center are found by calculating the center point of a circle that represents the outline of the tower's cross-section. The center of the roof is determined by modelling a best fit cone based on the roof-top points (Fig. 12c). The best fit cone is shifted horizontally by 25 cm with respect to the center of the tower.

By taking into consideration the systematic errors and shifts, it is possible to unify the TLS and ALS point clouds. Although it is clear that ALS data are not as high-resolution nor accurate as TLS data, ALS can still be useful if there are no other means to measure certain objects. It is usually not possible to capture fine details with standard ALS campaigns, as the point density is not sufficient to clearly distinguish small objects, e.g. chimneys, drainage elements, ventilation equipment, etc. Therefore, ALS is useful in modelling rough shapes of roofs, when the shape can be approximated by using different shapes, e.g. planes, cones, pyramids, etc.

4.3.2. Monitoring coastal processes

This case study investigates the suitability of TLS and ALS for monitoring coastal processes. It attempts to widen the applicability and enhance the quality of standard ALS data products by using in situ TLS data for minimizing systematic errors between ALS and TLS datasets from different time epochs. The goal is to characterize not only the overall intensity of coastal processes but also to shed light to the changes in the internal structure of the beach, in particular to identify whether the most representative parts of the beach gain or lose sediment.

The data set used in this study consists of both ALS and TLS data. To reduce systematic elevation differences between the ALS and TLS data, the surface of a parking lot (which has not changed since the ALS flights) near the beach is used as a horizontal reference. All ALS surfaces are reduced to the TLS reference surface by applying elevation corrections similarly as in the previous section. The reference surface is measured with TLS using reference points that are linked to points located at the beach. The points representing beach surface (in both ALS and TLS data) are extracted by using the MCC ground filtering algorithm reviewed in Section 4.2.

A comparison of the beach surface for the years 2008 and 2010 (both measured using the ALS technique) first demonstrates that the entire study area gained sand (Fig. 13a). Erosion is observed only in a few spots. Spatial changes in the beach height according to the ALS survey in 2010 and a TLS survey in December 2013 (Fig. 13b) reveal an opposite pattern: the entire study area lost sand, only a small vicinity in the middle of the study area (where a small stream is located) gained some sand. The total loss of sand over three years (2010–2013) is almost equal to the total gain in 2008–2010.

The described radical difference of the change pattern within the two discussed time intervals suggests that the properties of driving forces are likely quite different in these intervals. The years 2009–2010 were relatively mild, whereas 2011–2013 were relatively stormy. Therefore, it is not unexpected that the changes to the study area during the five years (2008 ALS – December 2013 TLS) are minor and have a variable spatial pattern (Fig. 13c). The proportions of the erosion and accumulation regions are almost equal. The largest accumulation rates are near the mouth of the small stream but these apparently do not characterise properly the processes in other parts of the study area. These few small patches of accumulation around the stream are evidently connected with the relocation of the stream and filling the stream bed with sand from adjacent locations. The overall pattern of changes in the almost six years covered by the LS data coincides with the common understanding of the nature of coastal processes and sand movement at the Pirita Beach (Soomere et al. 2008).

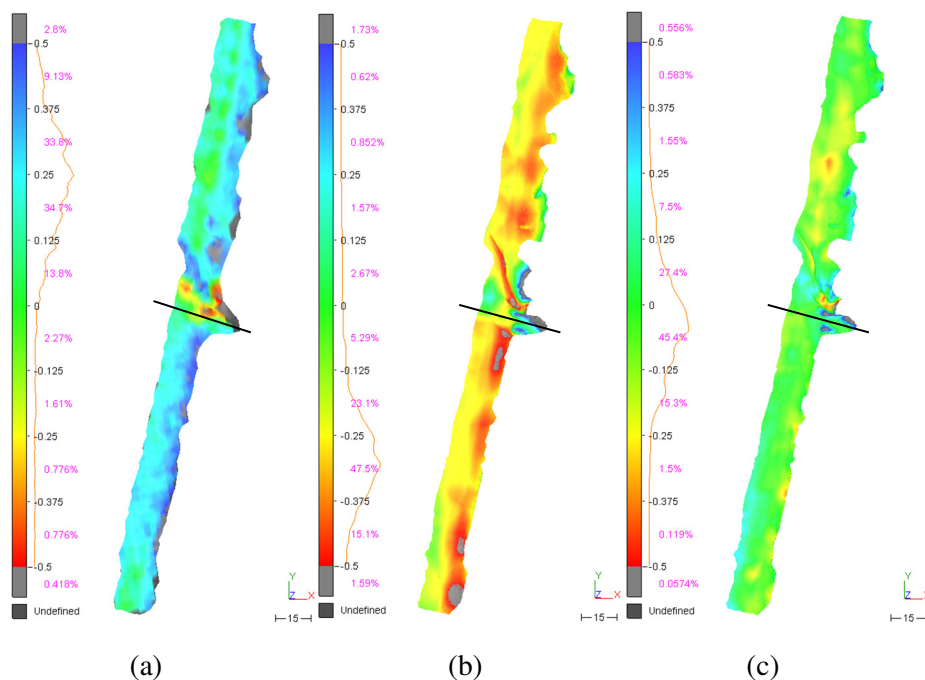


Fig. 13 Changes to the beach height from ALS in 2008 to 2010 (a), from ALS in 2010 to TLS in 2013 (b) and from ALS in 2008 to TLS in 2013 (c). The scale shows the extent of the differences (m) and the percentage of the scanned surface with a change rate within an interval of such rates. The black line indicates the location of a profile along a stream previously used for monitoring coastal processes. (**Paper V**)

The presented material suggests that the technology of repeated ALS and TLS is accurate and reliable enough to recognize the internal structure of changes to the beach. The described major difference of the changes in 2008–2010 and 2010–2013 also vividly demonstrates one of the major shortcomings of classical coastal monitoring activities. As they largely rely on the observed changes along a few profiles, the credibility of the outcome crucially depends on the proper choice of the profiles. The presented material demonstrates that local processes govern the beach height along the profile near the stream (Fig. 13). Not only is this profile evidently not able to replicate any essential changes to the adjacent segments of beach but in the discussed time intervals behaves almost oppositely to the real course of changes to the beach. The major advantage of both ALS and TLS is their ability to recognise a “big picture” of the evolution of longer beach sections and to avoid deceptive conclusions based on strongly localised data sets.

This study used ALS and TLS for monitoring the erosion of a beach. Similarly, these surveys can be performed with a MLS system. MLS is much faster than TLS and ALS data is not always available. Using a backpack mounted (vehicles are often not allowed on beaches) MLS system for measuring a beach is discussed in Section 4.1. Based on that study, the prototype MLS system is a viable solution for monitoring coastal erosion faster and at a lower cost than with either TLS or ALS.

5. CONCLUSIONS

The main objective (see Section 1.2.) of this study was to analyze the use of LS technologies for surveying built environment and landforms. More specifically, the results in this thesis contribute to the methods of constructing and evaluating prototype MLS systems, using ground filtering algorithms and combining different LS technologies for surveying and modelling structures and landforms.

A thorough overview of constructing a compact, low-cost, easy-to-use mapping-grade prototype MLS system was presented in **Papers I** and **II**. The MLS system was based on Velodyne VLP-16 LIDAR and SBG Systems Ellipse-D GNSS/INS device. The methodology for sensor inter-calibration, including the time synchronization and boresight calibration using BOBYQA algorithm, was presented.

The MLS system can be mounted on several platforms. It was tested on a car and a backpack to determine the experimental accuracy from comparisons with TLS data. The methodology for assessing vertical, horizontal and relative accuracy was described. The RMSE were determined to be 8 cm, 15 cm and 3 cm, respectively. Therefore, the prototype satisfied the criteria for a mapping-grade MLS system (20 cm).

The main application of the MLS system would be mapping and modelling of road engineering structures in order to measure the width of the road, curb heights, locate traffic signs and lamp posts. In these kinds of corridor surveys an absolute accuracy of mapping-grade is sufficient, whereas the relative accuracy is more important. It was also demonstrated that the MLS system can be used on a backpack to monitor coastal areas.

Algorithms for automatically determining ground points (for generating surface models) in a point cloud were reviewed in **Paper III**. Six common algorithms (Adaptive TIN, Elevation Threshold with Expand Window, Maximum Local Slope, Progressive Morphology, Multiscale Curvature and Linear Prediction) available in freeware software were tested on ALS data. Each algorithm yielded various errors. In the comparisons between DEM-s constructed from test and reference data, the Multiscale Curvature algorithm yielded the best overall results with an average RMSE of 0.35 meters. Adaptive TIN was more suitable in urban areas, whereas Multiscale Curvature algorithm was better in wooded areas.

Although, the test data sets were gathered with ALS, the same algorithms function also on TLS and MLS data. However, their efficiency might be different and the algorithm parameters need to be optimized according to the point cloud density and the characteristics of the area. Multiscale Curvature algorithm was successfully used to extract the road and beach surface from MLS data in **Paper I** and the beach surface from TLS data in **Paper V**.

It was demonstrated that point clouds surveyed with different LS methods can be used together. Common (nearly) horizontal surfaces can be used to detect the vertical offset between datasets. Horizontal offset can be derived by

constructing shapes based on the point cloud data (e.g. intersecting surfaces, cones) and aligning the shapes. Since man-made objects have more distinct outlines and shapes, then this is more feasible in urban areas, whereas horizontally aligning natural landforms is more difficult.

The use of ALS and TLS data in conjunction were exemplified in empirical studies. ALS and TLS techniques were used to survey and model a complex structure of a historic water tower. TLS was used for the facade and ALS for the roof. The two methods enabled capturing a complete point cloud, which individually would have been impossible (**Paper IV**). ALS and TLS data were also used to monitor coastal erosion zones. After alignment the methods were comparable and provided a good overview of the coastal processes. The advantage of LS was the ability to cover the entire beach area as opposed to traditional methodology, which relies on individual profiles every few hundred meters. With LS it was possible to locate the erosion and accumulation areas and accurately calculate the volume of changes (**Paper V**).

In conclusion, the empirical studies presented in this thesis demonstrate that LS can be used in various engineering and geoscientific tasks. LS has become accessible to a wider userbase due to lowering prices of the equipment, several freeware software for data processing (e.g. ground filtering) and the availability of point cloud data (e.g. ALS data from national campaigns).

6. FUTURE RESEARCH

Although the MLS system, algorithms and methods presented in this thesis worked well, there is still room for improvement and issues that require further investigation. Main areas for future research include:

- A comprehensive study comparing the BOBYQA algorithm with other calibration methods (e.g. least squares methods) and using different (e.g. survey-grade) MLS datasets.
- Investigating the causes and finding solutions to the problem of decreased quality of the MLS system's results in backpack mode versus car mode. The motion during walking is more unpredictable than that of driving. It could be possible that low-budget INS devices used in this thesis are not accurate enough for these challenging circumstances.
- Comparing and adapting the ground filtering algorithms on TLS and MLS data.
- Using low-flight unmanned aerial vehicle (UAV) as a platform for the prototype MLS system. The sensors are compact and light-weight enough to be mounted on an UAV. However, some modifications are required to optimize the placement of the sensors. Also, the data logger (currently a laptop) would need to be replaced with a more compact and robust device.

The field of laser scanning research is evolving quickly and new research topics will undoubtedly emerge. Solving existing problems and finding new applications for laser scanning data is a never-ending process.

LIST OF REFERENCES

- Ahokas, E., Kaartinen, H., & Hyypä, J. (2008). On the quality checking of the airborne laser scanning based nationwide elevation model in Finland. *Int. Arch. Photogramm. Remote Sens. Spat. Inf. Sci.*, 37, 267-270.
- Artuso, R., Bovet, S., & Streilein, A. (2003). Practical methods for the verification of countrywide terrain and surface models. *International Archives for Photogrammetry, Remote Sensing and Spatial Information Sciences*, 34(6).
- Axelsson, P. (2000). DEM generation from laser scanner data using adaptive TIN models. *International Archives of Photogrammetry and Remote Sensing*, 33(B4/1; PART 4), 111-118.
- Barber, D., Mills, J., & Smith-Voysey, S. (2008). Geometric validation of a ground-based mobile laser scanning system. *ISPRS Journal of Photogrammetry and Remote Sensing*, 63(1), 128-141. doi:10.1016/j.isprsjprs.2007.07.005
- Bishop, G., & Welch, G. (2001). An introduction to the kalman filter. *Proc of SIGGRAPH, Course*, 8(27599-23175), 41.
- Bremer, M., & Sass, O. (2012). Combining airborne and terrestrial laser scanning for quantifying erosion and deposition by a debris flow event. *Geomorphology*, 138(1), 49-60. doi:10.1016/j.geomorph.2011.08.024
- Brooks, B. A., Glennie, C., Hudnut, K. W., Ericksen, T., & Hauser, D. (2013). Mobile Laser Scanning Applied to the Earth Sciences. *Eos, Transactions American Geophysical Union*, 94(36), 313-315. doi:10.1002/2013eo360002
- Carter, W. E., Shrestha, R. L., & Slatton, K. C. (2007). Geodetic laser scanning. *Physics Today*, 60(12), 41-47. doi:10.1063/1.2825070
- Carter, W., Shrestha, R., Tuell, G., Bloomquist, D., & Sartori, M. (2001). Airborne laser swath mapping shines new light on Earth's topography. *Eos, Transactions American Geophysical Union*, 82(46), 549-549. doi:10.1029/01eo00321
- Dorning, P., Székely, B., Zámolyi, A., & Roncat, A. (2011). Automated detection and interpretation of geomorphic features in LiDAR point clouds. *Vermessung & Geoinformation*, 2, 60-69.
- El-Sheimy, N., & Schwarz, K. P. (1998). Navigating Urban Areas by VISAT-A Mobile Mapping System Integrating GPS/INS/Digital Cameras for GIS Applications. *Navigation*, 45(4), 275-285. doi:10.1002/j.2161-4296.1998.tb02387.x
- Evans, J. S., & Hudak, A. T. (2007). A Multiscale Curvature Algorithm for Classifying Discrete Return LiDAR in Forested Environments. *IEEE Transactions on Geoscience and Remote Sensing*, 45(4), 1029-1038. doi:10.1109/tgrs.2006.890412
- Glennie, C. (2007). Rigorous 3D error analysis of kinematic scanning LIDAR systems. *Journal of Applied Geodesy*, 1(3). doi:10.1515/jag.2007.017

- Glennie, C. (2009). Kinematic Terrestrial Light-Detection and Ranging System for Scanning. *Transportation Research Record: Journal of the Transportation Research Board*, 2105, 135-141. doi:10.3141/2105-17
- Glennie, C., Brooks, B., Ericksen, T., Hauser, D., Hudnut, K., Foster, J., & Avery, J. (2013). Compact Multipurpose Mobile Laser Scanning System — Initial Tests and Results. *Remote Sensing*, 5(2), 521-538. doi:10.3390/rs5020521
- Gonçalves, G., & Gomes Pereira, L. (2010). Assessment of the performance of eight filtering algorithms by using full-waveform LiDAR data of unmanaged eucalypt forest.
- Groves, P. D. (2015). Principles of GNSS, inertial, and multisensor integrated navigation systems, 2nd edition [Book review]. *IEEE Aerospace and Electronic Systems Magazine*, 30(2), 26-27. doi:10.1109/maes.2014.14110
- Gruno, A., Liibusk, A., Ellmann, A., Oja, T., Vain, A., & Jürgenson, H. (2013). Determining sea surface heights using small footprint airborne laser scanning. *SPIE Remote Sensing*, 88880R1-88880R13.
- Haala, N., Peter, M., Kremer, J., & Hunter, G. (2008). Mobile LiDAR mapping for 3D point cloud collection in urban areas—A performance test. *The international archives of the photogrammetry, remote sensing and spatial information sciences*, 37, 1119-1127.
- Hauser, D., Glennie, C., & Brooks, B. (2016). Calibration and Accuracy Analysis of a Low-Cost Mapping-Grade Mobile Laser Scanning System. *Journal of Surveying Engineering*, 142(4), 04016011. doi:10.1061/(asce)su.1943-5428.0000178
- Hofton, M. A., Blair, J. B., Minster, J., Ridgway, J. R., Williams, N. P., Bufton, J. L., & Rabine, D. L. (2000). An airborne scanning laser altimetry survey of Long Valley, California. *International Journal of Remote Sensing*, 21(12), 2413-2437. doi:10.1080/01431160050030547
- Holopainen, M., Kankare, V., Vastaranta, M., Liang, X., Lin, Y., Vaaja, M., . . . Alho, P. (2013). Tree mapping using airborne, terrestrial and mobile laser scanning – A case study in a heterogeneous urban forest. *Urban Forestry & Urban Greening*, 12(4), 546-553. doi:10.1016/j.ufug.2013.06.002
- Huising, E., & Pereira, L. G. (1998). Errors and accuracy estimates of laser data acquired by various laser scanning systems for topographic applications. *ISPRS Journal of Photogrammetry and Remote Sensing*, 53(5), 245-261. doi:10.1016/s0924-2716(98)00013-6
- Hyypä, J., Hyypä, H., Leckie, D., Gougeon, F., Yu, X., & Maltamo, M. (2008). Review of methods of small-footprint airborne laser scanning for extracting forest inventory data in boreal forests. *International Journal of Remote Sensing*, 29(5), 1339-1366. doi:10.1080/01431160701736489
- Jaakkola, A., Hyypä, J., Kukko, A., Yu, X., Kaartinen, H., Lehtomäki, M., & Lin, Y. (2010). A low-cost multi-sensoral mobile mapping system and

- its feasibility for tree measurements. *ISPRS Journal of Photogrammetry and Remote Sensing*, 65(6), 514-522. doi:10.1016/j.isprsjprs.2010.08.002
- Jochem, A., Höfle, B., & Rutzinger, M. (2011). Extraction of Vertical Walls from Mobile Laser Scanning Data for Solar Potential Assessment. *Remote Sensing*, 3(12), 650-667. doi:10.3390/rs3030650
- Jozkow, G., Toth, C., & Grejner-Brzezinska, D. (2016). UAS TOPOGRAPHIC MAPPING WITH VELODYNE LiDAR SENSOR. *ISPRS Annals of Photogrammetry, Remote Sensing and Spatial Information Sciences, III-1*, 201-208. doi:10.5194/isprs-annals-iii-1-201-2016
- Julge, K., & Ellmann, A. (2014). Combining Airborne and Terrestrial Laser Scanning technologies for measuring complex structures. Cygas, D. *Selected papers of the 9th International Conference on Environmental Engineering*, Vilnius, Lithuania, 22-23, May, 2014. (1-7). Vilnius: Vilnius Gediminas Technical University Press "Technika". doi:10.3846/enviro.2014.213. **(Paper IV)**
- Julge, K., Eelsalu, M., Grünthal, E., Talvik, S., Ellmann, A., Soomere, T., & Tõnisson, H. (2014). Combining airborne and terrestrial laser scanning to monitor coastal processes. 2014 IEEE/OES Baltic International Symposium, May 26.-29.2014, Tallinn, Estonia: 2014 *IEEE/OES Baltic International Symposium "Measuring and Modeling of Multi-Scale Interactions in the Marine Environment"*: Tallinn, Estonia, May 26-29, 2014. IEEE, 1-10. (IEEE Conference Proceedings). doi:10.1109/BALTIC.2014.6887874. **(Paper V)**
- Julge, K., Ellmann, A., & Gruno, A. (2014). Performance analysis of freeware filtering algorithms for determining ground surface from airborne laser scanning data. *Journal of Applied Remote Sensing*, 8 (1). doi:083573-1-083573-15.10.1117/1.JRS.8.083573. **(Paper III)**
- Julge, K., Ellmann, A., Vajakas, T., & Kolka, R. (2016). Initial tests and accuracy assessment of a compact mobile laser scanning system. In: *The International Archives of the Photogrammetry, Remote Sensing and Spatial Information Sciences* (633-638). XXIII ISPRS Congress, 12-19 July 2016, Prague, Czech Republic: Copernicus publications. (ISPRS Commission I, ICWG I/Va). doi:10.5194/isprsarchives-XLI-B1-633-2016. **(Paper II)**
- Julge, K., Vajakas, T., & Ellmann, A., (2017). Performance analysis of a compact and low-cost mapping-grade mobile laser scanning system. *Journal of Applied Remote Sensing*, 11(4), 044003. doi:10.1117/1.JRS.11.044003. **(Paper I)**
- Kalman, R. E. (1960). A New Approach to Linear Filtering and Prediction Problems. *Journal of Basic Engineering*, 82(1), 35. doi:10.1115/1.3662552
- Kraus, K., & Pfeifer, N. (1998). Determination of terrain models in wooded areas with airborne laser scanner data. *ISPRS Journal of*

- Photogrammetry and Remote Sensing*, 53(4), 193-203. doi:10.1016/s0924-2716(98)00009-4
- Kukko, A. (2013). *Mobile Laser Scanning—System development, performance and applications*. Doctoral dissertation. Finnish Geodetic Institute.
- Kukko, A., Kaartinen, H., Hyypä, J., & Chen, Y. (2012). Multiplatform Mobile Laser Scanning: Usability and Performance. *Sensors*, 12(12), 11712-11733. doi:10.3390/s120911712
- Lato, M., Hutchinson, J., Diederichs, M., Ball, D., & Harrap, R. (2009). Engineering monitoring of rockfall hazards along transportation corridors: using mobile terrestrial LiDAR. *Natural Hazards and Earth System Science*, 9(3), 935-946. doi:10.5194/nhess-9-935-2009
- Leslar, M., Wang, J., & Hu, B. (2016). Bore-sight and Lever Arm Calibration of a Mobile Terrestrial LiDAR System. *Geomatica*, 70(2), 97-112. doi:10.5623/cig2016-202
- Liang, X., Hyypä, J., Kukko, A., Kaartinen, H., Jaakkola, A., & Yu, X. (2014). The Use of a Mobile Laser Scanning System for Mapping Large Forest Plots. *IEEE Geoscience and Remote Sensing Letters*, 11(9), 1504-1508. doi:10.1109/lgrs.2013.2297418
- Löhmus, H., Ellmann, A., Märdla, S., & Idnurm, S. (2017). Terrestrial laser scanning for the monitoring of bridge load tests – two case studies. *Survey Review*, 1-15. doi:10.1080/00396265.2016.1266117
- Madeira, S., Gonçalves, J. A., & Bastos, L. (2012). Sensor Integration in a Low Cost Land Mobile Mapping System. *Sensors*, 12(12), 2935-2953. doi:10.3390/s120302935
- Mandlbürger, G., Vetter, M., Milenkovic, M., & Pfeifer, N. (2011, December). Derivation of a countrywide river network based on airborne laser scanning DEMs—Results of a Pilot Study. In *MODSIM2011, 19th International Congress on Modelling and Simulation. Modelling and Simulation Society of Australia and New Zealand, December 2011* (pp. 2423-2429). The Modelling and Simulation Society of Australia and New Zealand Inc.: Perth, WA, Australia.
- Maybeck, P. S. (1979). *Stochastic Models, Estimation and Control. Volume 1 (Mathematics in science and engineering ; v. 141a)*. Elsevier.
- McGaughey, R. J. (2011). *FUSION/LDV: Software for LIDAR Data Analysis and Visualization*. U.S. Department of Agriculture Forest Service.
- Meng, X., Currit, N., & Zhao, K. (2010). Ground Filtering Algorithms for Airborne LiDAR Data: A Review of Critical Issues. *Remote Sensing*, 2(3), 833-860. doi:10.3390/rs2030833
- Mill, T., & Ellmann, A. (2017). Assessment of along-normal uncertainties for application to terrestrial laser scanning surveys of engineering structures. *Survey Review*, 1-16. doi:10.1080/00396265.2017.1361565
- Mill, T., Ellmann, A., Aavik, A., Horemuz, M., & Sillamäe, S. (2014). Determining ranges and spatial distribution of road frost heave by terrestrial laser scanning. *The Baltic Journal of Road and Bridge Engineering*, 9(2), 225-234. doi:10.3846/bjrbe.2014.28

- Mill, T., Ellmann, A., Kiisa, M., Idnurm, J., Idnurm, S., Horemuz, M., & Aavik, A. (2015). Geodetic monitoring of bridge deformations occurring during static load testing. *The Baltic Journal Of Road And Bridge Engineering*, 10(1), 17-27. doi:10.3846/bjrbe.2015.03
- Mohamed, A. H., & Schwarz, K. P. (1999). Adaptive Kalman Filtering for INS/GPS. *Journal of Geodesy*, 73(4), 193-203. doi:10.1007/s001900050236
- Mukupa, W., Roberts, G. W., Hancock, C. M., & Al-Manasir, K. (2016). A review of the use of terrestrial laser scanning application for change detection and deformation monitoring of structures. *Survey Review*, 1-18. doi:10.1080/00396265.2015.1133039
- Olsen, M. J. (2013). *Guidelines for the use of mobile LIDAR in transportation applications* (Vol. 748). Transportation Research Board, Washington, D.C.
- Pearson, K. (1901). LIII. On lines and planes of closest fit to systems of points in space. *Philosophical Magazine Series 6*, 2(11), 559-572. doi:10.1080/14786440109462720
- Petrie, G., & Toth, C. (2008). Terrestrial Laser Scanners. *Topographic Laser Ranging and Scanning*, 87-128. doi:10.1201/9781420051438.ch3
- Plasencia, M., Pedersen, A., Arnaldsson, A., Berthet, J., & Jónsson, H. (2014). Geothermal model calibration using a global minimization algorithm based on finding saddle points and minima of the objective function. *Computers & Geosciences*, 65, 110-117. doi:10.1016/j.cageo.2013.09.007
- Powell, M. J. (2009). The BOBYQA algorithm for bound constrained optimization without derivatives. *Cambridge NA Report NA2009/06*, University of Cambridge, Cambridge.
- Puente, I., González-Jorge, H., Arias, P., & Armesto, J. (2012). Land-Based Mobile Laser Scanning Systems: A Review. *ISPRS - International Archives of the Photogrammetry, Remote Sensing and Spatial Information Sciences*, XXXVIII-5/W12, 163-168. doi:10.5194/isprsarchives-xxxviii-5-w12-163-2011
- Puente, I., González-Jorge, H., Riveiro, B., & Arias, P. (2013). Accuracy verification of the Lynx Mobile Mapper system. *Optics & Laser Technology*, 45, 578-586. doi:10.1016/j.optlastec.2012.05.029
- Reshetnyuk, Y. (2009). *Self-calibration and direct georeferencing in terrestrial laser scanning*. Doctoral dissertation. KTH.
- Rieger, P., Studnicka, N., Pfennigbauer, M., & Zach, G. (2010). Boresight alignment method for mobile laser scanning systems. *Journal of Applied Geodesy*, 4(1). doi:10.1515/jag.2010.002
- Sithole, G., & Vosselman, G. (2004). Experimental comparison of filter algorithms for bare-Earth extraction from airborne laser scanning point clouds. *ISPRS Journal of Photogrammetry and Remote Sensing*, 59(1-2), 85-101. doi:10.1016/j.isprsjprs.2004.05.004

- Skaloud, J., & Lichti, D. (2006). Rigorous approach to bore-sight self-calibration in airborne laser scanning. *ISPRS Journal of Photogrammetry and Remote Sensing*, 61(1), 47-59. doi:10.1016/j.isprsjprs.2006.07.003
- Soininen, A. (2012). Terrascan user's guide. *Terrasolid: Helsinki, Finland*.
- Soomere, T., Kask, A., Kask, J., & Healy, T. (2008). Modelling of wave climate and sediment transport patterns at a tideless embayed beach, Pirita Beach, Estonia. *Journal of Marine Systems*, 74. doi:10.1016/j.jmarsys.2008.03.024
- Sulaiman, N. S., Majid, Z., & Setan, H. (2010). DTM generation from LiDAR data by using different filters in open-source software. *Geoinformation Science Journal*, 10(2), 89-109.
- Zhang, K. (2007, December). Airborne LiDAR data processing and analysis tools. In *AGU Fall Meeting Abstracts*.
- Zhang, K., & Whitman, D. (2005). Comparison of Three Algorithms for Filtering Airborne Lidar Data. *Photogrammetric Engineering & Remote Sensing*, 71(3), 313-324. doi:10.14358/pers.71.3.313
- Zhang, K., Chen, S., Whitman, D., Shyu, M., Yan, J., & Zhang, C. (2003). A progressive morphological filter for removing nonground measurements from airborne LIDAR data. *IEEE Transactions on Geoscience and Remote Sensing*, 41(4), 872-882. doi:10.1109/tgrs.2003.810682
- Zlot, R., Bosse, M., Greenop, K., Jarzab, Z., Juckes, E., & Roberts, J. (2014). Efficiently capturing large, complex cultural heritage sites with a handheld mobile 3D laser mapping system. *Journal of Cultural Heritage*, 15(6), 670-678. doi:10.1016/j.culher.2013.11.009
- Telling, J., Lyda, A., Hartzell, P., & Glennie, C. (2017). Review of Earth science research using terrestrial laser scanning. *Earth-Science Reviews*, 169, 35-68. doi:10.1016/j.earscirev.2017.04.007
- Tinkham, W. T., Huang, H., Smith, A. M., Shrestha, R., Falkowski, M. J., Hudak, A. T., . . . Marks, D. G. (2011). A Comparison of Two Open Source LiDAR Surface Classification Algorithms. *Remote Sensing*, 3(12), 638-649. doi:10.3390/rs3030638
- Vaaja, M., Hyypä, J., Kukko, A., Kaartinen, H., Hyypä, H., & Alho, P. (2011). Mapping Topography Changes and Elevation Accuracies Using a Mobile Laser Scanner. *Remote Sensing*, 3(12), 587-600. doi:10.3390/rs3030587
- Wallace, L., Lucieer, A., Watson, C., & Turner, D. (2012). Development of a UAV-LiDAR System with Application to Forest Inventory. *Remote Sensing*, 4(12), 1519-1543. doi:10.3390/rs4061519
- Wehr, A., & Lohr, U. (1999). Airborne laser scanning—an introduction and overview. *ISPRS Journal of Photogrammetry and Remote Sensing*, 54(2-3), 68-82. doi:10.1016/s0924-2716(99)00011-8
- Vosselman, G. (2000). Slope based filtering of laser altimetry data. *International Archives of Photogrammetry and Remote Sensing*, 33(B3/2; PART 3), 935-942.

- Vosselman, G., & Maas, H. G. (2014). *Airborne and Terrestrial Laser Scanning*. Dunbeath: Whittles Publishing.
- Yadav, M., Goel, S., Singh, A. K., & Lohani, B. (2014). Developing Basic Design and Mathematical Framework for a Mobile Mapping System—a Case Study Using Available Sensors. *Journal of the Indian Society of Remote Sensing*, 42(2), 301-310. doi:10.1007/s12524-013-0340-x

ACKNOWLEDGEMENTS

This thesis was conducted in the Road Engineering and Geodesy Research Group in the Department of Civil Engineering and Architecture in Tallinn University of Technology.

I would like to express my gratitude to my supervisor Professor Artu Ellmann for his encouragement, guidance and support throughout my doctoral studies. I also thank him for the effort and time he has put in helping me to write my papers and this thesis.

I would also like to thank my co-authors of the publications Toivo Vajakas, Anti Gruno, Maris Eelsalu, Erko Grünthal, Silja Märdla (also for proofreading the thesis), Tarmo Soomere, Hannes Tõnisson and Riivo Kolka for their valuable contributions, co-operation and help. Completing these studies without them would not have been possible.

Prof. Tarmo Soomere, the principal investigator of the grant SF0140007s11AP14, is thanked for enabling access to some of the equipment used in this study. The funding sources of the studies are listed in the acknowledgements of **Papers I-V**.

Finally, I would like to thank my family and friends for their support.

ABSTRACT

The overall objective of this thesis is to analyze the use of laser scanning technologies for surveying landforms and constructions. This includes (i) the construction of a low-cost prototype mobile laser scanning (MLS) system and developing a methodology to evaluate its accuracy; (ii) analyzing the effectiveness of ground filtering algorithms; (iii) exploring the possibility of using different laser scanning technologies in conjunction with one another.

First, the construction of a prototype MLS system based on a Velodyne VLP-16 LIDAR and SBG Systems Ellipse-D dual antenna GNSS/INS system is described. The accuracy of the MLS system is evaluated with comparisons to high accuracy terrestrial laser scanning (TLS) data. The vertical, horizontal and relative accuracy are determined to be 8 cm, 15 cm and 3 cm (root mean square error - RMSE) respectively. Thus, the achieved mapping-grade accuracy demonstrates that this relatively compact and inexpensive self-assembled MLS can be successfully used for surveying the geometry and deformations of terrain, buildings, road and other engineering structures.

Secondly, the performance of freeware ground filtering algorithms is evaluated. The algorithms Adaptive TIN, Elevation Threshold with Expand Window, Maximum Local Slope, Progressive Morphology, Multiscale Curvature and Linear Prediction are tested on four relatively large (4-8 km²) and diverse landscape areas (surveyed with airborne laser scanning (ALS)), which include steep sloped hills, urban areas, ridge-like eskers and a river valley. The results show that in diverse test areas each algorithm yields various errors. It appears that Adaptive TIN is suitable in urban areas whilst the Multiscale Curvature algorithm is best suited in wooded areas. The Multiscale Curvature algorithm yielded the best overall results with an average RMSE value of 0.35 meters.

Lastly, a simple methodology for ALS and TLS data, based on finding common surfaces, is presented. Even though the spatial resolution and accuracy of ALS and TLS are very different, it is demonstrated based on two empirical studies that they can be successfully used in conjunction with one another. These studies include using TLS and ALS to survey the facade and roof (respectively) of a historic structure and monitoring coastal erosion zones.

Keywords: *laser scanning, MLS, ALS, TLS, accuracy assessment, ground filtering.*

KOKKUVÕTE

Käesoleva doktoritöö üldeesmärk on analüüsida ehitiste ja looduslike pinnavormide mõõdistamiseks kasutatavaid laserskaneerimise tehnoloogiaid. See hõlmab (i) kompaktselt ja madala hinnaga mobiilse laserskaneerimise (MLS) süsteemi prototüübi ehitamist ja selle täpsuse hindamise meetodika väljatöötamist; (ii) maapinna filtreerimisalgoritmide tõhususe analüüsimist; (iii) erinevate laserskaneerimise tehnoloogiate kooskasutamise uurimist.

Esiteks on kirjeldatud MLS prototüübi ehitamist. See koosneb Velodyne VLP-16 LIDAR seadmest ja SBG Systems Ellipse-D kahe antenniga GNSS/INS seadmest. MLS süsteemi täpsuse hindamiseks võrreldi sellega saavutatud tulemusi kõrgtäpsuse terestrilise laserskaneerimise (TLS) andmetega. Leiti, et vertikaalne, horisontaalne ja suhteline täpsus on vastavalt 8 cm, 15 cm ja 3 cm (keskmine ruutviga - KRV). Saavutatud täpsus näitab, et seda suhteliselt kompaktselt ja odavat MLS süsteemi saab edukalt kasutada maastiku, hoonete, maanteed ning muude rajatiste geomeetria ja deformatsioonide mõõtmiseks.

Teiseks hinnati vabavaraliste maapinna filtreerimise algoritmide efektiivsust. Algoritme *Adaptive TIN*, *Elevation Threshold with Expand Window*, *Maximum Local Slope*, *Progressive Morphology*, *Multiscale Curvature* and *Linear Prediction* testiti neljal suhteliselt suurel (4-8 km²) testalal, mis olid mõõdistatud aerolaserskaneerimisega (ALS) ning hõlmasid järskude nõlvadega künkaid, linnapiirkondi, metsasid, lagendikke ja jõe orgu. Tulemused näitavad, et erinevatel katsealadel tekitavad algoritmid erinevaid vigu. *Adaptive TIN* on sobilik linnapiirkondades, samal ajal kui *Multiscale Curvature* algoritm sobib kõige paremini metsastele aladele. Parimad tulemused kõigi testaladele piires saavutati *Multiscale Curvature* algoritmiga, mille KRV oli 0,35 meetrit.

Seejärel esitatakse lihtne meetodika ALS ja TLS andmete kooskasutamiseks. Kahe empiirilise uuringu põhjal saab väita, et kuigi ALS ja TLS andmete ruumiline eraldusvõime ja täpsus on väga erinevad, saab neid siiski edukalt kombineerida. Need uuringud hõlmavad TLS-i ja ALS-i kasutamist, et mõõdistada ehitiste fassaadi ja katusepindasid ning rannikualade erosiooni.

Märksõnad: *laserskaneerimine, MLS, ALS, TLS, täpsuse hindamine, maapinna filtreerimine.*

PUBLICATION I

© 2017 Society of Photo-Optical Instrumentation Engineers (SPIE). Reprinted, with permission, from

Julge, K., Vajakas, T., Ellmann, A., (2017). Performance analysis of a compact and low-cost mapping-grade mobile laser scanning system. *Journal of Applied Remote Sensing*, 11(4), 044003, 10.1117/1.JRS.11.044003.

Performance analysis of a compact and low-cost mapping-grade mobile laser scanning system

Kalev Julge,^{a,*} Toivo Vajakas,^{b,c} and Artu Ellmann^a

^aTallinn University of Technology, School of Engineering,

Department of Civil Engineering and Architecture,

Road Engineering and Geodesy Research Group, Tallinn, Estonia

^bReach-U AS, Tartu, Estonia

^cUniversity of Tartu, Institute of Computer Science, Tartu, Estonia

Abstract. The performance of a low-cost, self-contained, compact, and easy to deploy mapping-grade mobile laser scanning (MLS) system, which is composed of a light detection and ranging sensor Velodyne VLP-16 and a dual antenna global navigation satellite system/inertial navigation system SBG Systems Ellipse-D, is analyzed. The field tests were carried out in car-mounted and backpack modes for surveying road engineering structures (such as roads, parking lots, underpasses, and tunnels) and coastal erosion zones, respectively. The impact of applied calculation principles on trajectory postprocessing, direct georeferencing, and the theoretical accuracy of the system is analyzed. A calibration method, based on Bound Optimization BY Quadratic Approximation, for finding the boresight angles of an MLS system is proposed. The resulting MLS point clouds are compared with high-accuracy static terrestrial laser scanning data and survey-grade MLS data from a commercially manufactured MLS system. The vertical, horizontal, and relative accuracy are assessed—the root-mean-square error (RMSE) values were determined to be 8, 15, and 3 cm, respectively. Thus, the achieved mapping-grade accuracy demonstrates that this relatively compact and inexpensive self-assembled MLS can be successfully used for surveying the geometry and deformations of terrain, buildings, road, and other engineering structures. © 2017 Society of Photo-Optical Instrumentation Engineers (SPIE) [DOI: 10.1117/1.JRS.11.044003]

Keywords: mobile laser scanning; light detection and ranging; calibration; Bound Optimization BY Quadratic Approximation optimization algorithm; point cloud; accuracy assessment.

Paper 170542 received Jun. 19, 2017; accepted for publication Nov. 14, 2017; published online Dec. 12, 2017.

1 Introduction

Mobile laser scanning (MLS) is used to acquire three-dimensional (3-D) point cloud data on the move. MLS systems consist of a light detection and ranging (LIDAR) scanner, an inertial navigation system (INS), and a global navigation satellite system (GNSS) receiver. These are time-synchronized and placed on a moving platform. MLS is a faster and cost-effective alternative to static terrestrial laser scanning (TLS), even though there is a slight trade-off in accuracy.

In the past decade, numerous commercial MLS systems have been constructed by different manufacturers, e.g., Riegl, Optech, Trimble, Dynascan, etc. Generally, these systems are expensive (exceeding \$250,000), large in size, and sometimes difficult to operate. A commercially manufactured MLS system is often used on a specially designed platform. Due to nonstandardized platforms, the installation to the nondesignated platforms can be impractical, cumbersome, and time-consuming, which makes it difficult to travel overseas with the MLS system and install it quickly on a new platform, e.g., to be hired locally. Often the required investment for purchasing a commercial MLS system is unaffordable for smaller companies, research institutes, and universities. Therefore, MLS systems consisting of inexpensive, small, and light-weight LIDAR

*Address all correspondence to: Kalev Julge, E-mail: kalev.julge@ttu.ee

Table 1 Summary of prototype MLS systems.

Paper authors	Systems/sensors used	Cost ^a of the LIDAR sensor (USD)	Accuracy
Jaakkola et al. (2010) ¹	<i>Ibeo Lux profile LIDAR</i>	~18,000	Horizontal 22 cm
	Novatel SPAN-CPT GNSS/INS		Vertical 9.2 cm
Wallace et al. (2012) ²	<i>Ibeo Lux profile LIDAR</i>	~18,000	Without structure from motion (SfM) observations:
	MEMS IMU—microstrain 3DM-GX3 35		Horizontal 60 cm
	GPS receiver (Novatel OEMV1-df)		Vertical 19 cm
	(HD video camera)		With SfM observations: Horizontal 32 cm Vertical 14 cm
Glennie et al. (2013) ⁴	<i>Velodyne HDL-32E LIDAR</i>	~30,000	Horizontal 16.9 cm
	Oxford Technical Services Inertial+2 INS		Vertical ~4 cm
	Novatel dual-frequency GPS antennae and receivers		
Jozkow et al. (2016) ⁶	<i>Velodyne HDL-32E or Velodyne VLP-16 LIDAR</i>	~30,000 or ~8000	Vertical 49 cm (initial estimate)
	Novatel GNSS receiver Epson M-G362PDC1 or MicroStrain 3DM-GX3-35 IMU		
Julge et al. (this study)	<i>Velodyne VLP-16 LIDAR</i>	~8000	Horizontal 15 cm
	SBG Systems Ellipse-D GNSS/INS		Vertical 8 cm
			Relative 3 cm

^aThe total cost of the MLS systems is difficult to approximate since this information is usually not listed in the publications (nor all the exact models of the sensors). Also, the cost of the GNSS/INS systems is generally not public (varies among different distributors). Therefore, only the approximate cost of the LIDAR scanners is presented.

and GNSS/INS sensors have been constructed¹⁻⁶ to overcome these shortcomings. The characteristics of such MLS systems are summarized in Table 1.

All the sensors in an MLS platform need to be time-synchronized, which is one of the most important steps in constructing an MLS system. This is usually achieved by sending a pulse-per-second (PPS) signal from the GNSS to the other sensors along with complementary data-packages. This ensures that all the datasets have the same timestamp. Alternatively, the time synchronization can be achieved using the time information from the data logging computer. Approaches of sensor integration and time synchronization have been discussed by El-Sheimy and Schwarz,⁷ Yadav et al.,⁸ and Madeira et al.⁹

Prototype MLS systems need verification through comparisons with higher accuracy reference data. For instance, a rigorous 3-D error analysis to calculate the theoretical achievable accuracy of MLS systems was performed by Glennie.¹⁰ This methodology is also utilized in this current study. Glennie¹¹ also used GNSS, tachymetric, and levelling control points to evaluate MLS accuracy. Barber et al.¹² compared MLS point clouds with control points measured with real-time kinematic (RTK) and static GNSS surveys. The horizontal accuracy was determined to be 10 cm, while the elevation accuracy was ± 4 cm. Haala et al.¹³ compared planar patches from MLS point clouds with existing models that yielded an agreement within a few cm. Puente

et al.¹⁴ compared multiple passes of the same MLS system and found that the relative accuracy was within a couple of cm. Hauser et al.¹⁵ analyzed the accuracy of a mapping-grade MLS system with respect to TLS and achieved a 3-D accuracy of 8 cm. Their study also determined a relative surveying accuracy of 4 cm for brick post widths, loading dock widths and heights, ramp widths, railing lengths, guard post heights, and stair landing insets. These and other similar studies have proved that after applying rigorous procedures the MLS data accuracy is sufficient for many mapping and surveying applications.

The accuracy of modern MLS systems can vary to a large extent depending on the quality of sensors used. Olsen et al.¹⁶ differentiated between mapping-grade and survey-grade accuracy systems. A mapping-grade MLS system yields 3-D point accuracy of 5 to 20 cm (2 sigma), whereas a survey-grade system yields accuracy of better than 5 cm (2 sigma).

There are many applications for MLS data. Most of these are related to mapping and surveying tasks. Generally, survey-grade accuracy is needed for as-built surveys of roads and other structures, corridor mapping, and monitoring deformations,¹⁶ whereas mapping-grade MLS accuracy is sufficient for geomorphological studies to detect landslides and sink-holes,^{17,18} monitor rock-falls,¹⁹ detect faults and measure their size,^{3,18} and evaluate the extent of topographical changes.²⁰ MLS has many uses in various multidisciplinary fields, beyond surveying and mapping. MLS has been implemented in forestry studies, e.g., mapping large forest plots²¹ and extracting tree and pole features,¹ as well as in archaeology²² and assessing solar potential.²³

The main research objective of this study is to construct a low-cost, light-weight, and easy-to-use MLS system that can be rapidly mounted on several platforms and meets the mapping-grade accuracy of 20 cm. The MLS accuracy will be evaluated by comparisons with high-accuracy TLS and survey-grade MLS systems. The main application of the developed MLS system would be mapping of the traffic corridors and road engineering structures to determine the width of the road, curb heights, locate traffic signs, and lamp poles. In these surveys, a mapping-grade absolute accuracy is sufficient, whereas the requirements for relative accuracy are stricter. The sensors to be used are a Velodyne VLP-16 LIDAR and dual antenna SBG Systems Ellipse-D GNSS/INS. The self-assembled MLS is tested in a car-mounted mode and a backpack mode.

The outline of this paper is as follows. First, the basic principles of MLS are reviewed. This includes the system components, postprocessing of trajectory, direct georeferencing, calibration of boresight angles, and theoretical accuracy of the MLS system. Thereafter, several conducted case studies are described along with the specifications of the used sensors, study areas, achieved results, and vertical, horizontal, and relative accuracy assessment. A brief summary concludes this paper.

2 MLS Principles

2.1 System Components

The main components of an MLS system are a LIDAR scanner, a GNSS receiver, and an INS. Complementary odometer data (i.e., the running distance) and dual GNSS antennas for determining the heading are often implemented to improve the quality of the result. GNSS/INS and GNSS base station data are integrated to calculate the trajectory (i.e., the position and attitude) of the MLS system, generally using Kalman filtering.²⁴ The relative position of the sensors with respect to each other has to be firm and accurately determined. This includes the lever arms, i.e., the distance between the origins of the sensors in the INS frame, and the boresight matrix, i.e., the pitch, roll, and yaw offsets. The trajectory and LIDAR data are combined to calculate a georeferenced point cloud.

2.2 Georeferencing

The point cloud is calculated based on the distance and horizontal/vertical angles measured with a LIDAR sensor and the position and attitude measured with a GNSS/INS system. Generally, the coordinates x , y , z of an individual survey point in the scanner frame can be calculated by

$$P_s = \begin{bmatrix} r \cdot \cos \beta \cdot \sin \alpha \\ r \cdot \cos \beta \cdot \cos \alpha \\ r \cdot \sin \beta \end{bmatrix}, \tag{1}$$

where P_s is the 3-D position of an individual LIDAR point in the scanner’s coordinate frame; r is the range from scanner to survey point; β is the vertical angle reckoned from horizontal plane defined by the x -, y -axes of the scanner; and α is the horizontal angle reckoned from the x -axis of the scanner.

GNSS/INS data, as well as the determined boresight angles and lever arms, are used for direct georeferencing, i.e., transforming point coordinates from the scanner frame to the geodetic frame. The direct georeferencing equation is given as

$$P_G(t) = P_{GNSS}(t) + R_l^G(t) \cdot R_b^l(t) \cdot [R_s^b \cdot P_s(t) + L^b], \tag{2}$$

where P_G is the 3-D position of the measured LIDAR point in global frame; P_{GNSS} is the position of the navigation sensor in global frame; R_l^G is the transformation between the global and the local horizontal frame; R_b^l is the rotation matrix from the body (INS) frame to the local horizontal frame defined by roll, pitch, and heading; R_s^b is the boresight rotation matrix, i.e., rotation from scanner’s frame to the body (INS) frame; L^b is the position of the scanner in the body frame, i.e., the lever arms between the scanner and the navigation sensor center (in this case the INS origin); and (t) is the time instant, not shown in further equations for simplicity.

As is evident from Eq. (2), calibration values, i.e., the boresight rotation matrix and the lever arm offsets, are necessary to accurately transform the point cloud from the scanner coordinate system into a global coordinate system. If these parameters are determined inaccurately, then the discrepancy between consecutive point clouds increases. Boresight and lever arms are determined during the calibration of an MLS system.

2.3 Theoretical Accuracy

The achievable theoretical accuracy of an MLS system in good surveying conditions (i.e., no obstructions for the GNSS signal and no interference for the INS) can be *a priori* estimated from the quoted measurement accuracies of individual MLS system components and the accuracy of determining the boresight angles and lever arms. This can be achieved with a simple error budget analysis described, e.g., by Jaakkola et al.¹ or Kukko²⁵ or with a more complex calculation, e.g., conditional variance analysis as described by Leslar et al.²⁶ Also, a theoretical accuracy analysis of ALS systems with detailed testing is presented by Goulden and Hopkinson.²⁷

In this study, the rigorous first-order error analysis of the LIDAR georeferencing equation as described by Glennie¹⁰ is used. In the direct georeferencing equation [Eq. (2)], we can assume that all the components, except the transformation between local and global coordinates (R_l^G), contain errors.¹⁰ Therefore, if we remove R_l^G component and find the coordinates of a point in local frame, then Eq. (2) can be expressed as

$$P_G^l = P_{GNSS}^l + R_b^l(R_s^b \cdot P_s + L^b), \tag{3}$$

where P_G^l are the coordinates of the measured LIDAR point in local frame and P_{GNSS}^l are the coordinates of the navigation sensor in local frame.

Equation (3) can be elaborated to show that the calculated local coordinates are dependent on 14 parameters that all contain errors¹⁰

$$\begin{bmatrix} X \\ Y \\ Z \end{bmatrix}_G^l = \begin{bmatrix} X \\ Y \\ Z \end{bmatrix}_{GNSS}^l + R_b^l(\omega \quad \varphi \quad k) \cdot \left\{ R_s^b(d\omega \quad d\varphi \quad dk) \cdot P_s(\alpha \quad \beta \quad r) + \begin{bmatrix} l_x \\ l_y \\ l_z \end{bmatrix} \right\}, \tag{4}$$

where X , Y , and Z are the 3-D coordinates of the navigation sensor determined by the GNSS measurements; ω , φ , and k are the roll, pitch, and heading of the MLS system, respectively, with respect to the local level frame given by the INS; $d\omega$, $d\varphi$, and dk are the boresight angles

(roll, pitch, and heading, respectively) between the scanner frame and the INS body frame determined with calibration; α , β , and r are the horizontal and vertical scan angle and range measured by the LIDAR sensor, respectively; and l_x , l_y , and l_z are the lever arm offsets measured during the assembly of the MLS system.

The 14 parameters are thus unknowns, and Eq. (4) is nonlinear. To examine the effects of errors in the measured parameters, the equation can be linearized by truncating a Taylor series expansion after the first term. Therefore, the impact of small differential errors in parameters is observable in the output point coordinates when solving a set of linear equations. Assuming all the error sources are statistically independent (since no error originates from another error) and by differentiating Eq. (4) against the 14 unknowns above, the general error equation can be expressed as¹⁰

$$\begin{bmatrix} \delta X \\ \delta Y \\ \delta Z \end{bmatrix}_G^l = \begin{bmatrix} \delta X \\ \delta Y \\ \delta Z \end{bmatrix}_{\text{GNSS}}^l + J \begin{bmatrix} \delta\omega \\ \delta\varphi \\ \delta k \end{bmatrix} + K \begin{bmatrix} \delta d\omega \\ \delta d\varphi \\ \delta dk \end{bmatrix} + B \begin{bmatrix} \delta\alpha \\ \delta\beta \\ \delta r \end{bmatrix} + C \begin{bmatrix} \delta l_x \\ \delta l_y \\ \delta l_z \end{bmatrix}, \quad (5)$$

where J , K , B , and C are the Jacobian matrices, which contain the partial derivatives of a point cloud coordinate calculated with respect to each error. They are defined as¹⁰

$$J = \begin{bmatrix} \frac{\partial P_G^l}{\partial\omega} & \frac{\partial P_G^l}{\partial\varphi} & \frac{\partial P_G^l}{\partial k} \end{bmatrix}; \quad K = \begin{bmatrix} \frac{\partial P_G^l}{\partial d\omega} & \frac{\partial P_G^l}{\partial d\varphi} & \frac{\partial P_G^l}{\partial dk} \end{bmatrix}; \quad B = \begin{bmatrix} \frac{\partial P_G^l}{\partial\alpha} & \frac{\partial P_G^l}{\partial\beta} & \frac{\partial P_G^l}{\partial r} \end{bmatrix}; \quad C = \begin{bmatrix} \frac{\partial P_G^l}{\partial l_x} & \frac{\partial P_G^l}{\partial l_y} & \frac{\partial P_G^l}{\partial l_z} \end{bmatrix}. \quad (6)$$

Note that J , K , B , and C are actually 3×3 matrices since P_G^l consists of x , y , and z components. Therefore, we can express J as

$$J = \begin{bmatrix} \frac{\partial X_G^l}{\partial\omega} & \frac{\partial X_G^l}{\partial\varphi} & \frac{\partial X_G^l}{\partial k} \\ \frac{\partial Y_G^l}{\partial\omega} & \frac{\partial Y_G^l}{\partial\varphi} & \frac{\partial Y_G^l}{\partial k} \\ \frac{\partial Z_G^l}{\partial\omega} & \frac{\partial Z_G^l}{\partial\varphi} & \frac{\partial Z_G^l}{\partial k} \end{bmatrix}, \quad (7)$$

and the same is applied to matrices K , B , and C .

These equations can be used to predict (based on the specifications of system components) the theoretical accuracy of an MLS system even prior to assembling the system. Estimated error parameters of the prototype MLS system are inserted into the error analysis to yield the expected accuracy for this system configuration, cf., Sec. 3.4. When the theoretical accuracy is better than the experimental accuracy, there are problems either with synchronization or data processing. Such a comparison of the expected and achieved accuracy can be used to validate whether the prototype MLS system is performing according to its potential.

2.4 MLS System Calibration and Principles of BOBYQA Optimization Algorithm

Ideally, MLS system calibration could be performed in a laboratory setting by measuring the offset and orientation of the scanner in relation to the INS. However, this can only be achieved for the lever arms and not for boresight angles because any small mistake amplifies errors in the field measurements. This makes boresight calibration in a laboratory impractical and very rarely (if ever) used. In practice, the boresight calibration can only be performed by analyzing the point cloud data acquired with the MLS system. This analysis can be done manually or by a statistical adjustment. The former calibration involves manually changing the boresight and subsequently reprocessing the data, until the point cloud is “visually correct.” This method is used by Kukko²⁵ and Jaakkola et al.¹ However, manual calibration is subjective and relies heavily on the skill of the operator. Therefore, in most cases, some kind of calculation method is used. Numerous methods can be used for determining calibration parameters (e.g., Rieger et al.²⁸ or Leslar et al.²⁹).

Usually, planar patches are aligned with control measurements. The alignment outcome is evaluated by least-squares method or other algorithms (e.g., Skaloud and Lichti³⁰). The parameters that result in the best alignment are considered as the optimized boresight values.

For the developed system, an optimization algorithm was implemented to determine the boresight angles and lever arms. The optimization is performed with point cloud data gathered without prior rigorous calibration of the MLS system. The optimization algorithm is based on Bound Optimization BY Quadratic Approximation (BOBYQA).³¹

BOBYQA is a numerical optimization algorithm that does not require calculating derivatives of the objective function to solve bound constrained optimization problems. It uses a trust region method by forming quadratic models with interpolation. In each iteration, a point is calculated, either by solving a trust region subproblem subject to the bound constraints or by choosing a point to replace an interpolation point to achieve linear independence in the interpolation conditions.³¹

The objective function g to be optimized was constructed to minimize “fuzziness” of the point cloud on selected objects (subsets in point cloud) by means of principal components analysis (PCA).³² PCA gives approximation of test points as ellipsoid. Ellipsoid axes lengths can be calculated as eigenvalues λ_1 , λ_2 , and λ_3 of covariance matrix for 3-D point coordinates data. Two types (T_k) of calibration objects (clusters) were used:

- Flat two-dimensional (2-D) areas (e.g., road surface and vertical wall). Objective function g is to have “flat” ellipsoid, i.e., to minimize the thickness of ellipsoid in surface normal direction.
- Straight and thin one-dimensional (1-D) objects (e.g., traffic sign poles and lamp posts). Objective function g is to minimize cross-section diameter of ellipse.

Description of the algorithm to find improved parameter vector P'' from the original estimate P' , i.e., to optimize the boresight angles and lever arm offsets, is shown in Algorithm 1.

Algorithm 1 The optimization of boresight angles and lever arms.

Inputs:

- initial parameter vector P'
- measured data D in LIDAR coordinates (not georeferenced)

Defined functions:

- coordinate transform $f(P, D)$ to convert measured data to Cartesian point cloud C
- goal function $g(P)$ for parameter P , using calibration objects $D_{1...K}$
 - for each calibration object $k = 1...K$, calculate value g_k
 - CALCULATE the eigenvalues λ_1 , λ_2 , and λ_3 of correlation matrix of coordinates of $f(P, D_k)$
 - CALCULATE depending on type T_k :
 - if $T_k = 1\text{-D}$, then $g_k = (\lambda_2^2 + \lambda_3^2)^{1/2}$
 - if $T_k = 2\text{-D}$, then $g_k = \lambda_3$
 - CALCULATE total goal function $g = \text{sum}(g_k)$, where $k = 1...K$.

Algorithm:

- DETERMINE manually or semiautomatically from the initial point cloud $C(P', D) = f(P', D)$ the K calibration objects (clusters) as subsets of measured data $D_k \subset D$. For each $k = 1...K$ define the type of subset T_k , where T_k can be 1-D (for linear objects) or 2-D (for flat surface objects).
 - FIND optimal vector of parameter values P'' that minimizes the goal function g using BOBYQA optimization.
 - COMPUTE georeferenced point cloud with adjusted parameters $C'' = f(D, P'')$.
-
-

If original test objects were not fully correct due to errors in initial parameters P' , then repeat the process again, with P'' value used as initial P' . The objective function is calculated for each test object separately and thereafter summed to determine the total objective function used in BOBYQA optimization.

The optimization process does not require additional reference data. However, for reliable calibration, it is important that at least some of the test objects are measured while pitch, roll, and yaw of vehicle are changing. This can be achieved by selecting test objects where the vehicle is performing turns. Otherwise, objective function does not have well-defined minimum for all calibration parameters.³³

3 Case Study

3.1 System Description

The MLS system is based on Velodyne VLP-16 LIDAR and SBG Systems Ellipse-D dual antenna GNSS/INS system. These are mounted on a purpose-built rigid frame that can be mounted on different platforms.

The Velodyne VLP-16 laser scanner has been used in mapping and surveying due to its small size, low weight, low power consumption, and relatively low cost. However, it was originally designed for use in the automotive industry as a collision avoidance sensor. Therefore, the accuracy of the sensor is not as high as with more sophisticated survey-grade scanners. It has been determined that the accuracy of distance measurement of the sensor is within the specification stated by the manufacturer and that the scanner does not require a long warm-up time.³⁴ VLP-16 has been mainly used in research and prototyping of autonomous vehicles and low-cost mobile scanners. For instance, commercially manufactured Leica Pegasus and Phoenix LIDAR MLS systems use VLP-16. In addition, the VLP-16 has been implemented in indoor mapping and autonomous vehicle designs.^{35,36}

The Ellipse-D is an entry level dual antenna GNSS/INS system manufactured by SBG Systems. It is based on microelectromechanical systems (MEMS) technology and is compact, light-weight, and relatively inexpensive. However, it is primarily designed for navigation purposes and not for survey-grade measurements. Hence, the accuracy of measuring attitude angles is about 0.1 deg, which can cause large errors on points measured further away from the scanner. However, the system does support GPS, GLONASS, and other GNSS satellites, as well as recording the raw GNSS and INS data for trajectory postprocessing. It can also be operated in RTK mode.

The navigation sensor center coincides with the INS origin. During postprocessing of the trajectory, the coordinates of the INS origin are calculated, after taking into account the lever arms from the INS center to the GNSS antenna phase center. Therefore, it is necessary to measure two sets of lever arms (from INS to GNSS antenna and from INS to LIDAR). Since the reported coordinates are of the INS center, in the georeferencing equation, the lever arms between the INS and LIDAR are used.

The sensors are mounted on a specially designed rigid frame, so the relative position with respect to each-other is fixed. The INS and LIDAR are mounted close to each other to improve the accuracy of determining the lever arms and boresight angles. The GNSS antennas, which are used for the dual-antenna heading measurement, are mounted to the sides to avoid obstruction of LIDAR measurements and for easier mounting on different platforms. The primary GNSS antenna is placed on the left-hand side, whereas the interantenna distance is 90 cm. The LIDAR sensor is pitched at a 45-deg angle.

The origins and the axis of the coordinate frames used in this study are as follows:

- Scanner's frame—the origin is located in the geometrical center of the VLP-16; the orthogonal axis of the horizontally aligned device is as follows: x —right (with respect to the y -axis), y —forward, and z —up (i.e., a right-handed system); and the scanner's frame is rotated with respect to the INS frame by the boresight angles (cf., Table 3) and the origin is offset by the lever arms.

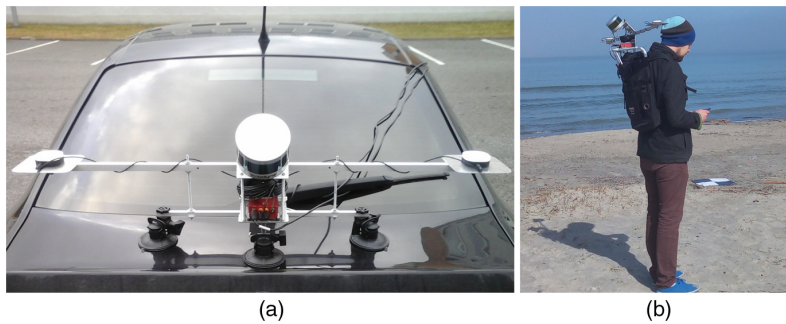


Fig. 1 MLS sensors on a purpose-built frame mounted on (a) car's rear side and (b) a backpack. The car-mounted LIDAR device is in the center, on top of the GNSS receiver, and an INS unit; dual GNSS antennae are located on the sides.

- INS (body) frame—the origin is the INS center and is marked on the Ellipse-D; the orthogonal axis of the horizontally aligned device is as follows: x —forward, y —right (with respect to the x -axis), z —down (right-handed system); the INS frame is aligned with the frame of the platform (e.g., car).
- Local frame—Earth-tangential reference system (Hofton et al.³⁷) where the origin is located at the INS center; x —north, y —east, z —down (right-handed system); the local frame is rotated with respect to the INS frame by roll, pitch, and heading values measured with the INS.
- Global frame—the coordinates are initially recorded in WGS84, which are transformed into some specific 2-D Cartesian coordinate system (e.g., Lambert-EST or UTM map projections, whereas the heights are reckoned from the ellipsoid or geoid) before using in the georeferencing equation.

The MLS system can be mounted on a suitable platform with adjustable suction cups or bolted to a horizontal surface. Thus, it can be placed on different types of cars, all-terrain-vehicles, backpacks, snowmobiles, trains, boats, etc. In Fig. 1, examples of the system are mounted to a car with suction cups (this setup was first tested on a road with lots of potholes with just the frame and no sensors) and bolted to a backpack frame. The technical characteristics of the used sensors are outlined in Appendix A.

3.2 Sensor Synchronization and Trajectory Postprocessing

The SBG Ellipse-D is a unit that combines GNSS and INS sensors. Therefore, these are already synchronized by the device itself. The VLP-16 LIDAR and the Ellipse-D data are synchronized by PPS signals generated with the GNSS device. The Ellipse-D output port and VLP-16 interface box are directly connected with a cable. No additional hardware or software synchronization module is necessary for such a setup.

Ellipse-D GNSS/INS device issues a PPS synchronization pulse in conjunction with a 1-Hz NMEA RMC sentence, which is issued sequentially. The PPS length is not critical, whereas the RMC sentence must be issued between 50 to 500 ms after the falling edge of the PPS pulse.

The synchronization was tested by introducing an incremental (positive and negative) time delay to the LIDAR data and evaluating the calculated point cloud. With the artificial time delays, the results deteriorated. Therefore, no constant time-delay was detected.

Raw data from all sensors (GNSS, INS, and LIDAR) are logged into a laptop computer onboard the measurement platform. The raw GNSS observations from the dual antennas (5-Hz data rate) are combined with Continuously Operating Reference Station GNSS base station data to determine a precise kinematic trajectory for the platform using the Waypoint/Novatel Inertial Explorer software package. In addition to the GNSS trajectory, 200-Hz raw inertial measurements are used in a tightly coupled Kalman filter with forward and backward processing. This results in an optimal estimate of platform position and attitude.

3.3 MLS System Calibration

The lever-arms are estimated using the engineering drawings of the components and the frame. It is assumed that the accuracy of direct mechanical measurement of the lever arms can be performed within a couple of millimeters accuracy since all the sensors are located close together on the same rigid metallic frame. The lever arm errors are generally small compared with others in the error budget, and these do not amplify with range or scan angle.

The boresight calibration is performed by the BOBYQA method, the principles of which were explained in Sec. 2.4. The method yielded good results in our study. The main advantages over some other calibration methods are the fast calculation time and that there is no need for additional reference data. This could be important in situations where the sensors must be mounted on a locally hired platform and the results are required in a limited time, e.g., carrying out MLS surveys overseas. BOBYQA is also a rigorous statistical optimization method, so the subjectivity by a human operator is eliminated. Case studies comparing this method to other existing calibration methods (e.g., least-squares method) and using data from different (e.g., survey-grade) MLS systems were outside the scope of this study and could be a subject of further research.

The data used in the optimization of boresight angles were acquired in a parking lot located next to a building facade and lined with street light poles. The system was mounted on a car, which drove parallel to the facade forward and backward and with slight (and intentional) swerving. Heading and pitch can be optimized while moving only in a straight line, provided that there are also vertical objects in the point cloud. However, the movement in both directions while turning is important for determining the roll value. On a straight road, roll misalignment does not influence the “sharpness” of the point cloud. The vehicle was moving at around 15 km/h. Therefore, the point cloud was dense due to significant overlap of subsequent measurements. At higher speeds, the overlap between consecutive point subsets reduces. This causes difficulties in optimizing the boresight pitch value.

Optimization was performed by manually selecting 20 clusters—12 on the road surface, 5 on the facade, and 3 around lamp poles (Fig. 2). The manual selection of clusters yielded a better calibration result than automatic selection. Therefore, the manual selections are used throughout this study. The radius for including points in the calculation of the total goal function g was defined as 2 m for the clusters on the road surface and lamp poles and 1 m for the clusters on the facade. The reasoning for such a limited radius on the facade is to exclude reflections from windows, which is a noisy area of the point cloud. A minimum of 10 clusters is required. According to our experiments, adding more clusters generally does not change the outcome significantly. The clusters on the road and lamp posts were given an equal weight of 1. The clusters on the building facade were given a weight of 0.75 since these were further away from the LIDAR sensor (note that a longer range decreases the accuracy of an MLS system).

The optimization was performed in four iterations. The initial boresight values were the estimated values based on the engineering drawings of the frame and the sensors (0 deg for heading and roll, -45 deg for pitch). In the subsequent iterations, the values that resulted from the previous iteration were used. The optimization process was finished after the g value for the user defined clusters did not improve. The results are shown in Table 2.

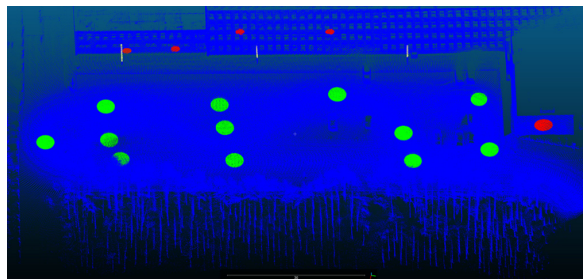


Fig. 2 User-defined clusters used in the optimization process (green, clusters on the road; red, clusters on the facade; and yellow, clusters around lamp poles).

Table 2 A sample of optimization of boresight angles.

Iteration	Heading (deg)	Pitch (deg)	Roll (deg)	<i>g</i>
1	1.3367	-45.1973	-0.5983	0.1071
2	1.3932	-45.2742	-0.6038	0.1011
3	1.4105	-45.2732	-0.5963	0.1010
4	1.4091	-45.2734	-0.5982	0.1010

Note: The bold values are the final boresight angles.

Overall, the relatively low accuracy of the used sensors yields a situation where the calculated point cloud is somewhat noisy. This challenges the rigorous calibration of the MLS system.

3.4 Theoretical (a priori) Accuracy

The theoretical accuracy of the prototype MLS system is calculated with the method developed by Glennie¹⁰ (reviewed also in Sec. 2.3). The estimated errors used for the instrument parameters were based on the manufacturer specifications (see Appendix A). However, the accuracy for the GNSS position in PPK estimated by the manufacturer seems overly optimistic. Therefore, the error is assigned to be 2 cm for X-, Y-coordinates and 3 cm for Z-coordinate, as described by Hauser.³⁸ The errors in the boresight angles and lever arms were approximated based on characteristics of the system. All the assigned error estimates are summarized in Table 3.

Inserting these estimates and likely parameters into Eq. (5) and solving it, the theoretical accuracy of the system was calculated. The prototype mapping-grade MLS system should ensure a 3-D theoretical accuracy of $\sim \pm 19.5$ cm at 10-m range to target, which is the usual range limit that contains most of the useful measurements. It is clear that the accuracy of an MLS system depends heavily on the range to the measured point. To illustrate this, the theoretical error with respect to range was plotted (Fig. 3). The system suffers a significant decrease in accuracy at longer ranges due to the inaccuracies in determining the attitude of the system.

Another common parameter in ALS and MLS campaigns that affects the accuracy is the scan angle, i.e., the angle between the laser beam and the vertical plane. Changing the scan angle does not affect the theoretical 3-D accuracy of the points measured with an MLS system. However, it does affect the components of vertical and horizontal accuracies. The dependency of the theoretical vertical and horizontal accuracies on the scan angle (at the constant 10-m range) is depicted in Fig. 4.

Table 3 Assigned error estimates of MLS system component parameters.

Parameter	<i>X</i>	<i>Y</i>	<i>Z</i>
Assigned error (m)	0.02	0.02	0.03
Parameter	ω	φ	<i>k</i>
Assigned error (deg)	0.1	0.1	0.2
Parameter	<i>d</i> ω	<i>d</i> φ	<i>d</i> <i>k</i>
Assigned error (deg)	0.05	0.05	0.05
Parameter	α	β	<i>r</i>
Assigned error	0.02 deg	0.02 deg	0.03 m
Parameter	<i>l</i> _{<i>x</i>}	<i>l</i> _{<i>y</i>}	<i>l</i> _{<i>z</i>}
Assigned error (m)	0.003	0.003	0.003

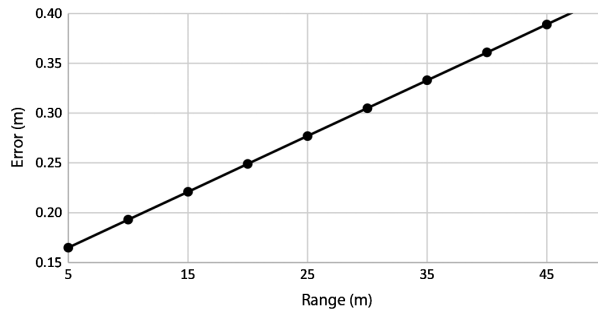


Fig. 3 The range dependency of the theoretically estimated 3-D accuracy of the prototype MLS system [cf., Eq. (5) and Table 3].

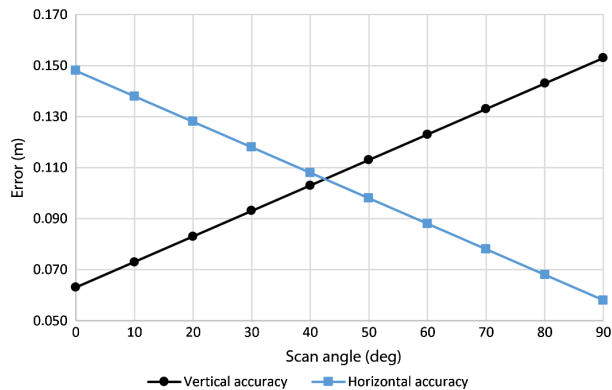


Fig. 4 The dependency of the theoretically estimated vertical and horizontal accuracy on the scan angle at a constant range of 10 m.

As can be seen, the vertical accuracy reduces further away from nadir. The effect of attitude errors near nadir mostly influences the planimetric/horizontal accuracy. Its effect on vertical accuracy at the near-zero scan angle is negligible and in that case the vertical accuracy is mostly dependent on the GNSS height and range.

It should be noted that, generally during MLS campaigns, at the near-zero scan angle the range to objects is shorter (e.g., road surface near nadir) than at the near-perpendicular scan angle (building facades, trees, lamp poles, etc.). Therefore, there is a correlation between the larger scan angle and smaller theoretical accuracy, but this is due to the longer range at higher scan angles. Further field tests were conducted to verify the theoretical estimates.

3.5 Field Tests

To assess the accuracy of the in-house MLS system in practice and to evaluate its suitability for field operations, a series of tests were conducted in both a car and backpack configuration. High-resolution and high-accuracy terrestrial and survey-grade MLS data were used for verifying the prototype MLS data accuracy.

Several distinguishable study areas were selected: a newly built concrete road, a parking lot, an underpass below a bridge, a tunnel, and an eroding beach area. The majority of these were measured with the car-mounted sensors. The MLS system is used in backpack configuration to survey eroding sandy beach areas that are inaccessible by car. Such a survey facilitates quantifying the beach erosion faster than with static TLS^{39,40} or with better accuracy estimates than that of airborne laser scanning.³⁹ The required accuracy for surveying beach erosion is less demanding compared with the requested surveying accuracy of engineering structures.

When on a car platform, all of the 16 channel lasers were used. When in backpack mode, only one laser was used, essentially turning the device into a laser profiler. The reasoning was that when moving at walking pace, the density of the data is much higher. Also, since the INS struggles to handle the walking induced jerky movements, the data are noisier. Therefore, such a reduction of the amount of measured points facilitates the data management and processing.

The speed during car-mounted measurements was generally about 40 to 50 km/h, resulting in an average point density of about 650 to 800 pts/m². The car mounted scanner was elevated from the ground 1.2 m and on a backpack 1.7 m; see Fig. 1. The laser spot diameter on the closest ground point was about 2.2 and 2.5 cm, respectively. The characteristics of each test area are summarized in Table 4.

The data georeferencing was performed as explained in Sec. 2.2. The software package developed by the research team uses the mathematical model for the VLP-16 scanner [Eq. (1)] and the LIDAR georeferencing equation [Eq. (2)]. Some examples of the generated point clouds are depicted in Fig. 5.

TLS and survey-grade MLS data were used to evaluate the accuracy of the prototype MLS system. For the TLS data acquisition, a Leica ScanStation C10 was used. It is a time-of-flight scanner yielding a 6-mm accuracy, i.e., an order of magnitude more accurate than the tested MLS prototype data. The average spatial resolution of the TLS-acquired point clouds was ~2500 points/m² (2 × 2 cm). The independent georeferencing of the TLS data to the common datum with the MLS data was conducted based on reference points coordinated with survey-grade GNSS measurements. The scanning was performed from several scan positions to cover the study areas entirely. Measurement noise, vegetation, traffic, and other objects were removed from the MLS point cloud with a combination of manual deletions and ground filtering algorithms.⁴¹ TLS data were used in the “road,” “parking lot,” “underpass,” and “beach” study areas. In the “beach” area, a 400-m² stretch of the beach was used.

Additionally, survey-grade Riegl VMZ mobile laser mapping system equipped with a Riegl VZ-400 laser scanner was used to evaluate the accuracy in the “tunnel” study area (conducting TLS in the tunnel would have required closing it for traffic). According to technical specifications, Riegl VMZ/VZ-400 has a nominal accuracy of 5 mm. The point density was ~3000 points/m². As the scanner was “down-face,” the comparisons are based on the road surface only. The accuracy of the survey-grade MLS data was verified by comparing it with TLS results at the “road” study area. The two datasets agreed within a couple of centimeters [root-mean-square error (RMSE) 1.5 cm]. This indicates that the survey-grade MLS data is suitably accurate for use as a reference for verifying the prototype mapping-grade MLS data.

Table 4 Description of the study areas.

Study area	Platform	Area size (m ²)	Collection speed (km/h)	Distance from the GNSS base (km)	No. of points	Point density (pts/m ²)	Description
Road	Car	12,000	40	3.5	9,837,402	800	New concrete road (a 600-m long stretch) with clear road markings, lamp poles, and traffic signs
Parking lot	Car	3600	15	1	7,291,069	2000	Has a parallel building facade and lamp poles, was used during calibration run
Underpass	Car	2000	50	4.5	1,298,500	650	Sloped underpass below a bridge with poor GNSS reception
Tunnel	Car	6000	50	7	4,791,302	750	Two parallel tunnels (sloped and curved, 300 m). No GNSS reception
Beach	Backpack	15,000	5	10	5,625,817	375	Eroding sandy beach with some vegetation

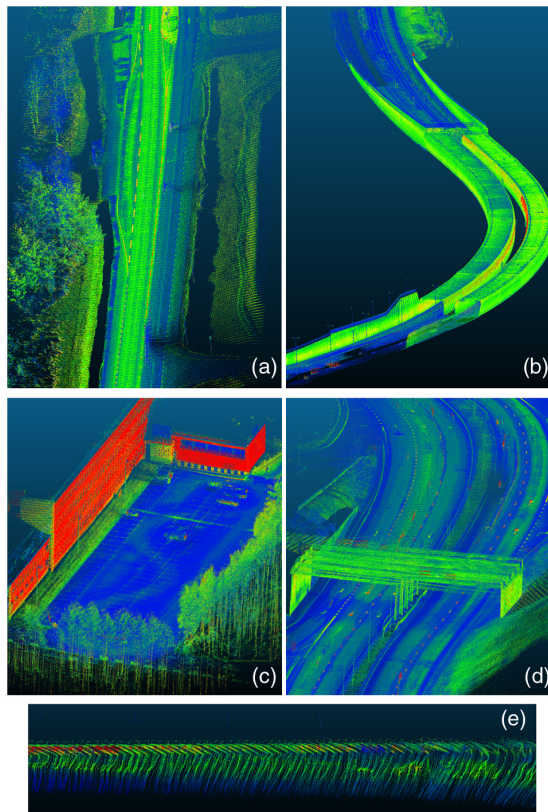


Fig. 5 Examples of MLS point clouds at study areas: (a) “road,” (b) “tunnel,” (c) “parking lot,” (d) “underpass,” and (e) “beach.”

4 Results and Accuracy Assessment

The prototype mapping-grade MLS data were compared against the terrestrial and survey-grade MLS data. The 3-D comparisons between point clouds are shown in Fig. 6. The discrepancy is calculated as a 3-D distance by measuring the shortest distance from a measured MLS point to the interpolated surface of the reference point cloud. The statistics of the 3-D comparisons are presented in Table 5.

The average RMSE value was 9 cm (note that the averaging included all the study areas). If the 3-D differences are absolute values, then the minimum 3-D error is 0. The maximum value can be very large when the comparison is made in an area where there is a gap in either of the point clouds. Therefore, the min and max values of the 3-D distance are not presented in Table 5.

However, simple 3-D differences are affected by the different densities and noise levels of point clouds, as well as from the fact that instable points (e.g., vegetation) are taken into consideration. Also, 3-D differences do not give an overview of the vertical, horizontal, and relative accuracy components. Therefore, these components are evaluated separately in the next sections.

4.1 Vertical Accuracy Assessment

To evaluate the vertical accuracy of the prototype MLS system data, triangulated irregular network (TIN) models were calculated based on the point clouds of only the road surface (the bare earth for the “beach” study area). The surface points were automatically extracted with a multi-scale curvature classification ground filtering algorithm.⁴² These surface models were compared with the reference TIN models along the Z-axis. The models were from (nearly) horizontal surfaces. Therefore, even if there is a horizontal shift between surveyed and reference data,

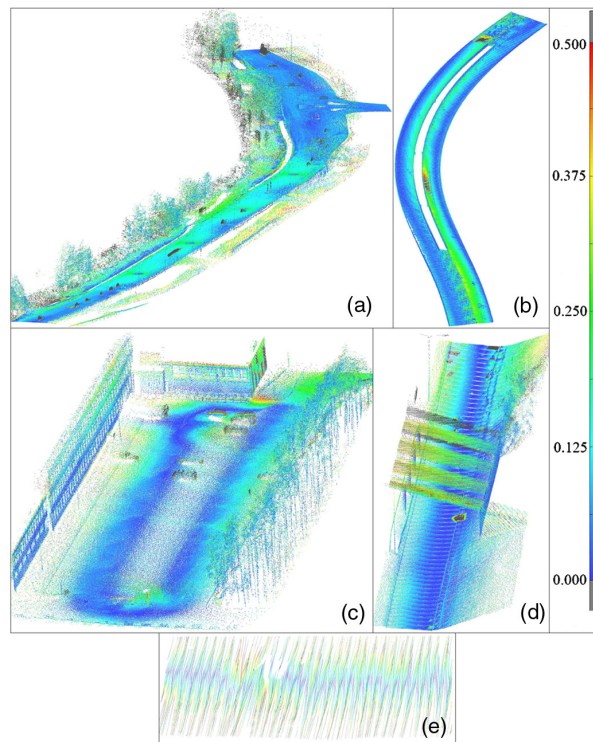


Fig. 6 3-D comparison between MLS point clouds and reference data at study areas: (a) “road,” (b) “tunnel,” (c) “parking lot,” (d) “underpass,” and (e) “beach.”

Table 5 3-D comparison between MLS point clouds and reference data (m).

Study area	Mean	RMSE
Road	0.065	0.078
Parking lot	0.059	0.072
Underpass	0.041	0.062
Tunnel	0.070	0.089
Beach	0.121	0.145
Average	0.071	0.090

it has a small (almost negligible) effect on the vertical accuracy. Statistics of the comparisons for all sites are presented in Table 6.

The results in Table 6 indicate that the reference data and mapping-grade MLS data agree at ~6 to 9 cm vertically. The data gathered with the backpack platform shows slightly worse agreement, at ~13 cm. This is due to the unpredictable and jerky motion of the backpack platform during the walking of the operator. Such irregular motion makes it difficult to compute an accurate trajectory, as well as determine the accurate values for roll, pitch, and heading. The mean offsets between MLS and reference data are both positive and negative. This indicates that these offsets are not caused by systematic errors in determining the lever arms and boresight angles. A more likely cause is the inaccuracy of the vertical component of GNSS positioning along with other error sources (due to range, boresighting, etc.). At the calculation of the theoretical

Table 6 Vertical comparison (along the z-coordinate) between MLS point clouds and reference data (m).

Study area	^a Min	^a Max	^a Mean	RMSE
Road	-0.350	0.412	0.029	0.072
Parking lot	-0.253	0.384	0.013	0.061
Underpass	-0.202	0.264	-0.015	0.064
Tunnel	-0.347	0.269	-0.034	0.089
Beach	-0.376	0.520	0.041	0.128
Average	-0.306	0.370	0.007	0.083

^aMLS minus reference.**Table 7** Vertical comparison (along the z-coordinate) between MLS point clouds and reference data with respect to the range and the scan angle at the “parking lot” study area (m).

	^a Min	^a Max	^a Mean	RMSE
Range (m)				
0 to 5	-0.023	0.035	0.010	0.029
5 to 10	-0.095	0.131	-0.019	0.051
10 to 20	-0.147	0.219	0.020	0.068
>20	-0.253	0.384	0.023	0.089
Scan angle (deg)				
0 to 10	-0.023	0.035	0.010	0.029
10 to 25	-0.082	0.117	-0.021	0.047
25 to 45	-0.126	0.219	0.016	0.072
>45	-0.253	0.384	0.023	0.089
Overall	-0.253	0.384	0.013	0.061

^aMLS minus reference.

accuracy, it is assumed that the GNSS reception is unobstructed, whereas in practical tests the GNSS reception was disturbed or even lost (e.g., in the tunnel).

A vertical accuracy assessment with respect to range and scan angle is performed on the “parking lot” study area (Table 7). As is predicted by the theoretical accuracy analysis, the accuracy is better at closer range and at smaller scan angles. Therefore, as expected, the most accurate elevation data are achieved on the close range ground/road.

4.2 Horizontal Accuracy Assessment

The horizontal accuracy of the MLS system was assessed by comparing the 2-D coordinates of clearly identifiable features in the MLS and reference point clouds. These were the edges of road markings measured very close to the LIDAR sensor. The edges of road markings that were measured further from the nadir of the scanner were not clearly identifiable. To evaluate horizontal accuracy further from nadir, vertical surfaces on the facade and the wall of the underpass were used. Small sections of point clouds (~1 m × 1 m) of the same vertical surface in both MLS and reference data were used to calculate a least squares best-fit plane for each point cloud independently. The plane equation is expressed as

$$ax + by + cz + d = 0, \quad (8)$$

where a , b , and c are the normal vector of the plane, and d is the shift of the plane from the origin.

The coefficients were determined from a system of linear equations by solving it in the least squares sense.

The distance between the planes was measured from the center of the MLS data plane along the normal vector. If tilted planes would have been used, then a horizontal vector would have been used instead of a normal vector (using horizontal planes for evaluating horizontal accuracy is impossible). Overall, 30 road markings and 10 best fit planes were used. Horizontal accuracy was not evaluated on the beach area since there were no clearly identifiable features or vertical surfaces.

The results in Table 8 show that the horizontal accuracy of the MLS data is ~ 15 cm. Generally, the horizontal error was slightly smaller near nadir. This is to be expected because points further away suffer more from the errors in attitude determination by the INS. Overall, the horizontal accuracy is clearly worse than vertical accuracy but it is still within the requirements for mapping-grade MLS systems (20 cm).

The large mean error does not indicate a systematic shift because in this case the absolute value of the distance in the XY -plane between the MLS surface and reference data is used. However, in this study, the shifts were random. The relatively large horizontal error is due to the vertical planes used to evaluate the horizontal accuracy being located farther away

Table 8 Planar comparison between MLS point clouds and reference data (m).

Study area	Min	Max	Mean	RMSE
Road	0.021	0.345	0.143	0.152
Parking lot	0.015	0.274	0.125	0.147
Underpass	0.019	0.257	0.153	0.136
Tunnel	0.052	0.372	0.162	0.185
Average	0.027	0.312	0.146	0.155

Table 9 Planar comparison between MLS point clouds and reference data depending on the range and the scan angle at the “parking lot” study area (m).

	Min	Max	Mean	RMSE
Range (m)				
0 to 5	0.015	0.127	0.075	0.079
5 to 10	0.035	0.178	0.124	0.136
10 to 20	0.114	0.236	0.163	0.159
>20	0.103	0.274	0.193	0.201
Scan angle (deg)				
0 to 10	0.015	0.127	0.073	0.075
10 to 25	0.035	0.162	0.122	0.124
25 to 45	0.125	0.236	0.192	0.181
>45	0.103	0.274	0.193	0.201
Overall	0.015	0.274	0.125	0.147

(generally 10+ m) from the sensor. The MLS system’s accuracy being range dependent explains the reduced horizontal accuracy achieved with this methodology.

A horizontal accuracy assessment with respect to range and scan angle is performed on the “parking lot” study area (Table 9). Similarly, with the vertical accuracy, and as predicted by the theoretical accuracy analysis, the horizontal accuracy is better at a closer range. However, even though the theoretical horizontal accuracy is better at near perpendicular scan angles, generally, objects at 90 deg are much further away (building facade, tunnel wall, etc; within 5 to 20 m) than objects at a near zero scan angle (near nadir road surface; <5 m away). This explains variations in the practical horizontal accuracies and noncorrelation with the scan angle—because in the MLS surveys the range at a scan angle of 90 deg is generally more distant than at 0 deg.

4.3 Relative Accuracy Assessment

Previous evaluations were performed to assess the absolute accuracy of the system. However, in many occasions, the absolute accuracy of the point cloud is not as crucial as the relative accuracy. To test the ability of the MLS point cloud to provide accurate relative measurements, several relevant dimensions were measured within the MLS data and the reference data. These measurements included road width, length of road markings, curb heights, facade dimensions, and height of lamp poles. Measurements were taken repeatedly and then averaged. Relative accuracy was not evaluated on the sandy beach area because there were no clearly identifiable

Table 10 Relative comparison between MLS point clouds and reference data (m).

Study area	Absolute min	Absolute max	Mean	RMSE
Road	0.015	0.040	0.030	0.028
Parking lot	0.010	0.045	0.030	0.031
Underpass	0.020	0.050	0.035	0.034
Tunnel	0.010	0.030	0.020	0.019
Average	0.014	0.041	0.029	0.028

Table 11 Relative comparison between MLS point clouds and reference data depending on the range and the scan angle at the “parking lot” study area (m).

	Min	Max	Mean	RMSE
Range (m)				
0 to 5	0.010	0.032	0.020	0.021
5 to 10	0.015	0.037	0.025	0.027
10 to 20	0.021	0.041	0.030	0.031
>20	0.038	0.045	0.041	0.042
Scan angle (deg)				
0 to 10	0.010	0.029	0.018	0.019
10 to 25	0.015	0.035	0.027	0.025
25 to 45	0.023	0.043	0.030	0.034
>45	0.038	0.045	0.041	0.042
Overall	0.010	0.045	0.030	0.031

features. The measurements of the MLS and reference data generally agreed within 3 cm, and the MLS measurements were nominally within 5% of the actual values (Table 10).

A relative accuracy assessment with respect to range and scan angle is performed on the “parking lot” study area (Table 11). As expected, the relative accuracy is better at a closer range. In theory, the scan angle should not affect relative accuracy. However, as mentioned in the previous section, in practice, objects at a scan angle of 90 deg are generally further away than objects near nadir. Therefore, the experimental relative accuracy reduces with a larger scan angle.

However, it can be concluded that the relative accuracy of the point cloud is significantly better than the absolute horizontal accuracy. This confirms that the MLS data have high relative accuracy in the short term. Taking measurements on the road surface, building facades, etc. can be performed with an accuracy of a couple of centimeters.

5 Discussion

The practical accuracy assessment yielded better results than the *a priori* error estimates. This indicates that some of the adopted *a priori* error estimates (obtained from manufacturer’s specifications and presented in Table 3) might be too pessimistic. However, without dedicated studies (which would require more sophisticated equipment than that used in this study for reference) to evaluate the errors of the sensors, it is difficult to estimate which ones and by how much. If more reliable values were available (e.g., from individual calibration in laboratory conditions), then these could be inserted into the theoretical accuracy equation [Eq. (5)].

As can be seen from the results, the prototype MLS system’s performance in backpack mode is worse as compared with the car mounted solution. There are many possible contributing factors. In the backpack mode, the motion profile of the system is not smooth. There are periodic changes in the roll of the system (usually varying within ± 7 deg) due to the walking motion of the operator. Also, the pitch and heading can change anytime and in any direction. Therefore, these characteristics become unpredictable. There is no bias toward forward-motion compared with a car platform. This means that the INS must be accurate and responsive enough to measure accurate values real time because the smoothing and optimization of the trajectory with Kalman filter will not be as effective. Most likely, a technologically less advanced MEMS INS system is not accurate enough for this task. Also, if the LIDAR and INS data are even slightly out-of-sync, then the errors in the point cloud are much more prevalent, larger, and more noticeable than that of a more stable platform, i.e., a car. However, no systematic time-delay between the sensors was detected.

In this study, the point cloud was intentionally georeferenced without independently coordinated reference points to test the MLS system accuracy before further alignment. With multiple passes in the same location (e.g., road intersection or forward and backward passes on a road), there will be both horizontal and vertical misalignments between different point clouds, which in some cases can be quite large (Fig. 7). These misalignment errors are mostly due to inaccuracies in GNSS positioning, and the extent of these can vary quite significantly depending on the

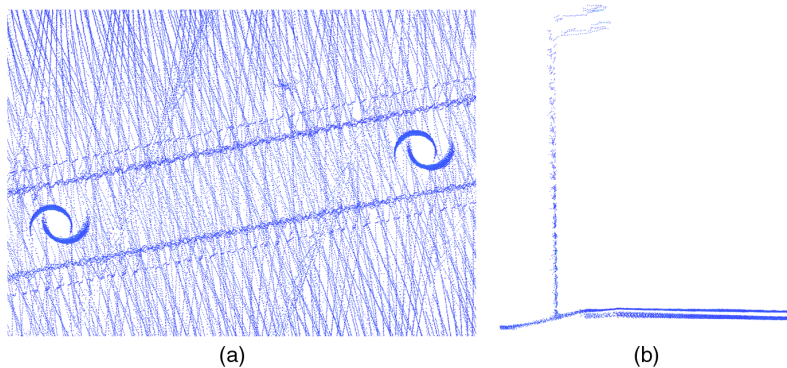


Fig. 7 Examples of MLS point clouds (a) horizontal (~10-cm error) and (b) vertical (~15-cm error) misalignments between different passes. Note the misalignment of the lamp poles (half circles) from different passes.

accuracy of the GNSS sensors and GNSS signal reception. In some cases, the discrepancies can reach up to several decimeters. Therefore, further alignment (e.g., using common control points) between point clouds is required. To improve absolute accuracy, some of these points should be independently coordinated with survey-grade geodetic measurements. This alignment can be achieved with several commercial airborne or MLS processing software.^{43,44} However, it was not implemented in this paper because it was not the intention of this study.

6 Conclusions

This paper presented an analysis of a relatively compact and low-cost mapping-grade MLS system that is mountable on a car and a backpack. The principles of direct georeferencing, calibration of the boresight angles, and theoretical accuracy of the MLS system were discussed in detail.

The results and accuracy assessment of the MLS system based on several study areas, as well as depending on the range and scan angle, were presented. Considering the achieved vertical accuracy of 8 cm, horizontal accuracy of 15 cm, and relative accuracy of 3 cm, the MLS system satisfies the objective of mapping-grade accuracy (RMSE better than 20 cm). The MLS system can be easily deployed on different platforms, as was demonstrated using it on car and backpack platforms. Mapping-grade accuracy is achievable without frequent control points, which allows faster data collection and processing.

The analysis demonstrates that the mapping-grade MLS system can be used to acquire point cloud data, including terrain, road, and building locations. With proper measurement techniques, the system can provide data that can be used effectively to model objects, such as building walls, flat surfaces from bridges and other structures, poles, tree trunks, curbs, etc. Basic engineering, structural, and architectural measurements can also be made with the MLS data, e.g., measuring road width, curb heights, dimensions of a building, etc. This makes the MLS system usable in situations that do not require survey-grade accuracy.

Further research on this topic would include a case study comparing BOBYQA optimization method with other existing calibration methods (e.g., least-squares method), improving the operation of the MLS system in backpack mode, and implementing a process for aligning point clouds using control points.

Appendix A

The technical characteristics of the sensors used to construct the prototype MLS system are presented in Table 12.

Table 12 Specifications of Velodyne VLP-16 and SBG Systems Ellipse-D

Velodyne VLP-16 LIDAR	
Sensor	Time of flight distance measurement
	16 channels
	Range up to 100 m
	Accuracy: ± 3 cm
	Vertical field of view: 30 deg
	Horizontal field of view: 360 deg
	Dual returns
	Vertical angular resolution: 2 deg
	Horizontal angular resolution: 0.1 deg to 0.4 deg
	Rotation rate: 5 to 20 Hz

Table 12 (Continued).

Velodyne VLP-16 LIDAR	
Laser	Class 1—eye safe Wavelength—903 nm
Mechanical	Weight: 830 g (without cabling) Dimensions: 103 <i>mm</i> diameter × 72 <i>mm</i> height
Electrical	Power consumption: 8 W Operating voltage: 9 to 32 V DC
Output	Up to 300,000 points/s 100 Mbps Ethernet connection UDP packets containing <ul style="list-style-type: none"> - Distances - Calibrated reflectivities - Rotation angles - Synchronized time stamps (μs resolution) \$GPRMC NMEA sentence from GPS receiver
SBG Systems Ellipse-D GNSS/INS system	
Navigation	Position accuracy (single point): 1.2 m Position accuracy (RTK): 0.02 m Position accuracy (PPK ^a): 0.01 m Roll and Pitch accuracy: 0.1 deg (0.05 deg with PPK) Heading accuracy: 0.2 deg (with dual GNSS) Velocity accuracy: 0.03 m/s
GNSS	Survey-grade GNSS receiver Antennas: 2 × ANT-ACM-G5ANT-1A196MNS-1 GPS L1, L2, L2C GLONASS L1, L2 GALILEO E1, E5 BeiDou B1, B2 Update rate: 5 Hz
Mechanical	Weight: 180 g (without cabling and GNSS antennas) Dimensions: 87 × 67 × 31.5 mm
Electrical	Power consumption: <2500 mW Operating voltage: 9 to 36 V DC
Output	Interface: RS-232, RS-422, USB Baudrate: up to 921,600 bps Protocol: Binary eCom protocol, NMEA, ASCII, TSS

^aPPK, postprocessing kinematic and postprocessing with Inertial Explorer.

Acknowledgments

This research has been supported by European Union Regional Development Fund as a research cooperation between Tallinn University of Technology and Reach-U AS, which was conducted within the frames of “Testing spatial data acquisition devices/sensors mounted in a mobile platform and corresponding data analysis” (Lep16116) and “Testing components of mobile mapping system and elaboration corresponding data processing methodology” (Lep17016). The used Velodyne VLP-16 LIDAR, SBG Systems Ellipse-D, and Leica ScanStation C10 were purchased within frames of Estonian Scientific Equipment Purchase Support Program (Project No. SF0140007s11AP14) and Estonian Research Infrastructures Roadmap Object Estonian Environmental Observatory (Project No. AR12019). The survey-grade MLS reference data used in this study was provided by REIB OÜ. Mr. A. Gruno of Estonian Land Board is thanked for the assistance in trajectory postprocessing. The two anonymous reviewers are thanked for their valuable and insightful comments.

References

1. A. Jaakkola et al., “A low-cost multi-sensoral mobile mapping system and its feasibility for tree measurements,” *ISPRS J. Photogramm. Remote Sens.* **65**(6), 514–522 (2010).
2. L. Wallace et al., “Development of a UAV-LiDAR system with application to forest inventory,” *Remote Sens.* **4**(12), 1519–1543 (2012).
3. B. Brooks et al., “Mobile laser scanning applied to the earth sciences,” *EOS Trans. Am. Geophys. Union* **94**(36), 313–315 (2013).
4. C. Glennie et al., “Compact multipurpose mobile laser scanning system—initial tests and results,” *Remote Sens.* **5**(2), 521–538 (2013).
5. K. Julge et al., “Initial tests and accuracy assessment of a compact mobile laser scanning system,” in *ISPRS—Int. Archives of the Photogrammetry, Remote Sensing and Spatial Information Sciences*, Vol. XLI-B1, pp. 633–638 (2016).
6. G. Jozkow, C. Toth, and D. Grejner-Brzezinska, “UAS topographic mapping with velodyne LiDAR sensor,” in *ISPRS Annals of Photogrammetry, Remote Sensing and Spatial Information Sciences*, Vol. III-1, pp. 201–208 (2016).
7. N. El-Sheimy and K. P. Schwarz, “Navigating urban areas by VISAT-A mobile mapping system integrating GPS/INS/digital cameras for GIS applications,” *Navigation* **45**(4), 275–285 (1998).
8. M. Yadav et al., “Developing basic design and mathematical framework for a mobile mapping system—a case study using available sensors,” *J. Indian Soc. Remote Sens.* **42**(2), 301–310 (2014).
9. S. Madeira, J. A. Gonçalves, and L. Bastos, “Sensor integration in a low cost land mobile mapping system,” *Sensors* **12**(12), 2935–2953 (2012).
10. C. Glennie, “Rigorous 3D error analysis of kinematic scanning LIDAR systems,” *J. Appl. Geod.* **1**(3), 147–157 (2007).
11. C. Glennie, “Kinematic terrestrial light-detection and ranging system for scanning,” *Transp. Res. Rec.: J. Transp. Res. Board* **2105**, 135–141 (2009).
12. D. Barber, J. Mills, and S. Smith-Voysey, “Geometric validation of a ground-based mobile laser scanning system,” *ISPRS J. Photogramm. Remote Sens.* **63**(1), 128–141 (2008).
13. N. Haala et al., “Mobile LIDAR mapping for 3D point cloud collection in urban areas—a performance test,” in *Int. Archives of the Photogrammetry, Remote Sensing and Spatial Information Sciences*, Vol. 37, pp. 1119–1124 (2008).
14. I. Puente et al., “Accuracy verification of the lynx mobile mapper system,” *Opt. Laser Technol.* **45**, 578–586 (2013).
15. D. Hauser, C. Glennie, and B. Brooks, “Calibration and accuracy analysis of a low-cost mapping-grade mobile laser scanning system,” *J. Surv. Eng.* **142**(4), 04016011 (2016).
16. M. J. Olsen et al., *Guidelines for the Use of Mobile LIDAR in Transportation Applications*, Transportation Research Board, Washington, DC (2013).
17. W. Carter et al., “Airborne laser swath mapping shines new light on Earth’s topography,” *EOS Trans. Am. Geophys. Union* **82**(46), 549–555 (2001).

18. W. E. Carter, R. L. Shrestha, and K. C. Slatton, "Geodetic laser scanning," *Phys. Today* **60**(12), 41–47 (2007).
19. M. Lato et al., "Engineering monitoring of rockfall hazards along transportation corridors: using mobile terrestrial LiDAR," *Natl. Hazards Earth Syst. Sci.* **9**(3), 935–946 (2009).
20. M. Vaaja et al., "Mapping topography changes and elevation accuracies using a mobile laser scanner," *Remote Sens.* **3**(12), 587–600 (2011).
21. X. Liang et al., "The use of a mobile laser scanning system for mapping large forest plots," *IEEE Geosci. Remote Sens. Lett.* **11**(9), 1504–1508 (2014).
22. R. Zlot et al., "Efficiently capturing large, complex cultural heritage sites with a handheld mobile 3D laser mapping system," *J. Cult. Heritage* **15**(6), 670–678 (2014).
23. A. Jochem, B. Höfle, and M. Rutzinger, "Extraction of vertical walls from mobile laser scanning data for solar potential assessment," *Remote Sens.* **3**(12), 650–667 (2011).
24. R. E. Kalman, "A new approach to linear filtering and prediction problems," *J. Basic Eng.* **82**(1), 35 (1960).
25. A. Kukko, "Mobile laser scanning–system development, performance and applications," PhD Thesis, Finnish Geodetic Institute (2013).
26. M. Leslar, B. Hu, and J. Wang, "Error analysis of a mobile terrestrial LiDAR system," *Geomatica* **68**(3), 183–194 (2014).
27. T. Goulden and C. Hopkinson, "The forward propagation of integrated system component errors within airborne lidar data," *Photogramm. Eng. Remote Sens.* **76**(5), 589–601 (2010).
28. P. Rieger et al., "Boresight alignment method for mobile laser scanning systems," *J. Appl. Geod.* **4**(1), 13–21 (2010).
29. M. Leslar, J. Wang, and B. Hu, "Boresight and lever arm calibration of a mobile terrestrial LiDAR system," *Geomatica* **70**(2), 97–112 (2016).
30. J. Skaloud and D. Lichti, "Rigorous approach to bore-sight self-calibration in airborne laser scanning," *ISPRS J. Photogramm. Remote Sens.* **61**(1), 47–59 (2006).
31. M. Powell, "The BOBYQA algorithm for bound constrained optimization without derivatives," Cambridge NA Report NA2009/06, University of Cambridge, Cambridge (2009).
32. K. Pearson, "LIII. On lines and planes of closest fit to systems of points in space," *Philos. Mag. Ser. 6* **2**(11), 559–572 (1901).
33. M. Plasencia et al., "Geothermal model calibration using a global minimization algorithm based on finding saddle points and minima of the objective function," *Comput. Geosci.* **65**, 110–117 (2014).
34. C. L. Glennie, A. Kusari, and A. Facchin, "Calibration and stability analysis of the Vlp-16 laser scanner," in *ISPRS–Int. Archives of the Photogrammetry, Remote Sensing and Spatial Information Sciences*, Vol. XL-3/W4, pp. 55–60 (2016).
35. R. Bogue, "Sensors for robotic perception. Part two: positional and environmental awareness," *Ind. Rob.: Int. J.* **42**(6), 502–507 (2015).
36. C. Toth and G. Józków, "Remote sensing platforms and sensors: a survey," *ISPRS J. Photogramm. Remote Sens.* **115**, 22–36 (2016).
37. M. A. Hofton et al., "An airborne scanning laser altimetry survey of Long Valley, California," *Int. J. Remote Sens.* **21**(12), 2413–2437 (2000).
38. D. L. Hauser, "Three-dimensional accuracy analysis of a mapping-grade mobile laser scanning system" Msc Thesis, University of Houston (2013).
39. K. Julge et al., "Combining airborne and terrestrial laser scanning to monitor coastal processes," in *IEEE/OES Baltic Int. Symp. (BALTIC)* (2014).
40. M. Eelsalu, T. Soomere, and K. Julge, "Quantification of changes in the beach volume by the application of an inverse of the Bruun Rule and laser scanning technology," *Proc. Est. Acad. Sci.* **64**(3), 240 (2015).
41. K. Julge, A. Ellmann, and A. Gruno, "Performance analysis of freeware filtering algorithms for determining ground surface from airborne laser scanning data," *J. Appl. Remote Sens.* **8**(1), 083573 (2014).
42. J. S. Evans and A. T. Hudak, "A multiscale curvature algorithm for classifying discrete return LiDAR in forested environments," *IEEE Trans. Geosci. Remote Sens.* **45**(4), 1029–1038 (2007).

43. E. Paska and J. A. Ray, "Influence of various parameters on the accuracy of LiDAR generated products for highway design applications," in *Proc. ASPRS 2007 Annual Conf.* (2007).
44. C. Hopkinson et al., *IP3 LiDAR Collaborative Research Data Report*, Applied Geomatics Research Group, Centre of Geographic Sciences, Nova Scotia (2008).

Kalev Julge received his MSc degree in geodesy from Tallinn University of Technology (TUT), Estonia, in 2013. Currently, he is pursuing his PhD and works as a research scientist at TUT. His main research interest is remote sensing by methods of airborne, mobile, and terrestrial laser scanning.

Toivo Vajakas received his MSc degree in applied math from the University of Tartu (UT), Estonia, in 1983. Currently, he is pursuing his PhD and works as a research scientist at Reach-U Ltd. His main research interest is mobile positioning methods, but he also works in the area of laser scanning and mobile mapping.

Artu Ellmann received his MSc degree in geodesy from Moscow State University of Geodesy and Cartography (formerly MIIGAiK) in 1993 and his PhD from the Royal Institute of Technology (KTH) in Stockholm in 2004. He is currently a professor in geodesy in the Department of Road Engineering, Faculty of Civil Engineering, TUT. He has been a national correspondent to the International Association of Geodesy (IAG) since 2006. His research interests include remote sensing, physical geodesy (gravity field and geoid modeling, in particular), and engineering surveying.

PUBLICATION II

© 2016 Authors. This work is distributed under the Creative Commons Attribution 3.0 License.

Julge, K., Ellmann, A., Vajakas, T., Kolka, R. (2016). Initial tests and accuracy assessment of a compact mobile laser scanning system. In: *The International Archives of the Photogrammetry, Remote Sensing and Spatial Information Sciences* (633–638). XXIII ISPRS Congress, 12–19 July 2016, Prague, Czech Republic: Copernicus publications. (ISPRS Commission I, ICWG I/Va).10.5194/isprsarchives-XLI-B1-633-2016.

INITIAL TESTS AND ACCURACY ASSESSMENT OF A COMPACT MOBILE LASER SCANNING SYSTEM

K. Julge^{a,*}, A. Ellmann^a, T. Vajakas^{b,c}, R. Kolka^b

^a Tallinn University of Technology, Faculty of Civil Engineering, Department of Road Engineering, Chair of Geodesy, Ehitajate tee 5, Tallinn, Estonia, 19086 - (kalev.julge, artu.ellmann)@ttu.ee

^b Reach-U AS, Riia 24, Tartu, Estonia - (toivo.vajakas, riivo.kolka)@reach-u.com

^c University of Tartu, Institute of Computer Science, Liivi 2, Tartu, Estonia - tvajakas@ut.ee

Commission I, ICWG I/Va

KEY WORDS: Mobile Laser Scanning, LIDAR, Point Cloud, Accuracy Assessment

ABSTRACT:

Mobile laser scanning (MLS) is a faster and cost-effective alternative to static laser scanning, even though there is a slight trade-off in accuracy. This contribution describes a compact mobile laser scanning system mounted on a vehicle. The technical parameters of the used system components, i.e. a small LIDAR sensor Velodyne VLP-16 and a dual antenna GNSS/INS system Advanced Navigation Spatial Dual, are reviewed, along with the integration of these components for spatial data acquisition. Calculation principles of 3D coordinates from the real-time data of all the involved sensors are discussed. The field tests were carried out in a controlled environment of a parking lot and at different velocities. Experiments were carried out to test the ability of the GNSS/INS system to cope with difficult conditions, e.g. sudden movements due to cornering or swerving. The accuracy of the resulting MLS point cloud is evaluated with respect to high-accuracy static terrestrial laser scanning data. Problems regarding combining LIDAR, GNSS and INS sensors are outlined, as well as the initial accuracy assessments. Initial tests revealed errors related to insufficient quality of inertial data and a need for the trajectory post-processing calculations. Although this study was carried out while the system was mounted on a car, there is potential for operating the system on an unmanned aerial vehicle, all-terrain vehicle or in a backpack mode due to its relatively compact size.

1. INTRODUCTION

MLS systems are used to gather 3D spatial data (i.e. point cloud) on the move. The main components of MLS systems are a LIDAR scanner, a GNSS (Global Navigation Satellite System) receiver and an INS (Inertial Navigation System), which are synchronized and placed on a moving platform. Odometer data and dual GNSS antennas for determining the heading are often implemented to improve the quality of the result. The scientific research of MLS, of which there is a considerable amount, has mostly dealt with calibrating and data processing, mainly the automatic extraction of features from a point cloud.

The point cloud calculation and direct georeferencing of MLS data share the same principles as Airborne Laser Scanning (ALS), see e.g. Wehr and Lohr (1999). In feature (such as pavements, technical utilities, terrain relief, facades) extraction most of the same principles apply as with terrestrial laser scanning (TLS). Such examples include extraction of building features by Pu et al. (2006), extraction of a tunnel liner by Yoon et al. (2009) and reconstructing tree crowns by Pyysalo et al. (2002). For bare-earth extraction algorithms and their performance analysis see Sithole and Vosselman (2004), Julge et al. (2014a) and references therein. Recognizing and extracting features from MLS point clouds has been discussed by e.g. Pu et al. (2011), Yang et al. (2013) and Guan et al. (2014).

Some examples of previous research of MLS include also a review of mobile mapping and surveying technologies (Puenté et al., 2013), geometric validation of ground-based MLS systems (Barber et al., 2008), creating and testing multiplatform MLS systems (Kukko et al., 2012), evaluating MLS systems for tree measurements (Jaakkola et al., 2010) and environment mapping (Jaakkola, 2015).

MLS has developed rapidly in the recent years and there are several commercial products available. Companies that provide commercial MLS systems include Riegl, Trimble, 3D Laser Mapping, TopScan, Dynascan, Optech etc. However, complete commercial MLS systems are usually expensive. Purchasing the required sensors separately is more cost-effective but does require time-consuming work to integrate the systems and calculate the final point clouds. However, there is a possibility to adapt and fine-tune the system according to the specifics of the task at hand. Complete hardware and software solutions utilizing Velodyne scanners, either VLP-16 or larger HDL-32E model, include Routescene LidarPod, Topcon IP-S3, Phoenix Aerial Systems, Hypack, etc.

Accordingly, this paper describes an in-house assembled compact and relatively low-cost MLS system consisting of a Velodyne VLP-16 LIDAR and Advanced Navigation Spatial Dual GNSS/INS system, as well as related data processing and the accuracy assessment of the initial results. The MLS data are compared with high resolution and high accuracy (sub-cm) TLS reference data. The ultimate goal is to use MLS point clouds in

* Corresponding author

conjunction with photos from a 360° spherical camera Ladybug5 to provide a possibility for reliable measurements in the Street-U street view application. However, this is not yet implemented.

The outline of the paper is as follows. First the specifications of the used sensors and the basic principles of point cloud calculation are reviewed, after which the case study at hand is described including the methodology. Then the achieved results and initial accuracy assessment are presented. Lastly, a brief summary and a description of goals for further research concludes the paper.

2. SYSTEM DESCRIPTION

2.1 Sensors

The assembled MLS system is based on a Velodyne VLP-16 compact LIDAR sensor and a dual antenna GNSS/INS system Advanced Navigation Spatial Dual. The specifications of the used sensors are outlined in Table 1. The two systems are synchronized with one another by sending a pulse-per-second (PPS) signal in conjunction with a once-per-second NMEA \$GPRMC sentence from the GNSS/INS system to the LIDAR. The Spatial Dual system is connected to a data logging computer with RS-232 cables. The data packets of VLP-16 are output through an Ethernet port.

2.2 Point cloud calculation

The point cloud coordinates are calculated by combining distance and horizontal/vertical angle data from the LIDAR sensor and the position and inertial data from the GNSS/INS system.

The point cloud calculation method (specific to Velodyne scanners) is as follows. The data packets received through an Ethernet port are parsed for rotational angles, measured range to the object, calibrated reflectivities and time stamp. The VLP-16 reports spherical coordinates (R , ω , α). Therefore, a transformation is needed to convert to x , y , z coordinates (Fig. 1). The vertical/elevation angle (ω) is fixed and is determined by the Laser ID, which is indicated by the position of the return in the data packet. The horizontal angle/azimuth (α) is reported at the beginning of every other firing sequence, and the distance is reported in the two distance bytes. Points within one-meter distance are ignored. (VLP-16 user manual)

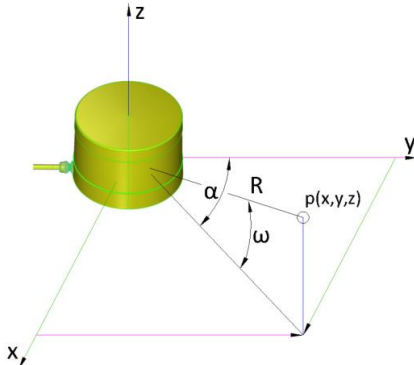


Figure 1. The interrelations between spherical polar coordinates of VLP-16 to x , y , z coordinates.

Velodyne VLP-16 LIDAR	
Sensor	Time of flight distance measurement 16 channels Range up to 100 m Accuracy: ± 3 cm Vertical field of view: 30° Horizontal field of view: 360° Dual returns Vertical angular resolution: 2° Horizontal angular resolution: $0.1^\circ \dots 0.4^\circ$ Rotation rate: $5 \dots 20$ Hz
Laser	Class 1 – eye safe Wavelength – 903 nm
Mechanical	Weight: 830 grams (without cabling) Dimensions: 103 mm diameter x 72 mm height
Electrical	Power consumption: 8 W Operating voltage: 9 - 32 V DC
Output	Up to 300 000 points/second 100 Mbps Ethernet connection UDP packets containing -Distances -Calibrated reflectivities -Rotation angles -Synchronized time stamps (μ s resolution) \$GPRMC NMEA sentence from GPS receiver
Advanced Navigation Spatial Dual GNSS/INS system	
Navigation	Horizontal accuracy: 1.2 m Vertical accuracy: 2.0 m Horizontal accuracy (RTK): 0.008 m Vertical accuracy (RTK): 0.015 m Roll and Pitch dynamic accuracy: 0.15° Heading dynamic accuracy: 0.1° Velocity accuracy: 0.007 m/s
GNSS	Model: Trimble BD982 Antennas: 2 x Antcom G5Ant-53A4T1 GPS L1, L2, L5 GLONASS L1, L2 GALILEO E1, E5 BeiDou B1, B2 Update rate: 20 Hz
Mechanical	Weight: 285 grams (without cabling and GNSS antennas) Dimensions: 90x127x31 mm
Electrical	Power consumption: 220 mA at 12 V Operating voltage: 9 - 36 V DC
Output	Interface: RS232 Baudrate: 4800...1 000 000 Protocol: AN Packet Protocol or NMEA

Table 1. Velodyne VLP-16 and Advanced Navigation Spatial Dual specifications (VLP-16 datasheet, Spatial Dual datasheet)

The coordinates x , y , z with respect to the VLP-16 centre can be calculated by:

$$\begin{bmatrix} x \\ y \\ z \end{bmatrix} = \begin{bmatrix} R \cdot \cos \omega \cdot \sin \alpha \\ R \cdot \cos \omega \cdot \cos \alpha \\ R \cdot \sin \omega \end{bmatrix} \quad (1)$$

where x , y , z = coordinates of an individual survey point
 R = range from scanner to survey point
 ω = vertical angle
 α = horizontal angle

These calculated 3D coordinates are in a local (sensor's) frame. In order to georeference the point cloud and display consecutive point clouds together as a unified point cloud, GNSS and INS data need to be taken into account. This is referred to as direct georeferencing, which is defined as a transformation between the sensor coordinates frame and the geodetic reference frame. This has been previously described by e.g. Schwarz et al. (1993) Cramer et al. (2000), Grejner-Brzezinska (1999) and Baltasviats (1999). Although these articles concentrate on direct georeferencing of photogrammetry and airborne laser scanning data, the same basic principles apply here as well.

The custom software for point cloud computations was written in Java programming language. The inputs are LIDAR data packets and a text file containing GNSS/INS data. The software checks the time-stamps of both datasets and calculates geodetic coordinates based on the rotational angles and range from the LIDAR, the position and heading data from the GNSS and the roll and pitch data from the INS. Output is a point cloud file in ASCII text format containing 3D coordinates and reflective intensity of points.

3. METHODOLOGY

3.1 Field work and study area

The initial MLS field measurements were done in December of 2015. The sensors were placed on a sturdy wood plate on the roof rack of a car. The LIDAR was positioned in the back of the car looking down at a 30° angle. The inertial measurement unit (IMU) was located in the centre and the dual GNSS antennas were located on either side of it, see Fig. 2. Real time kinematic GNSS and INS data were recorded, synchronously with the VLP-16 data packets.

The study area was a 50x100m parking lot of Tallinn University of Technology. The main objects of interest were the asphalt-surface of the parking lot and the façade of an adjacent building, see Fig. 2. Data was collected while moving straight in a steady speed, cornering, swerving and alternating between braking and accelerating.

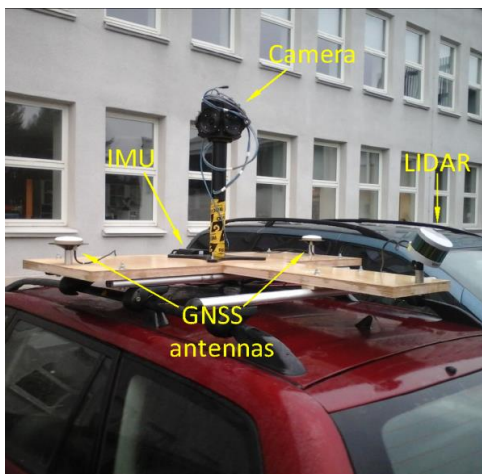


Figure 2. The placement of the VLP-16 and Spatial Dual sensors on the roof of a vehicle. 360° spherical camera Ladybug5 can be seen in the centre. The surveyed building façade in the background.

3.2 Reference data

The reference data was collected with a time-of-flight terrestrial laser scanner Leica ScanStation C10 with an average spatial resolution of ~2500 points/m² (2 × 2 cm). The scanner is rated for 6 mm positional accuracy. The point cloud registration and georeferencing of the TLS data were conducted based on 3 reference points which were coordinated with survey-grade GNSS measurements. The scanning was performed from three scan positions in order to sufficiently cover the asphalt-surface of the parking lot and the façade of the adjacent building. The TLS point cloud was clipped to only the area of interest and the measurement noise, as well as points reflected from obstructions (e.g. cars) were removed.

4. RESULTS AND ACCURACY ASSESSMENT

The resulting MLS point cloud (Fig. 3) was calculated with the method discussed in section 2.2. Overall more than 10 million points were measured during the MLS test survey.

The final MLS point cloud was compared with TLS data. The datasets indicated reasonable agreement near the trajectory of the vehicle. However, the errors became linearly larger when moving further away from the trajectory. The errors are mostly attributed to insufficient quality of the INS data, especially the roll misalignment. This is more evident during cornering and swerving. It should also be noted, that the accuracy of the distance measured with VLP-16 is ±3 cm (as shown in Table 1), which is considerably less accurate than that of TLS (see Section 3.2).

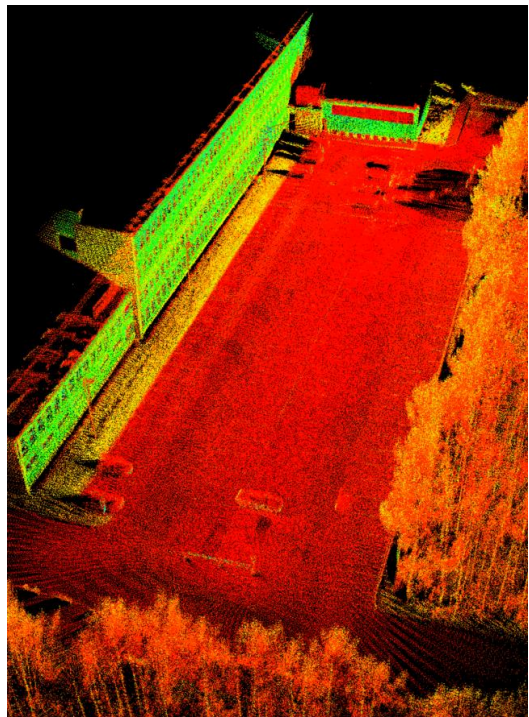


Figure 3. MLS point cloud of the study area. Colours show the calibrated reflectivities of surveyed points.

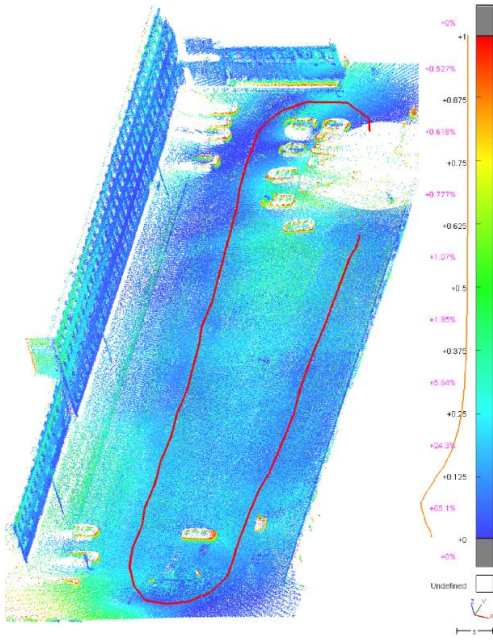


Figure 4. 3D discrepancies between TLS and MLS data (the absolute values of differences) in the test site. The red line denotes the clockwise trajectory of the vehicle. The empty data pockets are attributed to the cars in the parking lot. The horizontal scale denotes 5 metres.

The 3D discrepancies between the MLS and TLS clouds are shown in Fig. 4. The absolute values of the discrepancies mostly did not exceed 15 cm (blue points in Fig.4) with the root mean square error (RMSE) being 7.5 cm. The differences on the façade were mostly less than 10 cm but there is evidence of the two datasets being slightly tilted with respect to one another both horizontally and vertically. The first is presumably caused by the accuracy of position, i.e. GNSS data, and the second by roll misalignment. However, the dimensions (both height and width) of the building derived from TLS and MLS data indicated good agreement, within 1 cm vertically and within 3 cm horizontally.

According to the histogram (on the right hand side of Fig. 4), 65% of the detected discrepancies were within 12.5 cm and 90% of discrepancies within 25 cm. However, since the MLS data seem to be most affected by the roll misalignment error, then larger errors are observed with points measured while cornering and more than 5 metres away from the trajectory. Therefore, the isolated parts of the point cloud were evaluated separately.

On Fig. 5, vertical discrepancies between the TLS data and a segment of the MLS point cloud measured during cornering is shown. The differences increase during the cornering. At first, the roll is under-compensated (indicated by the higher (red) points on the “inside” corner at the top left of Fig. 5 which were measured at the start of the cornering manoeuvre) but later, the results show over-compensation (indicated by the higher (red) points on the “outside” corner at the bottom left of Fig. 5, which were measured in the end of the cornering manoeuvre).

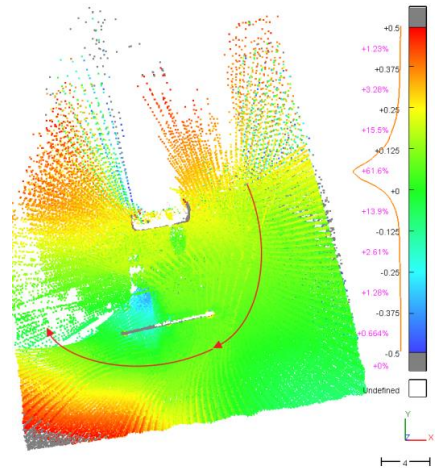


Figure 5. Vertical discrepancies between the TLS and MLS data acquired during cornering. The red arrowed line denotes the clockwise trajectory of the vehicle.

In the latter case the (red) points in the “outside corner” appear to be linearly higher than TLS data and vice versa, even though the roll of the vehicle in corners would cause the points in the “outside corner” to be lower if roll was not taken into account at all. Near the trajectory of the vehicle the discrepancies are within 10 cm (green points). It is worth noting that the density of points is higher near the trajectory and therefore 75% of the discrepancies are within 12.5 cm but larger than 50 cm differences occur further away from the trajectory.

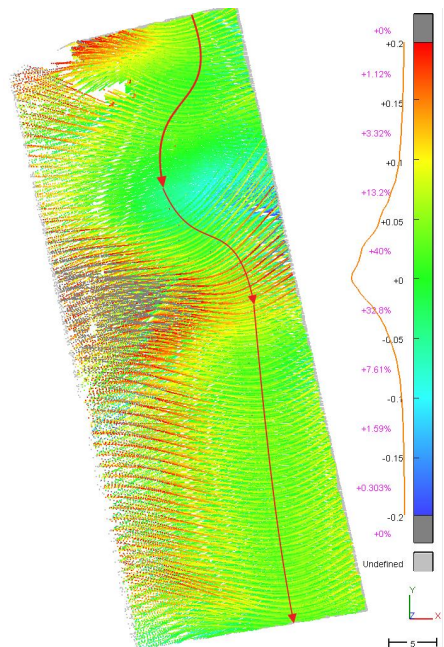


Figure 6. Vertical discrepancies between the TLS and MLS data gathered during a swerving manoeuvre. The red arrowed line denotes the trajectory of the vehicle.

The same effect can be observed by examining the results collected during a swerving manoeuvre (Fig. 6). At first the roll is under-compensated but at the end it is over-compensated. Although there are large errors further away from the trajectory, the accuracy of the points measured near the trajectory is within a couple of cm. Overall, ca 75% of the discrepancies do not exceed ± 5 cm.

5. CONCLUSION AND FUTURE RESEARCH

This paper presented the description of a relatively compact and low-cost MLS system, as well as the results and accuracy assessment of the initial case study. The initial tests indicated quite large errors mostly due to poor rotational angle data from the INS, especially roll misalignment.

The achieved results may be acceptable in some cases where high accuracy is not necessary, e.g. using single profiles to estimate the condition and smoothness of a road surface or estimating volumes of land mass transportations. For example, such MLS can also be used for quantifying the erosion and sedimentation over long portions of sand beaches. Our previous studies (Julge et al., 2014b, Eelsalu et al., 2015) have exploited both TLS and ALS data for this purpose. However, TLS survey is very time- and labour-consuming, whereas ALS data (acquired during national mapping campaigns) are not always available nor up-to-date. Even the current state of the assembled MLS system would provide a faster alternative with sufficient accuracy.

In order to make the results usable in other areas, further research and development is needed. Further experiments will include recording raw GNSS and INS data and using that information in post-processing trajectory calculations. Also there is a space for further calibration and improvements in the quality of inertial data. This will hopefully result in more accurate 3D point clouds.

Another direction for further research is to implement an algorithm which checks the distance of measured points from the scanner in overlapping areas and removes points that have been measured from adjacent/parallel MLS routes. These measurements are more susceptible to errors caused by poor inertial data and therefore less accurate. Also feature detection (mainly curb stones, posts and building outlines) will be integrated into the point cloud calculation software.

One of the main objectives is to use the MLS point clouds in conjunction with the image data from Ladybug5 camera (shown in Fig. 2) in order to add a possibility for reliable measurements in the existing Street-U street view online application (currently similar to Google Street View).

After the successful implementation of the MLS system on a car, other vehicles for mounting the system will be considered, e.g. an unmanned aerial vehicle, all-terrain vehicle or a "backpack".

ACKNOWLEDGEMENTS

This research has been supported by European Union Regional Development Fund. The used Velodyne VLP-16 LIDAR and Leica ScanStation C10 were purchased within frames of Estonian scientific equipment purchase support programme (project SF0140007s11AP14) and Estonian Research Infrastructures Roadmap object Estonian Environmental

Observatory (project No. AR12019). The participation in the XXIII ISPRS Congress in Prague is (partially) funded with SA Archimedes' Kristjan Jaak Scholarship.

REFERENCES

- "Advanced Navigation Spatial Dual datasheet" <http://www.advancednavigation.com.au/sites/advancednavigation.com.au/files/Spatial%20Dual%20Datasheet.pdf> (15 Feb. 2016)
- Baltsavias, E.P., 1999. Airborne laser scanning: basic relations and formulas. *ISPRS Journal of Photogrammetry and Remote Sensing*, 54(2), pp. 199-214.
- Barber, D., Mills, J. and Smith-Voysey, S., 2008. Geometric validation of a ground-based mobile laser scanning system. *ISPRS Journal of Photogrammetry and Remote Sensing*, 63(1), pp. 128-141.
- Cramer, M., Stallmann, D. and Haala, N., 2000. Direct georeferencing using GPS/inertial exterior orientations for photogrammetric applications. In: *International Archives of Photogrammetry and Remote Sensing*, 33(B3/1; PART 3), pp. 198-205.
- Eelsalu, M., Soomere, T. and Julge, K., 2015. Quantification of changes in the beach volume by the application of an inverse of the Bruun Rule and laser scanning technology. *Proceedings of the Estonian Academy of Sciences*, 64(3), pp. 240-248.
- Guan, H., Li, J., Yu, Y., Wang, C., Chapman, M. and Yang, B., 2014. Using mobile laser scanning data for automated extraction of road markings. *ISPRS Journal of Photogrammetry and Remote Sensing*, 87, pp. 93-107.
- Grejner-Brzezinska, D.A., 1999. Direct exterior orientation of airborne imagery with GPS/INS system: Performance analysis. *Navigation*, 46(4), pp. 261-270.
- Jaakkola, A., 2015. Low-cost Mobile Laser Scanning and its Feasibility for Environmental Mapping. (PhD thesis)
- Jaakkola, A., Hyypä, J., Kukko, A., Yu, X., Kaartinen, H., Lehtomäki, M. and Lin, Y., 2010. A low-cost multi-sensoral mobile mapping system and its feasibility for tree measurements. *ISPRS Journal of Photogrammetry and Remote Sensing*, 65(6), pp. 514-522.
- Julge, K., Ellmann, A. and Gruno, A., 2014a. Performance analysis of freeware filtering algorithms for determining ground surface from airborne laser scanning data. *Journal of Applied Remote Sensing*, 8(1), pp. 083573-083573.
- Julge, K., Eelsalu, M., Grunthal, E., Talvik, S., Ellmann, A., Soomere, T. and Tõnisson, H., 2014b. Combining airborne and terrestrial laser scanning to monitor coastal processes. In: *Baltic International Symposium (BALTIC), 2014 IEEE/OES* pp. 1-10.
- Kukko, A., Kaartinen, H., Hyypä, J. and Chen, Y., 2012. Multiplatform mobile laser scanning: Usability and performance. *Sensors*, 12(9), pp. 11712-11733.
- Pu, S., Rutzinger, M., Vosselman, G. and Elberink, S.O., 2011. Recognizing basic structures from mobile laser scanning data for road inventory studies. *ISPRS Journal of Photogrammetry and Remote Sensing*, 66(6), pp. S28-S39.

Pu, S. and Vosselman, G., 2006. Automatic extraction of building features from terrestrial laser scanning. *International Archives of Photogrammetry, Remote Sensing and Spatial Information Sciences*, 36(5), pp. 25-27.

Puente, I., González-Jorge, H., Martínez-Sánchez, J. and Arias, P., 2013. Review of mobile mapping and surveying technologies. *Measurement*, 46(7), pp. 2127-2145.

Pyysalo, U. and Hyypä, H., 2002. Reconstructing tree crowns from laser scanner data for feature extraction. *International Archives Of Photogrammetry Remote Sensing And Spatial Information Sciences*, 34(3/B), pp. 218-221.

Schwarz, K.P., Chapman, M.A., Cannon, M.W. and Gong, P., 1993. An integrated INS/GPS approach to the georeferencing of remotely sensed data. *Photogrammetric engineering and remote sensing*, 59(11), pp. 1667-1674.

Sithole, G. and Vosselman, G., 2004. Experimental comparison of filter algorithms for bare-Earth extraction from airborne laser scanning point clouds. *ISPRS journal of photogrammetry and remote sensing*, 59(1), pp. 85-101.

“Velodyne VLP-16 datasheet” http://velodynelidar.com/docs/datasheet/63-9229_Rev-C_VLP16_Datasheet_Web.pdf (19 Feb. 2016)

“Velodyne VLP-16 User’s manual and programming guide” <http://velodynelidar.com/docs/manuals/63-9243%20Rev%20B%20User%20Manual%20and%20Programming%20Guide,VLP-16.pdf> (11 Feb. 2016)

Wehr, A. and Lohr, U., 1999. Airborne laser scanning—an introduction and overview. *ISPRS Journal of Photogrammetry and Remote Sensing*, 54(2), pp. 68-82.

Yang, B., Fang, L. and Li, J., 2013. Semi-automated extraction and delineation of 3D roads of street scene from mobile laser scanning point clouds. *ISPRS Journal of Photogrammetry and Remote Sensing*, 79, pp. 80-93.

Yoon, J.S., Sagong, M., Lee, J.S. and Lee, K.S., 2009. Feature extraction of a concrete tunnel liner from 3D laser scanning data. *NDT & E International*, 42(2), pp. 97-105.

PUBLICATION III

© 2014 Society of Photo-Optical Instrumentation Engineers (SPIE). Reprinted, with permission, from

Julge, K., Ellmann, A., Gruno, A. (2014). Performance analysis of freeware filtering algorithms for determining ground surface from airborne laser scanning data. *Journal of Applied Remote Sensing*, 8(1), 083573-1–083573-15.10.1117/1.JRS.8.083573.

Performance analysis of freeware filtering algorithms for determining ground surface from airborne laser scanning data

Kalev Julge,^{a,*} Artu Ellmann,^a and Anti Gruno^{a,b}

^aTallinn University of Technology, Faculty of Civil Engineering, Department of Road Engineering, Chair of Geodesy, Ehitajate tee 5, Tallinn 19086, Estonia

^bEstonian Land Board, Mustamäe tee 51, Tallinn 10621, Estonia

Abstract. Numerous filtering algorithms have been developed in order to distinguish the ground surface from nonground points acquired by airborne laser scanning. These algorithms automatically attempt to determine the ground points using various features such as predefined parameters and statistical analysis. Their efficiency also depends on landscape characteristics. The aim of this contribution is to test the performance of six common filtering algorithms embedded in three freeware programs. The algorithms' adaptive TIN, elevation threshold with expand window, maximum local slope, progressive morphology, multiscale curvature, and linear prediction were tested on four relatively large (4 to 8 km²) and diverse landscape areas, which included steep sloped hills, urban areas, ridge-like eskers, and a river valley. The results show that in diverse test areas each algorithm yields various commission and omission errors. It appears that adaptive TIN is suitable in urban areas while the multiscale curvature algorithm is best suited in wooded areas. The multiscale curvature algorithm yielded the overall best results with average root-mean-square error values of 0.35 m. © 2014 Society of Photo-Optical Instrumentation Engineers (SPIE) [DOI: [10.1117/1.JRS.8.083573](https://doi.org/10.1117/1.JRS.8.083573)]

Keywords: airborne laser scanning; classification; algorithms; point cloud.

Paper 14079 received Feb. 5, 2014; revised manuscript received May 22, 2014; accepted for publication Jul. 1, 2014; published online Aug. 8, 2014.

1 Introduction

Airborne laser scanning (ALS) is a recent technology that utilizes laser pulses for acquiring relatively high-resolution three-dimensional (3-D) spatial data about objects. The height accuracy of the measured points is usually estimated^{1,2} to a range of within 0.05 to 0.15 m. Most modern scanners can detect and record several reflections per one laser pulse. This enables the pulse to travel all the way to the ground through various obstacles, even in densely forested areas. As the reflections are usually classified as “only” or “first,” “intermediate,” and “last,” then this information is useful in classifying points—“last” reflections are most likely ground, whereas “first” reflections could be, for example, treetops.

One of the main goals of ALS data processing is determining the ground points from the resulting ALS point cloud and forming digital elevation models (DEM). Since the point cloud initially contains points from all sorts of different features (buildings, vegetation, etc.) then identifying ground points is not always an easy task. The correct classification of ground/nonground points is crucial to the accuracy of subsequent ground surface models and to a large variety of spatial analyses that are based on them.

Filtering algorithms that automatically classify points as ground/nonground are usually developed with some specific terrain types in mind; thus, their efficiency is largely dependent on the type of landscape. In order to determine the all-round best ground classification algorithms, they all need to be tested on a variety of terrains and the results compared with some sort of “ground truth.”

*Address all correspondence to: Kalev Julge, E-mail: kalev.julge@ttu.ee

0091-3286/2014/\$25.00 © 2014 SPIE

Critical issues of ground filtering algorithms have been thoroughly reviewed by Meng et al.³ Different filtering algorithms have previously been compared, e.g., by Zhang and Whitman;⁴ Sithole and Vosselman;⁵ Tinkham et al.;⁶ Goncalves and Pereira;⁷ and Sulaiman et al.⁸ These contributions compare and evaluate various ground filtering algorithms (both freeware and commercial) on different data sets including urban areas, high and low vegetations, and mountainous terrains in areas ranging from a few hectares to a few square kilometers. The “ground truth” data are either gathered from separate ground measurements or generated by another ground filtering software and/or by manual classification. The numbers of correctly/incorrectly classified points are used for statistical analysis.

This contribution uses for ground classification diverse ALS data sets that cover rather large areas (covering 4 to 8 km²), as opposed to many previous ground classification studies, which utilize ALS data sets of relatively limited spatial coverage, see e.g., Tinkham et al.;⁶ Goncalves and Pereira;⁷ and Sulaiman et al.⁸

The present study uses reference data (“ground truth”) that are rather dense (almost “continuous”) and evenly cover each test area. This has a clear advantage over common cases using scarcely located discrete control points, see e.g., Zhang and Whitman.⁴ Recall that most ground classification errors tend to be localized at certain features (e.g., steep slopes, buildings, etc.); thus, large classification errors in such locations can be overlooked by relying on a selection of scarce control points. Thus, the magnitude of detected discrepancies over such areas may be underestimated in the statistical analyses.

Additionally, the selected approach is not affected by ALS positioning errors because the reference data originate from the same source as the test data. Recall that if the “ground truth” data are gathered from ground measurements (GNSS or total station surveys, e.g., Tinkham et al.;⁶ Goncalves and Pereira⁷), then the discrepancies between the ALS and reference data become also contaminated by the ALS positioning errors. In this study, the ALS height errors (which are definitely present) are the same in both the reference and test data. Therefore, in comparisons, they cancel each other out and the remaining differences between reference and test data can only be associated with classification errors. Note that investigating the ALS positioning errors is outside the scope of the present study.

Our testing approach requires that the ground truth classifications are correct. This is achieved by using manually corrected and visually verified ALS data. It is acknowledged that some errors will still remain after manual corrections. However, as the large majority of blunders have been corrected/removed, the remaining relatively small errors have only a little weight in the final solution since the entire data set is large.

Commercial software is usually expensive and thus used only in large companies or state-owned enterprises which perform a large amount of ALS data processing. Thus a nonassociated researcher or enthusiast would not have access to such commercial software. Hence, this paper focuses on the practical testing of algorithms in freeware programs which are readily available and freely downloadable.

The outline of the paper is as follows. This introduction is followed by a review of the basic principles of ground filtering algorithms; thereafter, the algorithms used in the present study are explained in more detail. Methodology used for comparing the algorithms is discussed. The performance of tested algorithms is assessed with respect to data products which have been reached using sophisticated commercial software and a thorough visual inspection. A brief summary concludes the paper.

2 Filtering Algorithms

Ground filtering algorithms are based on the assumption that the correlation between ground points is stronger than that between nonground points or between ground and nonground points. Using a threshold value that limits the allowed elevation difference or slope between points, it is possible to identify particular data points as being either as ground or nonground points. As the pulse returns with the lowest elevation are more likely to be ground points, these are primarily considered for the methods described below.

There are several basic ground classification methods. The first method considers the elevation difference between neighboring points. If the elevation difference is larger than a preset

threshold then the higher point is considered to be nonground. The second method calculates the slope between two neighboring points. If the slope value is steeper than the threshold, then the higher point is classified as nonground. Both of these methods can fail on landscapes with near vertical landforms such as sheer cliff faces.

An advanced way to filter point clouds is to create a model surface using raw ALS data or dividing the area into smaller cells and using the points with the minimum elevation in each cell. Then it is possible to compare the vertical distance of each individual point to this coarse ground surface. The points lower than the surface or within the threshold value are identified as ground points. This method is usually implemented iteratively, where all the points that are classified as ground in the iteration are used to calculate a new surface for the next iteration. The nonground points are discarded from further iterations.⁹ All of the abovementioned methods can be applied on their own or can be combined with each other as an iterative process or as a single step.

The filtering algorithms reviewed in this paper are as follows:

- Adaptive TIN (ATIN);¹⁰
- Elevation threshold with expand window (ETEW);⁴
- Maximum local slope (MLS);¹¹
- Progressive morphology 2D (PM);¹²
- Multiscale curvature (MCC);¹³
- Linear prediction (LP).¹⁴

The first four of these (ATIN, ETEW, MLS, and PM) are implemented in ALDPAT 1.0 (Airborne Lidar Data Processing and Analysis Tools, <http://lidar.ihrc.fiu.edu/lidartool.html>),⁹ MCC in MCC-Lidar 1.0 (current version 2.1, <http://sourceforge.net/p/mcclidar/wiki/Home/>)¹³ and LP in FUSION Metrics 0.85.0 (current version 3.42, <http://forsys.cfr.washington.edu/fusion/fusionlatest.html>)¹⁵ software. Out of these, ALDPAT has the window-based user interface while MCC-Lidar and FUSION make use of the command prompt. Accordingly, using ALDPAT is simpler at first but the script-based programs are more efficient in terms of automating the repeating calculation processes. The tested algorithms have changeable parameters (usually 6–8 except MCC which only has 2) e.g., the thresholds for elevation differences or slopes, number of iterations, and so on. Finding the most suitable combination of parameter values for each tested algorithm is essential for the correct classification of ground points.

The widely known Lastools software is omitted from the study on the basis that it is not completely freeware. The ground filtering module requires a license, as the unlicensed version will delete some of the data (intensity, GPS time, etc.) and add a bit of noise.¹⁶ It is also acknowledged that other free software (not included in this study) for ground filtering, such as BCAL LiDAR Tools (<https://code.google.com/p/bcal-lidar-tools/>) and GRASS GIS (<http://grass.osgeo.org/#>) exist. For instance, the performance of BCAL and GRASS GIS ground filtering algorithms has been previously reviewed by Tinkham et al.⁶ and Brovelli and Lucca,¹⁷ respectively.

2.1 Adaptive Triangulated Irregular Network

The ATIN algorithm uses the distance of a point from the surface of a triangulated irregular network (TIN) as the main constraint. The ALDPAT embedded ATIN algorithm is applied as follows. At first, the area is divided into small cells and the point cloud is thinned by keeping only one point (with a minimum elevation) per cell and discarding other points. Then, the local minimums are found and are considered to be ground. Thereafter, a coarse TIN is calculated based on these local minimums using the Delaunay triangulation. The position of the points not used in the TIN formation is then compared to the coarse TIN. The distance between a point and the surface of the closest triangle and the angles between the surface of the triangle and the lines connecting the point with triangle vertices are calculated. When both the distance and angles are less than predefined thresholds, then the point is classified as ground. These ground points are used in the next iteration to construct a new TIN. The distance to the surface and corresponding angles for the rest of the points is computed and compared with the thresholds. The process is terminated when no unclassified points can be classified as ground.¹⁰

2.2 Elevation Threshold with Expand Window

The ETEW algorithm is based on the assumption that the elevation differences among neighboring ground points are different from those between neighboring ground and nonground points. In order to determine the ground points, it is necessary to check the elevation differences of points in a predefined radius and compare them to the threshold values. The point cloud is divided into smaller (square-shaped) cells and within every cell the point with the minimum elevation is found. When the elevation difference of a point from the local minimum is less than the threshold value, the point is considered as ground. Points that are higher than the threshold are considered to be nonground. The method is implemented iteratively with the cell size expanding between sequential iterations.⁴

2.3 Linear Prediction

LP is based on linear least-squares interpolation, also known as linear prediction. It makes use of weights assigned to each point while calculating a surface and comparing the distance of the points to that surface. In the first iteration, all points have equal weights and a mean surface is constructed. Points that are below the mean surface by a predefined margin are given the weight 1, while the points that are higher from the mean surface than a threshold value are given the weight 0. Points that lie between these two limits are given a weight between 0 and 1 with more weight assigned to points that are lower. The weights are calculated using the weight function:

$$p_i = \begin{cases} 1 & \text{if } v_i \leq g \\ \frac{1}{1+[a(v_i-g)^b]} & \text{if } g < v_i < g + w, \\ 0 & \text{if } g + w < v_i \end{cases} \quad (1)$$

where v_i is the vertical distance of the point from the surface and p_i is the weight assigned to a point. Parameters a and b define the steepness of the weight function. Points that are lower than the surface by more than the shift parameter g value obtain the maximum weight of 1. The above-ground offset value w is used to reduce the effect of probable nonground points in the form of the surface for the next iteration. The above points farther than $(g + w)$ from the surface are given the weight 0. For the next iteration, a new mean surface is constructed, this time using weighted points. The process is repeated a predefined number of times. After the last iteration, points that are lower than the surface (or above the surface closer than a predetermined threshold value) are classified as ground.¹⁴

2.4 Multiscale Curvature

MCC uses an iterative multiscale approach to evaluate the distance of a point from a surface and gradually removes nonground points from the data set. The algorithm classifies last and only reflections as potential ground points and based on these interpolates a mean surface using thin plate spline interpolation. Thereafter, a 3×3 mean kernel is passed over the interpolated raster. The distance between each point and the surface is compared to the threshold value. If the point is lower than the surface or does not exceed the threshold, then it is considered as a potential ground point. All other points are classified as nonground. In the next iteration, a new mean surface is constructed based on the remaining potential ground points. The iterative process is repeated until the number of points removed is below the convergence threshold (usually 0.1%).¹³

2.5 Maximum Local Slope

The MLS algorithm determines ground points from a point cloud by using slope values between a point and its neighbors assuming that the ground slope is different from the slope between the ground and nonground points.¹¹ The point cloud is divided into smaller square-shaped cells

and within every cell the point with the minimum elevation is found. A point $p_0(x_0, y_0, z_0)$ is classified as ground when the maximum slope ($s_{0,max}$) between the point and its j 'th neighboring point $p_j(x_j, y_j, z_j)$ is less than a predefined threshold (s).

$$s_{0,j} = \frac{z_0 - z_j}{\sqrt{(x_0 - x_j)^2 + (y_0 - y_j)^2}}, \quad (2)$$

$s_{0,max} < s \Rightarrow p_0 \in \text{ground}$ where $s_{0,j}$ is the (unitless) slope between points $p_0(x_0, y_0, z_0)$ and $p_j(x_j, y_j, z_j)$.⁹

2.6 Progressive Morphology Two-Dimensional

PM is a filtering algorithm which makes use of mathematical morphology, i.e., operations based on a set theory to extract features from images. The point cloud is divided into cells usually smaller than the average spacing between LIDAR measurements. In each cell, the local minimum is found and these are used to construct an initial surface DEM. A mathematical morphological operation called opening (erosion and dilation) (see e.g., Haralick et al.¹⁸) is performed on the surface in order to derive a secondary surface. The elevation difference of a cell between the two surfaces is compared to a threshold value and points that do not exceed the threshold are considered to be ground. The threshold dh_{iT} is defined as follows:

$$dh_{iT} = \left\{ \begin{array}{ll} dh_0 & \text{if } f_i \leq 3 \\ s(f_i - f_{i-1})c + dh_0 & \text{if } f_i > 4 \\ dh_{max} & \text{if } dh_{iT} > dh_{max} \end{array} \right\}, \quad (3)$$

where dh_0 is the initial elevation difference threshold, dh_{max} is the maximum elevation difference threshold, s is the maximum terrain slope allowed, c is the size of the cell, and f_i is the size (length of side) of the filtering window in i 'th iteration.¹²

3 Comparison of Filtering Algorithms

3.1 Test Data Sets

The ALS data that were used were collected by Estonian Land Board in 2009 using the Leica ALS50-II airborne laser scanner. The ALS flight altitude of 2400 m resulted in a point cloud with an average point density of 0.45 p/m².

Flight parameters used in the ALS campaign:

- Field of view: 55 deg.
- Flight height: 2400 m.
- Width of the flight line: 2700 m.
- Scanning rate: 32.6 Hz.
- Laser pulse frequency with "multiple-pulses-in-the-air" (MPiA): 93.9 kHz.
- Minimum point density: 0.3 p/m².
- Average point density: 0.45 p/m².
- Scanning pattern-sinusoidal or "zig-zag."

The accuracy of a similar ALS data set in the nadir range was estimated² to be 0.06 m. The algorithms were tested on four diverse test areas located in Kiviõli, Neeruti, Purtsu, and Viitna, ranging from 4 to 8 km² in size (Fig. 1). The existence of a standard ISPRS testing data set ("ISPRS test on extracting DEMs from point clouds" <http://www.itc.nl/isprswgIII-3/filtertest/>) is acknowledged; however, in this study, ALS data over locally challenging landscapes were used for ground filtering tests. The areas were selected in a way that they would include a variety of terrains e.g., high and low vegetations, urban areas, high and low landforms, artificial landscape, and so on (Table 1).

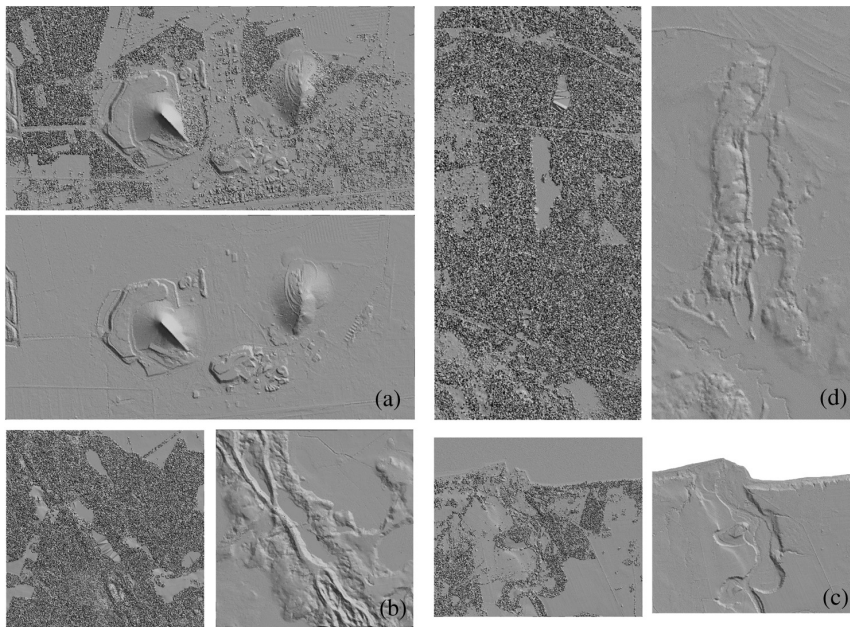


Fig. 1 The grayscale shaded relief maps of the test areas using raw ALS data (all points) and only ground points only. (a) Kiviõli “mixed” (steep-sloped-hills, combined with forests, urban structures and industrial buildings), (b) Neeruti “esker-1” (dense forest on top of eskers), (c) Purtse “river-valley” (river-valley and coastal cliffs), (d) Viitna “esker-2” (dense forest on top of eskers).

Table 1 The statistics of test areas.

Parameters	Test area			
	Kiviõli “mixed”	Neeruti “esker-1”	Purtse “river-valley”	Viitna “esker-2”
Landscape	Steep-slope-hills, urban areas, forests	Dense forest on top of eskers	River valley and coastal cliffs	Dense forest on top of eskers
Area	8 km ²	4 km ²	4 km ²	8 km ²
Wooded	28%	86%	40%	90%
Open landscape	37%	11%	28%	8%
Urban	18%	—	—	—
Water	—	3%	32%	2%
Industrial waste deposits	17%	—	—	—
Maximum height	163.5 m	126.5 m	32.2 m	100.7 m
Minimum height	42.9 m	86.2 m	-0.4 m ^a	67.6 m
Number of measured points	3 615 691	2 185 610	1 535 137	4 562 412
Number of ground points (Estonian Land Board classification)	2 366 839	545 087	789 769	1 492 746
Mean slope	5.1 deg	8.2 deg	4.3 deg	4.2 deg

^aPurtse is located by the sea and the water level at the time of the measurements was lower than the long-term average. Therefore, after the removal of points registered from the surface of the water, some of the ALS data reflected from the (temporarily dry) sea floor remained.

The Kiviõli test area [Fig. 1(a), in further text to be referred to as “mixed”] consists of the most diverse terrain. There are high and low vegetations, open landscape, urban areas, and artificial terrains. It includes semi-coke landfills which are formed from the ash and other by-products (industrial waste) of burning oil shale. The landfills possess very steep slopes that can, at places, reach near vertical. The elevation differences in the area reach 120 m. In the eastern part of the area, there are urban areas which include some large flat-roofed industrial/factory buildings.

Neeruti [Fig. 1(b), “esker-1”] and Viitna [Fig. 1(d), “esker-2”] are predominantly covered with a thick mixed forest, which grows on a relatively complicated landscape. These areas are characterized by long, ridge-like eskers which have occurred due to the latest deglaciation. The vegetation varies from <1 m tall bushes to 25 m tall trees. Most of it is trees about 10–15 m tall.

In the Purtse [Fig. 1(c), “river-valley”] test area, there are, in addition to some forested areas, steeply banked coastal cliffs and valleys with a river mouth. This represents typical river valleys, the width of which varies from 150 to 400 m.

3.2 Reference Data Model

Key works on the topic of ALS data ground filtering and DEM extraction include Meng et al.³ and Briese.¹⁹ There are different methods for generating reference data (“ground truth”). In some previous work, the reference data have been classified by some well-known algorithm; for example, a modified ATIN algorithm implemented in Terrasolid Terrascan.⁸ However, this may not be the best approach since no algorithm produces error-free results.

Another option has been to gather the “ground truth” data with GNSS or total station surveys. Clearly, this can be conducted over limited areas because this kind of data acquisition is very time consuming. Also, additional positioning discrepancies between test and reference data sets occur due to the data positioning errors, i.e., the elevation discrepancies between the test and reference data are not solely due to classification errors. For example, if a height error of 5 cm (easily possible) occurs in calculating the trajectory of the ALS flight, then this yields an additional 5 cm systematic error in the ALS data absolute heights. It should be emphasized that the aim of this study is to investigate the classification errors, not the influence of ALS positioning errors to ground classification (see also Introduction for the reasoning).

A third option is to randomly select a number of points, determine their classification, and statistically compare the number of omission and commission errors.⁴ This approach only includes a small percentage of points in the comparison which can result in nonidentification of possible gross errors.

The most accurate reference data are gained by manually verifying each point’s classification (using information from orthophotos, field measurements, etc.). This is time consuming and is not even thinkable on a point cloud containing millions of points.

Since this study focuses on large data sets, the reference data are generated by combining an algorithm with manual classification. This is first preceded by applying a widely known algorithm (ATIN in the Terrasolid Terrascan²⁰ software, to be further referred to as “commercial ATIN”) to the point cloud. Commercial ATIN has been found to achieve better results than other algorithms (by 1–5%).⁷ The main differences between the commercial ATIN as compared to the ALDPAT embedded ATIN seem to be the following: commercial ATIN works with the original point cloud, i.e., there is no initial thinning of the point cloud, see also Sec. 2.1. Also after each iteration, statistics of the ground classified points are generated, i.e., the surface normal angles and elevation differences in the form of histograms. These histograms are used for adjusting the values of the thresholds to be used in the iterative process.⁷

Since more than 50% of Estonia is covered with forests or underwood, the parameters for automatic filtering with Terrascan (Finland) software are set in ELB (from which the reference data originates) in a way to best remove vegetation. In particular, the angle and distance parameters in iterations are set to 6 deg and 1.4 m, respectively (see also Sec. 2.1). However, this may yield errors on steeper slopes. The removal of these errors is accomplished by visual verification. Within these DEM (formed of points initially classified as ground by the Terrascan software) areas, obvious mistakes are easily identifiable because summits of slopes appear to be “cut off.”

In these suspicious locations, cross sections of both the DEM and the point cloud are inspected. If the ground surface is identifiable in the point cloud, i.e., there is a row of points with small height discrepancies, then these are manually classified as ground. This process is iteratively repeated until the ground classifications appear to be correct. In questionable cases, complementary data sources, such as large-scale orthophotos, are used for additional verification.

This means that the reference data involves the entire test area and the large majority of blunders have been corrected so that the remaining relatively small errors have only a little weight because the entire data set is very large. With this method, the ALS positioning errors do not influence the results because the data source for both the reference and test data are the same, i.e., the possible ALS positioning errors are equal in both data sets (as opposed to using ground measurements for “ground truth” where the ALS errors would affect the differences between reference and ALS data). Therefore, all the detected height discrepancies are most likely solely caused by classification errors.

3.3 Methods for Finding the Parameters and Analyzing the Ground Determination Results

The aim of the study was to find an optimum algorithm and parameter combination that would perform reasonably within any given (excluding the most extreme cases, such as mountain peaks) area, without the need to account for area-dependent characteristics (e.g., tall vegetation, short vegetation, urban areas, hills, etc.). Therefore, the most suitable parameter values for every algorithm were empirically determined on a 1 km² area (from the “mixed” area, with the most challenging relief and a mixture of forested and urban areas). For each tested algorithm, various values and their combinations were tested. To remove obvious gross errors and outliers, the resulting point clouds and shaded relief maps were visually examined. This allowed for clearly identifying the ground classification errors (Fig. 2). The parameter combinations that yielded inaccurate results were discarded and three or four promising parameter combinations were selected for final computations.

These parameter combinations were applied on the four test areas “mixed,” “esker-1,” “esker-2,” and “river-valley.” To analyze the achieved results, both the results of the test data sets and the reference data sets were interpolated with a 5-m grid using Delaunay triangulation. The 5-m grid was selected since the resolution of the raw data was 0.45 p/m² (out of which only roughly half were ground points), whereas the use of a smaller (2 × 2 m) grid size did not yield significant improvements in the statistical analysis. Therefore, the conclusions in Sec. 4 (with some reservations) may also apply to somewhat denser or sparser data sets.

The formed DEMs had identical planar coordinates (x, y) for the pixel center points. Using these DEMs, the discrepancies between the results associated with the algorithms and the reference data were found:

$$\theta_i(x_i, y_i) = h_{\text{ref}}(x_i, y_i) - h_{\text{alg}}(x_i, y_i), \quad (4)$$

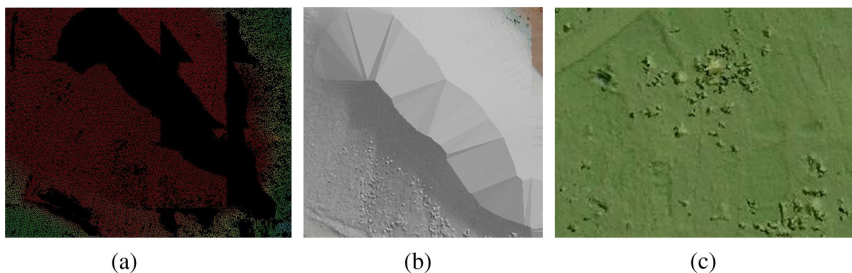


Fig. 2 Samples of visually obvious signs that point to ground classification errors in the “mixed” test area. (a) Voids in the point cloud on a hill, (b) unnaturally long interpolation lines on the shaded relief maps on a hill, (c) “peaks” or “bumps” on the shaded relief maps on over forested area.

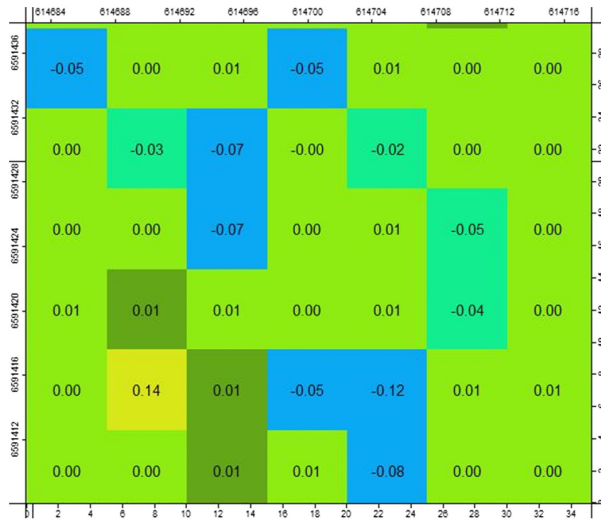


Fig. 3 Sample of a 5 × 5 m model of elevation discrepancies (zoomed in view). Pixel values are the elevation discrepancies between outcome of the ground filtering algorithms and the reference data. Units in meters.

where θ_i is the i 'th discrepancy from the reference data, $h_{ref}(x_i, y_i)$ is the reference data elevation, and $h_{alg}(x_i, y_i)$ is the algorithm generated elevation.

This resulted in a new model where the pixel values were no longer elevations but were the elevation discrepancies between the test and reference data (Fig. 3). These discrepancies were also used to calculate root-mean-square errors (RMSE) within each test area as follows:

$$RMSE = \sqrt{\frac{\sum_1^n \theta_i^2}{n}}, \tag{5}$$

where n is the number of observations (in this case the number of DEM pixels) and $i = 1, 2, \dots, n$.

Out of the three to four parameter combinations, the results with the smallest RMSE were selected for final analysis in this study. The parameters that yielded the best results on these test areas are presented in Table 2.

Note that these parameter combinations were selected to represent the entire data set in each test area. In areas where the landscape is more uniform or the point cloud is denser (or sparser), other combinations may be better suited for determining ground points. For example, in urban areas the “Init TriGrid Size” parameter of ATIN should be set larger than the maximum dimensions of the existing buildings. This would classify nonground features more accurately. However, in this particular case, it was not feasible since it yielded large errors for the classification of the ground at hilltops.

The final results were analyzed and compared by their RMSE values and also by the distribution of errors ranging from insignificant errors (less than 1 cm) to small errors (1–5 cm) up to gross errors (over 1 m).

4 Results

The analysis of the filtering results revealed that all the tested algorithms cause classification errors to some extent. As expected, the errors were more pronounced in areas with diverse landscape. The most common errors were commission errors, i.e., errors where nonground points were wrongly classified as ground (actually—vegetation and buildings); and omission errors, i.e., errors where ground points were classified as nonground, e.g., on steeper slopes. The

Table 2 The final parameter combinations for the ground filtering algorithms tested.

Parameter	Value	Unit
Adaptive TIN		
Cell size	1	m
Z difference	0.2	m
Angle threshold	0	deg
Init TriGrid size	25	m
Tile X width	50	m
Tile Y width	50	m
Tile buffer	5	m
Elevation threshold with expanding window		
Width	1	m
Height	1	m
Maximum Z	9999	m
Minimum Z	-9999	m
Slope	0.25	
Loop times	7	
Linear prediction		
Cell size	5	m
<i>g</i>	-2	
<i>w</i>	2.5	
<i>a</i>	1	
<i>b</i>	4	
Tolerance	0.2	m
Iterations	10	
Multiscale curvature		
Scale	2.5	
Curvature threshold	0.4	
Maximum local slope		
Width	1	m
Height	1	m
Maximum Z	9999	m
Minimum Z	-9999	m
Search radius	10	m
Minimum distance	1	m
Maximum slope	0.5	

Table 2 (Continued).

Parameter	Value	Unit
Progressive morphology		
Cell size	3	m
Slope	0.08	
Init threshold	0.6	m
Maximum threshold	9999	m
Window base	1	m
Power increment	1	
Window series length	8	
Init radius	1	m

best results were achieved with MCC (see Table 3) with an average RMSE of 0.35 m. Determining the MCC parameter combinations was the easiest since MCC has only two variables as opposed to 6–8 in the other algorithms.

None of the tested algorithms were able to flawlessly classify the most challenging areas, e.g., steep-slope hills and buildings. This is illustrated by the “mixed” test area (Fig. 4) where it is very challenging to correctly classify steep slopes and buildings with the same set of parameters. The green parts illustrate the areas where the discrepancies between reference and test data sets were negligible (<1 cm). The red represents the steep slopes and hilltops which were wrongly removed (omission error) from ground points. The purple and blue colors show the buildings and vegetation, respectively, which were not removed (commission error) from ground points.

The ATIN omission errors appeared mostly on hilltops and the commission errors on larger buildings. Areas covered with vegetation and smaller buildings have been classified more or less correctly [Fig. 4(a)]. ETEW yielded large omission errors on hilltops (resulting in a very large RMSE of 3.4 m, see Table 3) and quite large commission errors in forested areas [Fig. 4(b)]. LP yielded numerous commission errors on buildings and some omission errors on the steepest slopes, but the ground classification in forested areas was quite reasonable [Fig. 4(c)]. The MCC commission errors were practically absent. However, some omission errors were detected on buildings and forested areas [Fig. 4(d)]. This resulted in the smallest RMSE of 0.5 m in

Table 3 The RMSE values of ground filtering results within the test areas.

Algorithm	Root mean square error (m)				Average
	Kiviõli “mixed”	Neeruti “esker-1”	Purtse “river-valley”	Viitna “esker-2”	
ATIN	0.882	0.921	0.298	0.457	0.640
ETEW	3.410	1.481	0.628	0.315	1.459
LP	0.991	0.457	0.289	0.256	0.498
MCC	0.510	0.387	0.238	0.249	0.346
MLS	0.706	0.469	0.259	0.275	0.427
PM	1.117	0.735	0.384	0.340	0.644
Average	1.269	0.742	0.349	0.315	

Note: Bold values mark the lowest RMSE value for the test area.

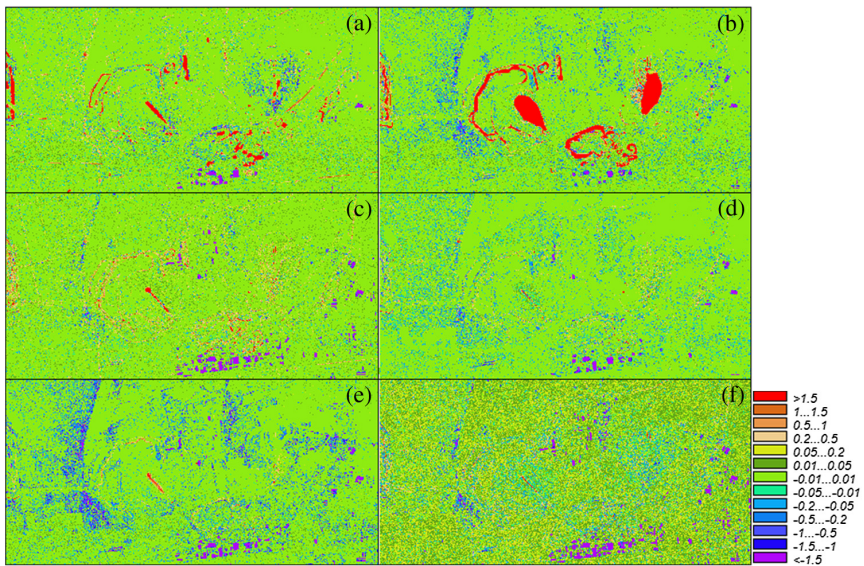


Fig. 4 Detected discrepancies between tested ground filtering algorithm results and the reference data in the “mixed” test area (a) ATIN, (b) ETEW, (c) LP, (d) MCC, (e) MLS, (f) PM. The legend units are meters.

the “mixed” area, see Table 3. The MLS-related large omission errors are associated with the vegetation and buildings. Commission errors were present only on the steepest hills [Fig. 4(e)]. The PM-related omission errors are due to buildings and, to some extent, vegetation. Hardly any PM-related commission errors were detected [Fig. 4(f)].

However, it is clear that the large RMSE values are mostly caused by gross errors which are localized at certain landscape features (such as steep slopes). The error distribution analysis reveals that most of the errors are insignificant (less than 1 cm); as much as 75% of the errors in the “mixed” test area are insignificant, see Fig. 5. However, this percentage drops significantly in more forested areas like “esker-1” and “esker-2.” RMSE values drop due to the small amount of gross error, but only about 40–60% of the errors are insignificant, see Table 4.

Within the mixed area (urban, steep hills, low and high vegetations), it is almost impossible to achieve good results with only one combination of parameters or only one algorithm. The area should be divided into subareas containing more or less similar features and thereafter apply the algorithm more suitable for the situation. For example, in urban areas that are otherwise

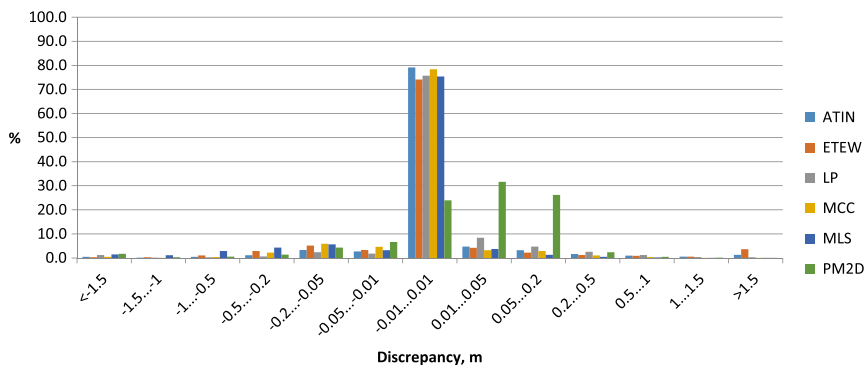


Fig. 5 The distribution of discrepancies between the ground filtering results and the reference data in the “mixed” test area.

Table 4 Distribution of area related ground filtering errors.

Area	Error [m]	Occurrence %					
		ATIN	ETEW	LP	MCC	MLS	PM
Kiviõli "mixed"	<0.01	79.1	74.1	75.7	78.4	75.3	24.0
	0.01...0.05	7.5	7.6	10.3	7.9	7.0	38.3
	>1	2.5	4.8	2.1	0.7	2.8	2.3
Neeruti "esker-1"	<0.01	46.6	42.4	51.5	44.8	47.2	32.4
	0.01...0.05	10.2	10.5	14.4	14.6	10.0	24.8
	>1	9.6	9.7	3.3	2.5	4.1	6.4
Purtse "river-valley"	<0.01	51.8	75.5	77.2	80.5	77.6	25.3
	0.01...0.05	29.1	8.3	10.4	6.5	7.9	41.0
	>1	1.5	3.5	1.1	0.8	1.6	1.5
Viitna "esker-2"	<0.01	58.0	54.7	61.3	51.1	55.6	36.9
	0.01...0.05	14.5	14.9	17.1	19.3	14.3	35.4
	>1	2.2	1.0	0.3	0.2	0.7	0.6

relatively flat the best algorithm is ATIN, but since it tends to remove points from the tops of hills, it cannot be used on complex terrain with the same parameter combinations. MCC, on the other hand, is efficient in wooded areas.

For all the algorithms, some general rules for choosing the values of parameters were identified. On a relatively flat and open landscape, where all of the laser pulse returns are ground points with similar elevations, the choice of the values is not of utmost importance because the same results can be practically achieved with every reasonable (e.g., the allowed elevation difference threshold should never be set to 0) parameter combination. The optimum parameter combinations are more important in areas where the landscape is inclined (e.g., hills). In that case, it should be noted that the elevation and slope thresholds need to be set large enough so that ground points would not be classified as nonground.

In diverse situation regions, the selection of a suitable parameter set is more difficult, e.g., steep slopes that need to be classified as ground, or buildings and vegetation that need to be classified as nonground. Hence, it is always necessary to determine a compromise which minimizes the classification errors. However, completely avoiding them is usually impossible.

5 Conclusions

ALS is a very useful remote sensing technique that enables the quick acquisition of spatial data over large areas. Freeware ground filtering algorithms make automatic ground detection from ALS data more accessible to researchers.

Theoretically, the best ground classification results are achieved by segmenting the areas based on their characteristics (complexity of landscape, type of vegetation, etc.). Thereafter, the most suitable algorithm and parameters for these circumstances need to be applied, complemented by visual verifications and manual corrections. Such procedures are difficult to automatize and require manual work. For a very quick and coarse ground classification, using a single algorithm and parameter combination, such as in the present study, might be useful.

In this study, the best ground determining results were achieved with the MCC algorithm. Since the script-based MCC algorithm can be easily automated and the determination of suitable parameters is relatively straightforward, it can be used as an alternative to expensive commercial

programs. It is, however, important to keep in mind that although filtering algorithms have been constantly refined, they are still far from an ideal where their results could be blindly trusted. The results still need to be visually checked to confirm that the classifications are correct.

All the tested filtering algorithms rely only on 3-D coordinates. As seen, this approach causes errors in more complex conditions. To counter this effect, future research should aim to include other constraints to the process. For example, using the ALS intensity values or making use of aerial photographs which are sometimes simultaneously taken with ALS flights or finding a way to automatically segment areas by their characteristics, followed by the filtering parameter selection and application of the most suitable algorithm for different segments.

Acknowledgments

This study is supported by the Estonian Environmental Technology R&D Programme KESTA, research project ERMAS AR12052. The ALS data used in this study were received from the Estonian Land Board under the license (Contract No. ST-A1-2422, 22/06/2012). The two anonymous reviewers are thanked for their constructive comments.

References

1. E. J. Huising and L. M. Gomes Pereira, "Errors and accuracy estimates of laser data acquired by various laser scanning systems for topographic applications," *ISPRS J. Photogramm. Remote Sens.* **53**(5), 245–261 (1998).
2. A. Gruno et al., "Determining sea surface heights using small footprint airborne laser scanning," in *Proc. Remote Sensing of the Ocean, Sea Ice, Coastal Waters, and Large Water Regions 2013 (Conference 8888)*, p. 88880, SPIE, Dresden, Germany (2013).
3. X. Meng, N. Currit, and K. Zhao, "Ground filtering algorithms for airborne LiDAR data: a review of critical issues," *Remote Sens.* **2**(3), 833–860 (2010).
4. K. Zhang and D. Whitman, "Comparison of three algorithms for filtering airborne lidar data," *Photogramm. Eng. Remote Sens.* **71**, 313–324 (2005).
5. G. Sithole and G. Vosselman, "Experimental comparison of filter algorithms for bare-earth extraction from airborne laser scanning point clouds," *ISPRS J. Photogramm. Remote Sens.* **59**(1–2), 85–101 (2004).
6. W. T. Tinkham et al., "Comparison of two open source LiDAR surface filtering algorithms," *Remote Sens.* **3**, 638–649 (2011).
7. G. Goncalves and L. G. Pereira, "Assessment of the performance of eight filtering algorithms by using full-waveform LiDAR data of unmanaged eucalypt forest," in *Proc. SilviLaser 2010*, pp. 187–196, Freiburg, Germany (2010).
8. N. S. Sulaiman, Z. Majid, and H. Setan, "DTM generation from LiDAR data by using different filters in open-source software," *Geoinform. Sci. J.* **10**(2), 89–109 (2010).
9. K. Zhang and Z. Cui, *Airborne LIDAR Data Processing and Analysis Tools*, National Center for Airborne Laser Mapping, Miami, Florida (2007).
10. P. Axelsson, "DEM generation from laser scanner data using adaptive TIN models," *Int. Arch. Photogramm. Remote Sens.* **XXXIII**(Part 4), 111–118 (2000).
11. G. Vosselman, "Slope based filtering of laser altimetry data," *Int. Arch. Photogramm. Remote Sens.* **XXXIII**(Part 3), 935–942 (2000).
12. K. Zhang et al., "A progressive morphological filter for removing non-ground measurements from airborne LIDAR data," *IEEE Trans. Geosci. Remote Sens.* **41**, 872–882 (2003).
13. J. S. Evans and A. T. Hudak, "A multiscale curvature algorithm for classifying discrete return LiDAR in forested environments," *IEEE Trans. Geosci. Remote Sens.* **45**, 1029–1038 (2007).
14. K. Kraus and N. Pfeifer, "Determination of terrain models in wooded areas with airborne laser scanner data," *ISPRS J. Photogramm. Remote Sens.* **53**, 193–203 (1998).
15. R. J. McGaughey, *FUSION/LDV: Software for LIDAR Data Analysis and Visualization*, U.S. Department of Agriculture Forest Service, Seattle, Washington (2011).
16. M. Isenburg, "lasground README," http://www.cs.unc.edu/~isenburg/lasground/download/lasground_README.txt, RapidLasso LAStools, Gilching, Germany (2014).

17. M. A. Brovelli and S. Lucca, "Filtering LiDAR with GRASS: overview of the method and comparisons with Terrascan," *Ital. J. Remote Sens.-Rivista Italiana Di Telerilevamento* **43**(2), 93–105 (2011)..
18. R. M. Haralick, S. R. Sternberg, and X. Zhuang, "Image analysis using mathematical morphology," *IEEE Trans. Pattern Anal. Mach. Intell.* **PAMI-9**(4), 532–550 (1987).
19. C. Briese, "Extraction of digital terrain models," in *Airborne and Terrestrial Laser Scanning*, G. Vosselman and H. G. Maas, Eds., pp. 135–168, CRC Press LLC, Boca Raton, FL (2010).
20. A. Soininen, "TerraScan User's Guide," Terrasolid, Helsinki, Finland (2012).

Kalev Julge received his MSc degree in geodesy from Tallinn University of Technology (TUT, Estonia) in 2013. Currently, he is pursuing studies towards a PhD degree and works as a research scientist at the TUT. His main research interest is remote sensing by methods of airborne and terrestrial laser scanning.

Artu Ellmann received his MSc degree in geodesy from Moscow State University of Geodesy and Cartography in 1993 and his PhD degree from the Royal Institute of Technology (KTH) in Stockholm in 2004. Currently, he is a professor in geodesy at the Faculty of Civil Engineering in TUT, national correspondent to the International Association of Geodesy (IAG) since 2006. His research interests include remote sensing, physical geodesy (gravity field and geoid modeling in particular), and engineering surveying.

Anti Gruno received his MSc degree in geodesy from Tallinn University of Technology in 2011. He has worked since 2007 in the Department of Photogrammetry at the Estonian Land Board and also as a researcher at TUT. His research interests include ALS data enhancements and applications.

PUBLICATION IV

© 2014 Authors. This work is distributed under the Creative Commons Attribution 3.0 License.

Julge, K., Ellmann, A. (2014). Combining Airborne and Terrestrial Laser Scanning technologies for measuring complex structures. Cygas, D. *Selected papers of the 9th International Conference on Environmental Engineering*, Vilnius, Lithuania, 22-23, May, 2014. (1–7). Vilnius: Vilnius Gediminas Technical University Press "Technika".10.3846/enviro.2014.213.



Combining Airborne and Terrestrial Laser Scanning technologies for measuring complex structures

Kalev Julge, Artu Ellmann

Tallinn University of Technology, Faculty of Civil Engineering, Dept. of Road Engineering, Chair of Geodesy, Ehitajate tee 5, Tallinn 19086, Estonia

Abstract

In recent years using laser scanning has gained popularity in measuring different objects, complementarily to traditional surveying and mapping methods. Terrestrial Laser Scanning (TLS) is often used for high-resolution accurate data acquisition of complex structures such as buildings, facades, etc. Airborne Laser Scanning (ALS) on the other hand can be used for remote surveying of large areas. Although TLS and ALS are generally used in separate applications, there are some possibilities where they may efficiently complement each other. In this study TLS and ALS data are combined for surveying a water tower where the façade is measured with TLS and the roof-top with standard high-elevation ALS. The advantages and shortcomings of using TLS along with ALS for measuring complex and non-standard structures are analyzed, the possible sources for errors are determined and some recommendations for methodology of field measurements and data processing in order to eliminate/reduce systematic errors are given. The estimated accuracy of combining TLS and ALS data after implementing the necessary adjustments was found to be about 5 cm.

Keywords: LIDAR; Airborne Laser Scanning; Terrestrial Laser Scanning; Point Cloud.

1. Introduction

Laser scanning is a remote sensing method which utilizes Light Detection and Ranging (LIDAR). It uses laser pulses to measure distances to objects and based on these distances (and the angles of laser beams) calculates the 3D coordinates of measured points. The LIDAR device can be mounted on a tripod (terrestrial laser scanners – TLS), an aircraft (airborne laser scanning – ALS) or a ground vehicle (mobile laser scanning – MLS). In this study combining TLS and ALS is analyzed. TLS and ALS are usually used separately due to their very different characteristics, to our present knowledge there is no dedicated research published on combining them at surveying complex structures or buildings. However, a practical experiment for creating a 3D model of the medieval Old Town in Tallinn (Estonia) was accomplished in 2012. The resulting 3D model consists of over 700 buildings (and streets between them) covering an area of 121 ha. The facades of the buildings were captured with a combination of TLS and MLS at a resolution of at least 1000 points/m². The ALS campaign, conducted specially for the project, was helicopter-flown at a low altitude (500 m), thus resulting in a relatively dense point cloud of 100 points/m² [1].

In many countries nation-wide ALS campaigns have been launched. These are proceeded at higher elevation (up to a few kilometers), thus resulting in sparser data (~0.3...1.5 points/m²). However, these national programmes make ALS data more accessible to a common user, as there is no need for arranging expensive single-purpose ALS campaigns. Therefore, this study analyses the possible use of standard high-altitude ALS campaigns for capturing complex structures.

Standard high-altitude ALS is generally considered not suitable for the task in hand due to the relatively low resolution and accuracy compared to TLS. Therefore it is/should be used as more of a last resort when TLS of the entire object is not feasible. TLS is much more detailed with an average spatial resolution of up to a point for every few mm, while ALS point cloud is less dense. Therefore TLS is used for surveying of in situ objects such as buildings, bridges, road surfaces, etc., whereas ALS to measure large areas such as pit mines, infrastructure objects and ground surfaces for compilation of Digital Terrain Models. In some instances some parts of the structures cannot be covered with only TLS. An example of this are high-rise buildings with pitched roofs. This means that either the scanner cannot be placed on the roof-top or the roof-top is not measurable from the ground. In these cases ALS data can be used to complete the point cloud of the structure. This case

study is based on laser scanning a water tower, where the facades were measured with TLS. However TLS of the roof proved to be impossible. In order to complete the point cloud, ALS data was used.

The outline of the paper is as follows. First the basic principles of laser scanning methods and aspects that affect this study are reviewed, after which some possible applications and problems of combining TLS and ALS data are discussed. Then the case study at hand is described including the methodology and achieved results. Lastly, a brief summary concludes the paper.

2. Review on TLS and ALS principles

TLS is used to gather high-resolution accurate spatial data about objects such as buildings, bridges, statues, road surfaces or other structures. It is especially useful in situations where the traditional surveying techniques do not provide enough accuracy or details, e.g. complicated facades, curved objects, etc. With TLS it is possible to gather data with an accuracy of cm or even more [2] and at a resolution up to a few mm. However, in order to save time and decrease the file sizes, the resolution is usually set at a few cm depending on the complexity of the measured object.

Point clouds measured from different stations are registered, i.e. a spatial transformation that aligns different point sets by common targets or overlapping surfaces is used. The point cloud may be calculated in some known coordinate system or in some relative coordinate system specific to the certain project. In the first case, it is achieved by using coordinated geodetic reference points.

TLS can theoretically be used to capture surfaces within 300 m range but in practice the reasonable distance to an object is about 50–100 m, varying according to specific scanner and characteristics of the surface. The laser beam has a tendency to diverge, i.e. the laser “foot-print” gets increasingly larger the further it travels. It is advantageous that the laser beam size remains small as it reaches a target, thus shorter ranges are preferable. This enables acquiring finer details.

In ALS the LIDAR device is placed on an aircraft, e.g. plane, helicopter or unmanned aerial vehicle (UAV). ALS is used more in applications where there is a need to quickly cover large areas, for example measuring ground surfaces for compilation of Digital Elevation Models, infrastructure objects, etc., or areas otherwise inaccessible, such as deserts or glaciers. As a rule, ALS point cloud is much less dense than a TLS point cloud and varies usually from 0.1...20 points per m² depending on many factors. Basically, acquiring more high-resolution data requires more time, flight hours and most importantly more funds.

In order to determine the position and orientation of the aircraft at any moment, a Global Navigation Satellite System (GNSS) receiver and an Inertial Measurement Unit (IMU) are used. GNSS receiver measures the position and IMU records the pitch, roll and yaw of the aircraft. Since the coordinates from GNSS are used then the resulting point cloud is in geodetic coordinates and can be transformed to any local system. Given that the calculation involves so many parameters, then the accuracy of ALS is less than that of TLS, usually estimated at 5–15 cm in favorable conditions [3][4].

As ALS is generally performed at an altitude of 1000...4000 m, the divergence of the laser beam is much more pronounced and can reach up to 0.5 m in diameter. This means that capturing fine detail is impossible and it can cause some measurements errors on surfaces that are at an angle to the laser beam as it hits a large area that is not the same distance from the LIDAR device.

In many countries nation-wide ALS campaigns have been launched. Some are an on-going process, some have been completed and some are already on next cycles. Examples in Europe include Germany, Netherlands, Austria [5], Switzerland [6], Finland [7] and Estonia. ALS is cost effective when used to cover very large areas, so for using ALS in small projects is usually not practical. This existing data makes ALS much more accessible. Using UAV as a platform for laser scanning has evolved recently and with further refinement can probably become a viable cost-effective option for use in smaller applications.

3. Combining TLS with ALS – advantages, shortcomings and applications

In some cases combining these laser scanning technologies can be useful – in applications where it is not possible to cover the entire object with only one method or in projects where for different steps of the process, different methods are better suited. For example, in creating 3D models of buildings, structures or built environment as a whole. With TLS it is possible to gather high-resolution data about building facades but the roofs are most likely not visible and often not accessible. Contrastingly in ALS data, the roof-tops are captured well, whereas there is little usable data about the facades.

Another use would be monitoring the volume of earthworks at large sites. ALS could be used to create the initial model of the whole area, where as TLS could be used to monitor the cut and fill volumes during the process. It would also be possible to monitor coastal processes by using ALS to detect whether there are significant changes and in case there are, to use TLS to accurately measure the extent of the changes. Another example would be combining ALS and TLS to monitor the extent of land slides or debris flows by using ALS data to reconstruct a pre-event surface and TLS to measure and create a post-event surface [8]. These are just a few possible examples.

Now although combining TLS with ALS obviously has potential, there are some issues. ALS data is much less dense and less accurate than TLS. In applications where the desired accuracy and data resolution are that of TLS, ALS does not meet the expected demands. Also given the relatively large differences in spatial resolution, the methods for data processing

have to be altered to best suit the data in hand. This is especially pronounced while using automatic filtering, segmenting, modelling, etc. algorithms that require the use of different parameters depending on the point cloud density.

Additionally, combining different laser scanning methods raises a few accuracy problems. The main issue is how to ensure that the TLS and ALS data are aligned to each other, i.e. there are no systematic errors present between them. First of all, TLS could adopt an arbitrary coordinate system where the x, y, z coordinates as well as the orientation are random. This saves time from coordinating reference points and is usually proceeded if the location of the object in the national coordinate system is not required. ALS results are most commonly always referred to national geodetic reference frame.

Even if the TLS and ALS point clouds are using the same coordinate system then there is still a possibility that systematic errors would occur. This is caused by the fact that most likely TLS and ALS measurements are done by using different reference marks. For example the TLS is done by using geodetic points on the ground and ALS uses data from GNSS systems and IMU to calculate the position and orientation.

The problem of unifying ALS and TLS point clouds could be easily solved by finding distinguishable points in both point clouds and moving one of the clouds to the correct location. Unfortunately, ALS data is usually not dense enough to accurately determine the coordinates of a certain point. Therefore it is necessary to find the value of the systematic errors by other means.

The systematic error of elevation can be determined by finding horizontal surfaces (e.g. a nearby parking lot) that are present on both point clouds. By comparing the elevation differences between the same surface measured by TLS and ALS, the extent of the systematic error should become evident. Points near the edge of the surface should be discarded to minimize the errors caused by shifts at the x, y plane and the large size of the ALS laser beam footprint on the ground caused by divergence. For example, a part of the ALS pulse might reflect from a curbstone instead of the pavement. The larger the surface area the better because a larger sample amount reduces the influence of inaccurate points.

Eliminating systematic errors in planar coordinates can be a bit more complicated. As mentioned earlier, ALS point clouds tend not to be dense enough to accurately determine certain points or edges. For this the ALS data need to be processed first. The aim is to find planar surfaces that meet, e.g. facets of a pitched roof. Now although the edge is not clearly defined in the point cloud (Fig. 1a), the points on the surfaces can be used to construct planes and the line of intersection between these planes is the edge (Fig. 1b). If there are three intersecting planes then this results in a single corner point.

Using these common edges or points, it is possible to match the location in ALS and TLS data and register the point clouds. Obviously, this method can be proceeded only in urban areas where there are clearly defined artificial sharp edges. Finding clearly defined natural features in non-built areas is unlikely though. Also since these edges and points are most likely found on roofs in ALS data, then there is no guarantee that they are visible in TLS point clouds.

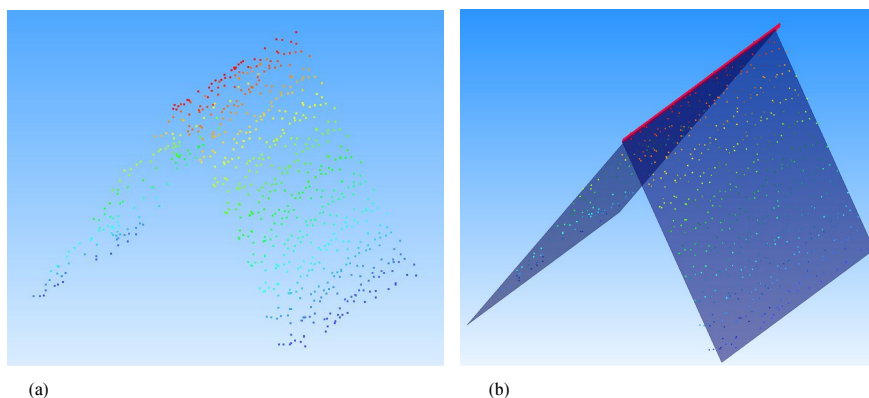


Fig. 1. Finding edges from (a) an ALS point cloud of a pitched roof by (b) constructing planes on roof facets and finding the intersection (red line)

4. Case study

This study tackles a TLS survey of a 30 m tall historic water tower (Fig. 2a). In this case the scanning of the roof-top proved to be impossible because the cone shaped pitched roof of the high-rise water tower was not visible from the ground and it was impossible to place the scanner tripod on it. Note also, that the surrounding buildings were lower than the water tower, thus it would not have been beneficial to place the scanner on a balcony or a roof of a neighboring building. So the only possibility was using ALS data to complete the point cloud of the water tower (Fig. 2b).

The TLS facade survey was conducted with a pulse-based Leica ScanStation C10. The resolution of the TLS data was 2500 points/m² (2x2 cm). The ALS data were received from the Estonian Land Board which uses a Leica ALS50-II airborne laser scanner. The ALS data tested originated from four different years – 2008, 2009, 2012 and 2013 (see also Table 1). The 2008 campaign was flown at a height of 1500 m and the point density was 1.2 points/m². The other three campaigns had a flight height of 2400 m with resulting point density of 0.3...0.4 points/m².

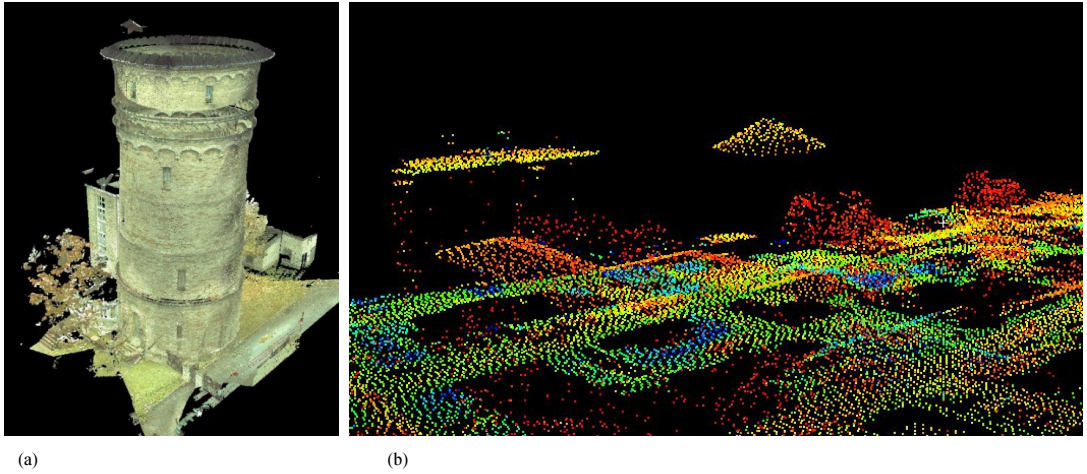


Fig. 2. (a) Point cloud of TLS data where the roof-top is missing. (b) Point cloud of ALS data where the cone shaped roof is clearly visible

In order to take into account the possible systematic errors in elevation, three horizontal reference surfaces near the water tower were selected (Fig. 3a). One of these was a 200 m² parking lot right next to the water tower (surface 1) and the others were terraces of a large building with an area of 100 m² each (surface 2&3) located some 125 m away. These were the only horizontal surfaces near-by that had remained unchanged (no roadwork, etc.) since the first ALS flight in 2008. The reference surfaces were measured with a regular 1.5 m steps by a total station using the same initial points that were used for the TLS orientation.

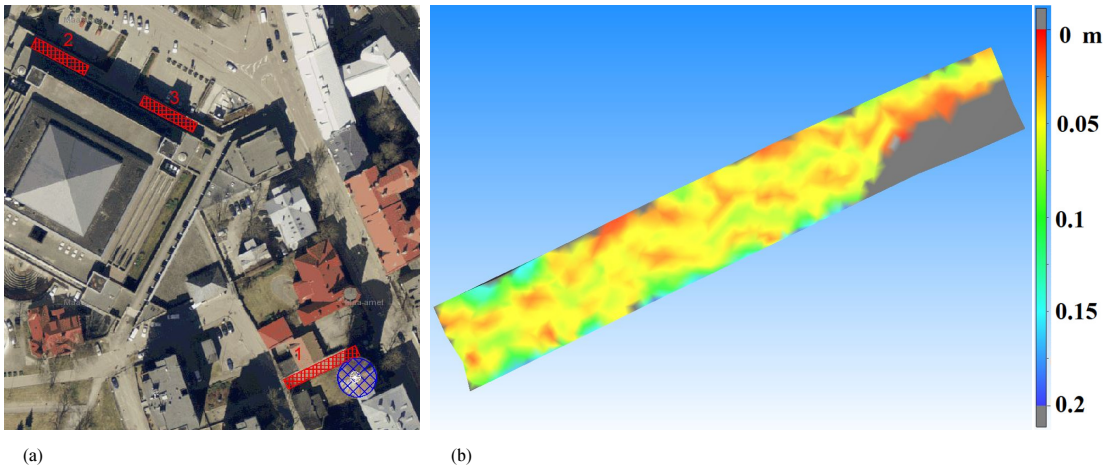


Fig. 3. (a) The location of the ALS reference surfaces (red hatch) with respect to the water tower (blue hatch). (b) Elevation differences of 2008 ALS points from the reference surface 1. ALS points are on average 0.05 m higher than the reference surface

5. Data processing and results

In order to find the systematic errors in elevation, the three surfaces were separated from the rest of the ALS point cloud and obvious measurement blunders were removed. Based on these cleaned point clouds Triangulated Irregular Network (TIN) models were formed. TIN models derived from ALS data were compared to reference TIN models derived from total station measurements in TLS coordinate system. The average elevation differences were found along with the standard deviation, cf. Table 1 and Fig. 3b.

It was found that the detected discrepancies between the less dense (0.3...0.4 points/m²) ALS data (the 2009, 2012 and 2013 flights) and reference surfaces appeared to be inadmissible. The standard deviations of detected discrepancies were also considerably large. The average of discrepancies exceeded 10 cm and standard deviations 4 cm, thus it was impossible to accurately estimate the presence and values of systematic errors and shifts in elevation. To use the sparser data, larger reference surfaces are required to increase the sample size, which would allow reducing the influence of measurement errors. This would enable more accurately determining the systematic error values.

Table 1. The statistics of ALS data and the comparisons between the ALS and reference surfaces

ALS data			Average elevation difference between the ALS and reference surfaces [m] / No. of ALS points on reference surface / Standard deviation [m]			
Year	Flight height [m]	No. of ALS roof-top points	Reference surface 1 (200 m ² , 51 ground survey points)	Reference surface 2 (100 m ² , 36 ground survey points)	Reference surface 3 (100 m ² , 38 around survey points)	Average
2008	1500	225	0.054 / 181 / 0.028	0.051 / 94 / 0.024	0.047 / 107 / 0.018	0.051 / 127 / 0.023
2009	2400	62	0.111 / 54 / 0.059	0.040 / 27 / 0.027	0.060 / 25 / 0.036	0.070 / 35 / 0.040
2012	2400	61	0.015 / 54 / 0.041	-0.016 / 24 / 0.033	0.003 / 25 / 0.030	0.001 / 34 / 0.034
2013	2400	50	0.028 / 55 / 0.045	0.011 / 25 / 0.038	0.015 / 26 / 0.035	0.018 / 35 / 0.038

Using the distorted data would have probably decreased the accuracy by adding more noise to the point cloud. Since these ALS campaigns were flown at a height of 2400 m as opposed 1500 m of the 2008 campaign, the laser beam divergence was larger resulting in less accurate measurements. Also there were fewer points which magnifies the influence of erratic ALS points. This makes it difficult to correctly register TLS and ALS point clouds which would in return distort the model of the object (Fig. 4).

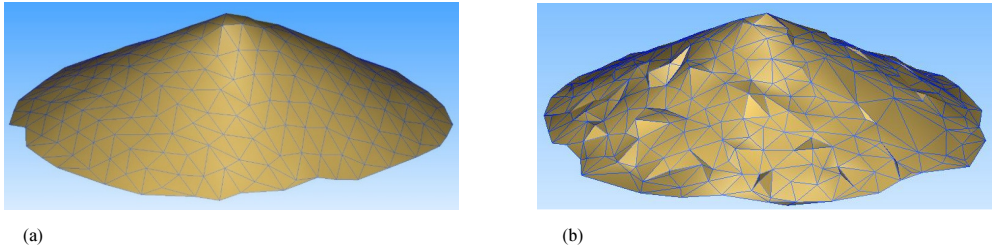


Fig. 4. Mesh models of the roof-top (a) based on the ALS 2008 points only, (b) based on all ALS points from the four campaigns illustrating the distortions to the model shape caused by alignment and measurement errors

Since it was impossible to distinguish the values of the systematic errors, the measurements seemed to be less accurate and there was a risk of incorrect alignment, then it was decided to discard the 2009, 2012 and 2013 ALS data and use only denser 2008 ALS data for modeling the shape of the roof-top.

In more dense (1.2 points/m²) ALS data from 2008, the elevation differences were more uniform and a systematic bias as of 0.051 m was detected (Fig. 3b). In other words, the ALS data appeared to be higher than the TLS data. This 1D bias was removed from the ALS point cloud to conform with TLS data. The resulting average standard deviation between the two datasets obtained was 2.3 cm, cf. Table 1.

Based on this, it can be presumed that a point density of at least 1 point/m² is required to properly register different point clouds. If this is the case, then finding a systematic error is possible. Otherwise the data is too sparse and inaccurate to distinguish a clear trend with any certainty.

This left the problem of the alignment in the horizontal x, y plane. The roof-top was not visible from the ground and therefore was not represented in TLS point cloud either. Unfortunately, no other features (point, edge) were clearly distinguishable in ALS point cloud either, thus finding common points in TLS and ALS data was impossible. However, since the water tower was circular with a cone shaped roof, then this allowed to align the centers of the tower (originating from the TLS data) and that of the roof (ALS data).

The planar coordinates of the tower's center were found by calculating the center point of a circle that represented the outline of the tower's cross-section. The roof's center was not distinguishable directly from the point cloud or the TIN model of the roof (see also Fig. 4a). Instead the center was determined by modelling a best fit cone based on the roof-top points. In this case the cone's vertex defines also the center of the roof.

The resulting best fit cone is still an approximation. To find the extent of deviations, the root mean square error (RMSE) of the modeled cone with respect to the ALS points was found using:

$$RMSE = \sqrt{\frac{\sum_{i=1}^n \theta_i^2}{n}} \quad (1)$$

where θ_i is the distance of i -th ALS point from the best fit cone along the surface normal, n is the number of observations (225 ALS points in this particular case, see Table 1) and $i = 1, 2, \dots, n$.

The RMSE was found to be 0.050 m with the errors distributed quite evenly between $-0.1 \dots 0.1$ m (Fig. 5). The accuracy of approximating a shape depends on the relative accuracy of point coordinates, as well as the number of available points.

The more accurate and high-resolution the data are, the better results of the best fit shape approximation can be achieved. This means that modelling based on sparse ALS point clouds can cause significant errors. First, because there are larger gaps between points, yielding thus that some details get lost. Secondly, a smaller amount of points reduces the quality of shape approximation.

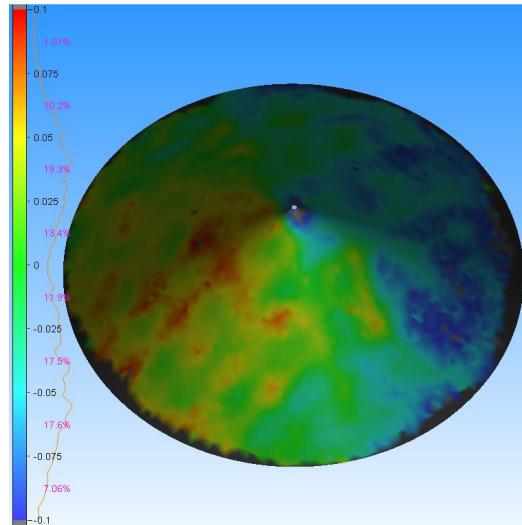


Fig. 5. Comparison between the best fit cone model of the roof-top and the initial TIN model derived from the 2008 ALS points. The root mean square error of discrepancies RMSE = 0.05 m. Next to the legend is a line histogram presenting the percentages of deviations from the cone in the given range

Approximating shapes can potentially cause additional shifts and errors. This was also evident in this case, since the best fit cone had to be shifted horizontally by as much as 25 cm with respect to the center of the tower (Fig. 6a). Such a large shift is unlikely to be only caused by measurement errors or systematic errors between TLS and ALS data. The shift in planar coordinates of ALS data was adjusted by moving the best fit cone in the 2D horizontal plane, so that the cone vertex coincided with the tower's center. This method can potentially be performed with other types of roofs as well. For example, aligning the ridge of a gabled roof with the center line of a building.

By taking into consideration the systematic errors and shifts, it is possible to unify the TLS and ALS point clouds (Fig. 6b). Although it is clear that ALS data is not as high-resolution nor accurate as TLS data, ALS can still be useful if there are no other means to measure certain objects. It is usually not possible to capture fine details with standard ALS campaigns, as the point density is not sufficient to clearly distinguish small objects, e.g. chimneys, drainage elements, ventilation equipment, etc. For example, in this case, the gable dormer on the roof is almost indistinguishable in the ALS data.

Therefore ALS is useful in modelling rough shapes of roofs, when the shape can be approximated by using different shapes, e.g. planes, cones, pyramids, etc. Considering all the possible errors – measurement errors; systematic errors in elevation and in planar coordinates between TLS and ALS; shape approximation errors and shifts caused by shape approximation, then the accuracy of combining TLS and ALS data can reach ca 5 cm. This is after making the necessary adjustments to correct (or at least reduce) these errors and it also depends on the quality of data. Further research with a larger sample size is necessary to confirm this estimation. If there are no distinguishable features (common points, edges, horizontal surfaces) to register different point clouds and reduce systematic errors, then the accuracy reduces significantly.

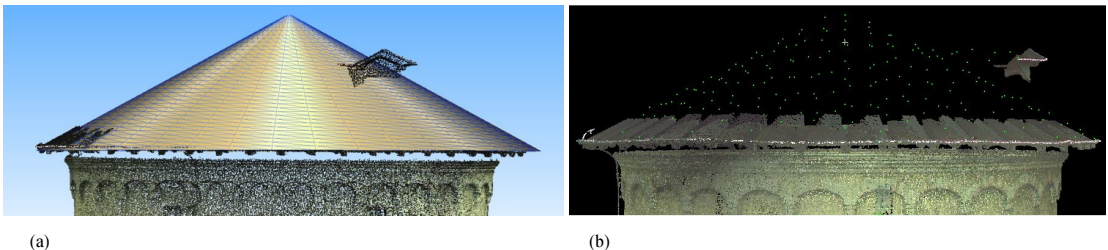


Fig. 6. (a) Best fit cone model of the roof-top before eliminating the shift. Note the TLS points of roof soffit are showing through the roof surface on the left-hand side. (b) Combined point cloud of the water tower, both TLS and ALS data are used. Note the different resolutions of ALS and TLS data. The gable dormer partially captured with TLS is almost indistinguishable in ALS data

6. Conclusions

TLS and ALS are usually used in different applications due to the difference in their characteristics. However, there are some cases where their combination could be beneficial. In this study ALS data made possible the completion of the point cloud of a water tower.

ALS data becomes much more accessible for practical use, provided that there are ALS data from country-wide campaigns available. Otherwise the expenses of single-purpose ALS campaigns might be too large to be practical and feasible. In standard ALS campaigns capturing as fine details is usually impossible. This is caused by the lower resolution of the data and the larger divergence of the laser beam. Also based on this study, significantly better results can be achieved if the point cloud density is at least 1 point/m². Even though fine detail is lost, the basic shapes can be approximated by using best fit shapes - planes, cones, pyramids, etc.

In order to find the shifts and systematic errors between TLS and ALS data, common features need to be distinguished from both point clouds. Finding common points outright from the point clouds is usually impossible because the resolution of the data is not sufficient. Therefore other methods are to be used. To find the extent of elevation systematic errors, horizontal surfaces that are present in both point clouds can be used by comparing the average elevations between the surfaces. A clear trend should be looked for. If the discrepancies are very large then that suggests measurement errors and the results might be distorted. To find the shifts in planar coordinates, common edges should be identified. This can be achieved by constructing intersecting planes using surfaces in the point cloud (or some other approximate shape and surface). The intersection line between planes is the edge. By finding a number of these, there is a possibility to register the point clouds. In this study the planar shift was corrected by approximating a cone and aligning it with the center of the tower.

The estimated accuracy of combining TLS and ALS data, after adjusting for the systematic errors, is about 5 cm, depending also on the quality of data. If there is no possibility to find the values of systematic errors, then the accuracy reduces significantly. TLS data are significantly higher-resolution and more accurate than ALS data, thus with TLS most of the details are captured, whereas with ALS fine detail is normally lost. Therefore modelling based on TLS and ALS data is slightly different caused by the different resolutions. Modelling based on ALS requires more approximation and interpolating, whereas modelling based on TLS is more precise. This will be further looked at in upcoming research.

Acknowledgements

This study is supported by the Estonian Environmental Technology R&D Programme KESTA, research project ERMAS AR12052. The ALS data used in this study was received from the Estonian Land Board under the license contract ST-A1-2422, 22/06/2012. The used Leica ScanStation C10 and licensed data processing software were acquired within frames of the Estonian Research Infrastructures Roadmap object Estonian Environmental Observatory (funding source 3.2.0304.11-0395, project No. AR12019). The prime author is supported by a NORDPLUS co-operation project AGES (Access to Geodetic Education for Society, HI-2012_1A-30040).

References

- [1] Terratec Terrapro. 2012. Report of Aerial Photography, Airborna Laser Scanning, Mobile Laser Scanning, Terrestrial Laser Scanning for City of Tallinn.
- [2] Dorminger, P.; Szekely, B.; Zamolyi, A.; Roncat, A. 2011. Automated Detection and Interpretation of Geomorphic Features in LiDAR Point Clouds, *Vermessung & Geoinformation* 2011(2): 60–69.
- [3] Gruno, A.; Liibus, A.; Ellmann, A.; Oja, T.; Vain, A.; Jürgenson, H. 2013. Determining sea surface heights using small footprint airborne laser scanning, in *Remote Sensing of the Ocean, Sea Ice, Coastal Waters, and Large Water Regions 2013 (Conference 8888)*, Dresden, Germany, 2013. Spie – International Society For Optical Engineering. <http://dx.doi.org/10.1117/12.2029189>
- [4] Huising, E. J.; Gomes Pereira, L. M. 2004. Errors and accuracy estimates of laser data acquired by various laser scanning systems for topographic applications, *ISPRS Journal of Photogrammetry and Remote Sensing* 53(5): 245–261. [http://dx.doi.org/10.1016/S0924-2716\(98\)00013-6](http://dx.doi.org/10.1016/S0924-2716(98)00013-6)
- [5] Mandlbürger, G.; Vetter, M.; Milenkovic, M.; Pfeifer, N. 2011. Derivation of a countrywide river network based on Airborne Laser Scanning DEMs - results of a pilot study, in *Proc. of the 19th International Congress on Modelling and Simulation, Perth, Australia, 2011*, 2423–2429.
- [6] Artuso, R.; Bovet, S.; Streilein, A. 2003. Practical Methods for the Verification of Countrywide Terrain and Surface Models, in *The internal archives of photogrammetry, remote sensing and spatial information sciences, Dresden, Germany, 2003*.
- [7] Ahokas, E.; Kaartinen, H.; Hyypä, J. 2008. On The Quality Checking of the Airborne Laser Scanning Based Nation Wide Elevation Model in Finland, in *The internal archives of the photogrammetry, remote sensing and spatial information sciences, Beijing, China, 2008*, 267–270.
- [8] Bremer, M.; Sass, O. 2012. Combining airborne and terrestrial laser scanning for quantifying erosion and deposition by a debris flow event, *Geomorphology* 138: 49–60. <http://dx.doi.org/10.1016/j.geomorph.2011.08.024>

PUBLICATION V

© 2014 IEEE. Reprinted, with permission, from

Julge, K., Eelsalu, M., Grünthal, E., Talvik, S., Ellmann, A., Soomere, T., Tõnisson, H. (2014). Combining airborne and terrestrial laser scanning to monitor coastal processes. 2014 IEEE/OES Baltic International Symposium, May 26.-29.2014, Tallinn, Estonia: 2014 *IEEE/OES Baltic International Symposium "Measuring and Modeling of Multi-Scale Interactions in the Marine Environment"*: Tallinn, Estonia, May 26-29, 2014. IEEE, 1–10. (IEEE Conference Proceedings).10.1109/BALTIC.2014.6887874.

Combining Airborne and Terrestrial Laser Scanning to Monitor Coastal Processes

K. Julge¹, M. Eelsalu², E. Grünthal^{1,4}, S. Talvik¹, A. Ellmann¹, T. Soomere², H. Tõnisson³

¹Department of Road Engineering, Tallinn University of Technology, Ehitajate tee 5, 19086 Tallinn, Estonia

²Institute of Cybernetics at Tallinn University of Technology, Akadeemia tee 21, 12618 Tallinn, Estonia

³Institute of Ecology, Tallinn University, Uus-Sadama 5, 10120 Tallinn, Estonia

⁴Estonian Land Board, Mustamäe tee 51, 10621 Tallinn, Estonia

Abstract—This study explores the potential of joint use of terrestrial (TLS) and airborne laser scanning (ALS) to quantify rapid and spatially inhomogeneous changes to the subaerial beach and to characterize the intensity of coastal processes. This remote sensing technology that uses scanning laser pulses for acquiring high-resolution three-dimensional surface of the measured object is applied to beach segment of the Piritä Beach (Tallinn Bay, the Baltic Sea). The extent and distribution of erosion and accumulation spots are analyzed by means of creating and comparing two digital terrain models of these areas from scanning point clouds obtained in different seasons. After elimination of systematic errors the ALS/TLS combination yields sub-decimeter accuracy for height determination of the beach. The analysis reveals not only the corresponding volume changes in the study area but also several features of internal dynamics of the beach across and along the waterline that are overlooked by classical monitoring methods. The benefits and shortcomings of combining the two laser scanning methods for monitoring coastal processes and the accuracy of the results are also discussed.

I. INTRODUCTION

The beaches of the Baltic Sea (Fig. 1) develop in relatively rare conditions of a large, relatively young and shallow, micro-tidal, seasonally ice-covered water body of extremely complicated shape [1]. Their key driving mechanism is a highly intermittent wave regime that is accompanied by aperiodic variations of the water level, seasonal ice cover [2], and frequent presence of conditions favorable for unexpectedly high run-up [3] and set-up [4]. The most interesting coastal segment in this respect is the southern coast of the Gulf of Finland where the beaches mostly overlie ancient dunes in deeply indented bays that are geometrically sheltered from a large part of the directions of strong winds. The volume of sediment and the magnitude of littoral drift are modest here and the entire coast in question generally suffers from sediment deficit [5],[6]. The beaches are to some extent stabilized by relatively rapid postglacial uplift (up to 2 mm/year) [7].

A specific feature of this coast is that the strongest storms tend to blow from directions from which winds are not very frequent [8]. Thus, differently from the classical examples of bay beaches [9], the bayhead beaches here are only partially sheltered from intense waves. This uplift combined with relatively low but intermittent hydrodynamic activity and limited supply of sand has led to a specific type of “almost equilibrium” beaches [10]. They often reveal step-like evolution: slow evolution is interspersed with rare but rapid

events that take place when high waves from an unusual direction occur simultaneously with high water levels before or after the ice season [11],[12].

A significant challenge in the understanding of the functioning of such beaches is to characterize and quantify the changes during the stages of their slow evolution. The key question is whether these beaches (or sections) gain or lose sediment in these stages. As the depth of mobilization of sediments frequently is fairly shallow and only a thin veneer of unconsolidated material may become mobile during these stages [9], the accuracy and spatial resolution of standard profiling of beaches is not sufficient to resolve the resulting changes, in particular, to recognize whether the middle parts of the beach show a healthy (concave) or problematic (convex) shape.

This contribution investigates the suitability of novel remote sensing methods like terrestrial (TLS) and airborne laser scanning (ALS) for monitoring coastal processes. ALS datasets are often used for different modelling and engineering



Figure 1. The Baltic Sea and the Gulf of Finland. The box indicates the study area in Tallinn Bay (see Fig. 2).

applications such as quantification of sediment volume transported by a major debris flow event [13] or assessments of riverbank erosion [14]. In particular, one of the well-known applications of ALS technique is forming Digital Elevation Models (DEM). The ALS equipment is mounted in an aircraft. The altitudes of surveying routes could reach up to a few kilometers, thus resulting in comparatively sparse data ($\sim 0.1\text{--}4$ points/m²). Repeated ALS measurements over the same area makes possible the creation of exact surface models for different time epochs and therefore enables the detection of inter-epoch volume and mass changes.

The laser scanning technique is capable of gathering accurate and high-resolution 3D data which covers the entire surface area of the beach. The advantage is that the entire area of interest can be included in the analysis while only changes along single profiles can be identified using classical methods of coastal monitoring. Thus, the ALS enables more accurate determination of the exact location and volumes of erosion and accumulation. In many countries nation-wide ALS campaigns have commenced, including Estonia [15]. Therefore ALS data of various vintages may already be accessible for regions of interest. Monitoring of coastal processes using ALS data has already been carried out, e.g. along the Baltic Sea shoreline by [16],[17].

This study attempts to widen the applicability and enhance the quality of standard ALS data products by using in situ TLS data for minimizing systematic errors between ALS and TLS datasets from different epochs. Combining TLS and ALS has been used, for example, to quantify the sediment volume transported by a major debris flow event in the Austrian Alps [13]. We explore the potential of the joint use of the TLS (mounted on a tripod) and ALS to quantify spatial changes to the subaerial beach. The goal is to characterize not only the overall intensity of coastal processes but also to shed light to the changes in the internal structure of the beach, in particular to identify whether the most representative parts of the beach gain or lose sediment.

We start from the description of the basic features of the ALS technique and the set-up of the terrestrial laser scanner. A case study is carried over a test area in Pirita Beach (Tallinn Bay, the Baltic Sea). The means of elimination of systematic and random errors of the ALS and TLS, creating and comparing of the resulting Digital Terrain Models (DTM) of test areas from scanning point clouds are discussed next. The main message is that the proposed technique is accurate enough to adequately recognize not only the overall volume changes but also to highlight local spots of accumulation and erosion and, most importantly, relatively small but systematic changes in the shapes of the coastal profiles.

II. LASER SCANNING

Laser scanning is a remote sensing method which utilizes laser pulses to measure distances to objects. Based on these distances and the angles of laser beams, the coordinates of measured points are calculated. This results in a 3D point

cloud of measured objects. The scanning device can be mounted on different platforms, i.e. a tripod (TLS), an aircraft (ALS) or a ground vehicle (mobile laser scanning).

1. Terrestrial laser scanning

TLS is used to acquire high-resolution accurate spatial data about objects such as buildings, bridges, statues, road surfaces or other structures. With TLS it is possible to gather data with an accuracy of about 1 cm or even better [18] and at a resolution up to a few mm. However, in order to save time and decrease the file sizes, the resolution is usually set at a few cm, depending also on the complexity of the measured object and the desired result.

Theoretically, TLS can be used for surveying surfaces within a 300 m range. However, in practice the maximum reasonable distance to a vertical surface is about 50–100 m and to a horizontal surface about 25–50 m, varying according to the specific scanner and the characteristics of the surface. A laser beam has a tendency to diverge, yielding the laser “foot-print” to increase in size the further it travels. Therefore, using shorter ranges enables acquiring finer details.

2. Airborne laser scanning

In ALS the scanning device is placed on an aircraft, e.g., plane, helicopter or unmanned aerial vehicle. ALS is cost-effective in applications where large areas need to be covered, for example measuring ground surfaces for compilation of terrain models, infrastructure objects, etc. Generally, an ALS point cloud is much less dense than a TLS point cloud. It usually varies from 0.1–20 points/m² depending on many factors. Acquiring more high-resolution data requires more time, flight hours and therefore more funds.

In order to determine the position and orientation of the aircraft at any instant, a Global Navigation Satellite System (GNSS) receiver and an Inertial Measurement Unit (IMU) are used. GNSS receiver records the position and IMU the pitch, roll and yaw of the aircraft. Since the calculation involves many parameters, the accuracy of ALS is less than that of TLS, and usually estimated at 2–15 cm in favorable conditions [15][19].

As ALS is generally performed at an altitude of up to 6000 m, the divergence of the laser beam is much more pronounced and the beam can reach up to a meter in diameter in ground surface. This means that capturing very fine details is impossible and measurement errors are more likely to occur. The possible errors are still negligible in many applications and the excellent cost/benefit ratio makes this technique highly attractive.

3. Combining ALS and TLS

Combining the results from different TLS and ALS campaigns raises some problems. First of all, in applications where the desired accuracy and data resolution are that of characteristic to TLS, ALS does not meet the expected demands. Also given the relatively large differences in spatial resolution, the methods for data processing have to be slightly altered. These differences are especially pronounced while

using automatic filtering, segmenting and modelling algorithms that require the use of different parameters depending on the point cloud density.

Additionally, combining different laser scanning methods and campaigns raises problems of accuracy. The main issue is how to ensure that the datasets are aligned to each other and determine whether systematic errors are present between them. Such errors can be due to ALS and TLS campaigns using different reference benchmarks. Usually TLS is performed using geodetic points on the ground while ALS uses data from GNSS systems and IMU to calculate the position and orientation.

Unifying point clouds from different campaigns could be accomplished by finding distinguishable points in both point clouds and moving one of the clouds to the correct location. Unfortunately, ALS data is usually not dense enough to accurately determine the coordinates of a particular point. Therefore, it is necessary to detect and quantify the systematic errors by other means.

The systematic error of elevation can be determined by using horizontal surfaces that are present in all point clouds. Such reference surfaces (e.g., a nearby parking lot at Pirita Beach, see below) need to be changeless during all the campaigns. By comparing the elevation differences between the same surface measured by TLS and ALS campaigns, the extent of the systematic error can be determined. Points near the edge of the surface should be discarded to minimize the errors caused by shifts in the (x, y) -plane and the large size of the ALS laser beam footprint on the ground. For example, a part of the ALS pulse might reflect from a curbstone instead of the pavement. The larger the reference surface area the better is the accuracy and reliability of linking of the ALS and TLS measurements.[20].

III. STUDY AREA

The test area of this study, Pirita Beach at the south-eastern bayhead of Tallinn Bay, Estonia, is a typical small, embayed beach of the southern coast of the Gulf of Finland (Fig. 2). This beach is one of the most popular recreational areas of the City of Tallinn, located next to the venue of the 1980 Olympic sailing regatta and hosting more than 3000 visitors daily on warm summer days. The beach is aligned between the northern mole of Pirita (Olympic) Harbor and a moraine scarp located about 400 m southwards from Merivalja jetty. The length of the sandy area is about 2 km and the dunes are relatively low: the maximum height of the scarp at the edge of the coastal forest is 1.5 m.

The stability of Pirita Beach has been discussed for several decades see [21],[22] and references therein). Prior to the mid-20th century, this beach was apparently stabilized by the postglacial uplift and natural sediment supplies but still suffered from a certain loss of sand [21]. Several attempts to refill the beach with material dredged from a neighboring harbor or transported from mainland quarries were undertaken in the 1970s. The entire subaerial beach from the waterline to

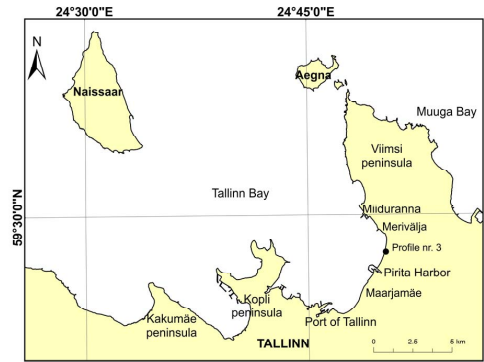


Figure 2. Location scheme of Pirita Beach in Tallinn Bay.

the scarp of the coastal forest was covered by an about 0.5 m thick sand layer. A total volume of 30 000 m³ with a typical grain size of 0.3 mm (which is considerably coarser than the native sand) was used to refill an about 1800 m long section. Additionally, finer sand was pumped to the southern (widest) section of the beach from the Pirita River mouth (see [23] and references therein). As the grain size of this sand volume was considerably smaller than the native sand, a large volume was probably relatively rapidly (in a few years) transported into deeper areas.

In recent decades, a gradual decrease of the beach width, recession of the scarp at the northern end of the beach, and extensive storm damage to the coastal forest have continued [22]. Although alterations of natural conditions such as an increase in storminess in the 1960s [24] may have caused increasing loads on Baltic beaches [11], a more probable reason for these changes at Pirita was the human intervention that has cut down the major natural sand supplies to the beach [10],[22]. For example, construction of Pirita Harbor substantially decreased the supply of river sand. The largest damage to the beach occurred in November 2001 and in January 2005 when high and long waves attacking the beach from northwest or west were accompanied with exceptionally high water level [22].

The recent status of the beach, a short overview of the local wave regime and the overall patterns of wave-induced sediment transport processes along the beach are presented in [22],[25]. The wave climate in the vicinity of the beach is relatively mild and the closure depth evaluated according to [26] is in the range of 2.4–2.6 m. The average net loss of sand from the entire beach was estimated to be in the range of 1000–1250 m³/yr in 1986–2006 based on the relocation of the waterline and the local uplift rate [27].

Southward transport dominates in the northern section of the beach whereas no prevailing transport direction exists in the southern sections. Consequently, different sections of the beach may have different level of erosion or accretion. Approximately 50% of Pirita Beach suffers from substantial

damage at times [25]. In the southern part, the width of the beach (up to 100 m, elevation up to 2 m above the mean water level) and the total sand volume has increased. This tendency is apparently long-term, since even the most violent storms in 2001 and 2005 have not affected the beach width in this relatively stable sector. The central part of the beach is in a near equilibrium state. The bluff at the back of the beach is at times eroded to some extent in strong storms but relatively intense aeolian sand transport into the dune forest [25] can be interpreted as an expression of an excess of sand and a generally healthy state of the beach.

Strong storms caused extensive regression of the bluff over an approximate 1 km long northern sector of the sandy beach in 1999–2005. The changes are marked northwards from the mouth of a small stream about 900 m to the north of Pirita Harbor (see its location in Fig. 4 below). The recession of the bluff was on average 1–2 m (at a few sections even 3–5 m) in 1999–2001. The most intense erosion occurred at the interface between the sandy and till coasts at the northern end of the beach.

Based on the described pattern of the alongshore sediment transport and erosion and deposition patterns, the central area of the beach in the vicinity of the above-mentioned stream mouth seems to be most sensitive with respect to changes in the hydrodynamic and meteorological forcing. Also, this area possibly has variable erosion and accumulation patterns and was selected as test region for this study.

IV. FIELD MEASUREMENTS AND DATA PROCESSING

The data set used in this study consists of both ALS and TLS data (Table I). The ALS data were gathered by the Estonian Land Board with a Leica ALS50-II airborne laser scanner. The Estonian Land Board also performed the ground filtering and classification of the measured points. In this

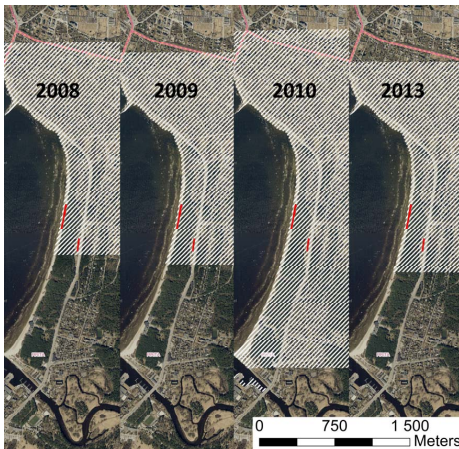


Figure 3. Flight corridors (hatch) of different ALS campaigns. Note a match between the location of the 2008, 2009 and 2013 flight corridors. The studied beach area and the parking lot used as a reference surface (Fig. 4) are marked in red.

analysis only the points classified as ‘ground’ were used. The test area is entirely located within a single flight corridor (Fig. 3), therefore the results are not affected by flight line matching errors.

TABLE I
AIRBORNE AND TERRESTRIAL SCANNING IN 2008–2013

Type of scanning	Day	Water level ^a , m	Flight height, m	Density of point cloud, points/m ²
ALS	6.05.2008	-0.18	2400	0.45
ALS	3.05.2009	-0.36	2400	0.45
ALS	4.06.2010	-0.04	3800	0.15
ALS	25.04.2013	-0.05 ^b	2400	0.45
TLS	18.12.2013	+0.35	-	2500

^a with respect to the long-term mean at Tallinn Harbor; ^b the same but measured at Pirita Harbor by the Estonian Environmental Agency, cf. Fig. 2.

The TLS survey was conducted with a pulse-based Leica ScanStation C10 with an average spatial resolution of ~2500 points/m² (2 × 2 cm). The beach survey was performed from six scanning stations (Fig. 4). For future surveys, nine reference points were established near the beach (Fig. 4) and coordinated by total station measurements from GNSS determined base lines (see Fig. 4). The heights of the points were determined with respect to a nearby located levelling benchmark.

To reduce systematic elevation differences between the

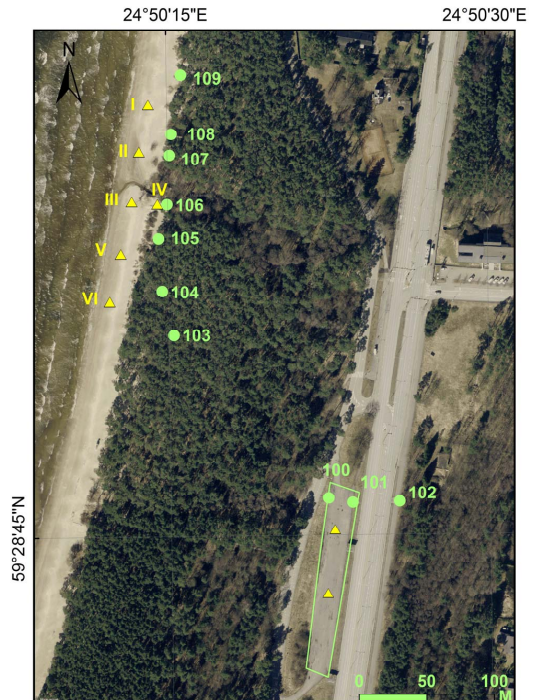


Figure 4. The reference points (numbered green circles) and TLS stations (yellow triangles). Reference points 100, 101, 102, 105 and 106 were measured with GNSS. Reference point no. 106 also marks the beginning of a profile no. 3.

ALS and TLS data, we used the surface of a parking lot near the beach (Fig. 3) as a horizontal reference. This surface has been changeless (i.e. no repaving) since the first ALS flight in 2008. The reference surface was measured with TLS using reference points that were linked to points located at the beach.

All ALS surfaces were reduced to the TLS reference surface by applying elevation corrections (ΔH in Table II). Doing so improved the accuracy of the process of detection of deformations of the beach surface. These 1D corrections (ΔH) were derived from the average height differences of ground profiles of each ALS data-set from the TLS surface. The accuracy estimations are calculated from the TLS–ALS DEM differences for the reference parking lot. After elimination of the systematic errors the ALS/TLS combination yields sub-decimeter accuracy for height determination of the beach, cf. the last column in Table II.

TABLE II
HEIGHT CORRECTIONS APPLIED TO ALS DATA

Campaign	Elevation correction ΔH [m]	Average elevation difference from TLS measurements [m]	Standard deviation [m]
2008_ALS	0.036	0.030	0.024
2009_ALS	0.204	0.018	0.025
2010_ALS ^a	-0.176	-0.020	0.055
2013_ALS	0.010	0.004	0.022
2013_TLS	0	0	0

^a The 2010 ALS campaign was flown higher (cf. Table I) which affects the resolution and accuracy of the data.

The adjusted and aligned point clouds were used to form DTM's of the beach. Both raster based Digital Elevation Models and vector based Triangulated Irregular Network (TIN) models were used. The constructed DTMs were used to analyze and visualize the changes that had occurred through the years. The resulting DTMs constructed from ALS make it possible to highlight relatively long-term changes within 2008–2013 whereas a comparison of similar results from the ALS and TLS campaigns in 2013 allow for the identification of changes within one stormy season (this will be discussed elsewhere). Finally, the ALS data from different years enable us to recognize an interesting shift in the nature of changes to the beach around the year 2010.

V. LONG-TERM CHANGES

1. Single profiles

The study area is an about 250 m long strip in the central part of the beach (Fig. 5) where the earlier data and above discussion suggest a moderate loss of sand. This area contains one coastal profile (No. 3 in the relevant database) that is monitored regularly by the Geological Survey of Estonia in the framework of the national coastal monitoring programme [28]. Data for this profile, available for the years of 2003–2012 (Fig. 6), indicate the range of changes that can be identified using the classical methods of coastal monitoring. Although certain fluctuations occurred in the exact position of the beach surface and the zero-height line, none of these



Figure 5. The study area in Pirita Beach and its cross-sections (profiles) used in Fig. 6 and 7. The profile in the centre of the test area matches profile No. 3 monitored by the Geological Survey of in the framework of the national coastal monitoring programme.

changes are systematic; in particular, and almost no changes to the sand volume of the dry beach have occurred during this decade. The data reveal much larger variations in the location and height of an underwater sand bar that seems to move onshore by about 4 m/yr.

To properly interpret the described data, it is important to note that this profile is located just next to the mouth of a small stream. Although this stream is evidently not capable of bringing substantial volumes of sand to the beach, even a small sediment supply may keep its immediate vicinity in an almost equilibrium on the background of a gradually eroding beach section. Also, the meandering of its mouth under bi-directional littoral flow [25] may to a certain extent affect the location of the waterline and the volume of sediment present exactly along the profile. However, making strong conclusions from the described behavior may not be justified.

The ALS and TLS data in 2008–2013 for this and neighbouring cross-sections located about 70 m to the south

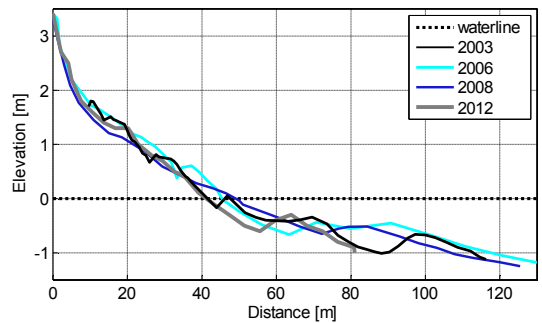


Figure 6. Beach profile No. 3 measured in 2003–2012. Data courtesy of the Geological Survey of Estonia.

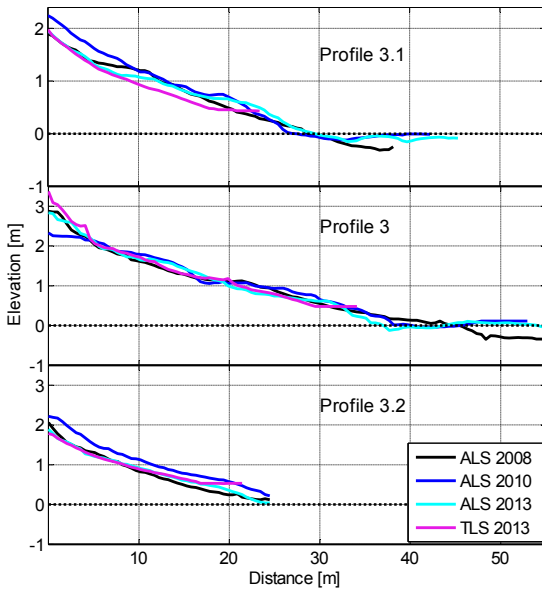


Figure 7. Beach profiles (see the location in Fig. 5) in 2008–2013 based on ALS and TLS data.

and about 60 m to the north of it (Fig. 5) add substantial information about the nature and course of the changes to the study area. Profile 3 in Fig. 7 matches the one routinely used in the national coastal monitoring programme [28] and portrayed in Fig. 6. The data at a distance of 0–10 m from the starting points of each profile are affected by the particular flying line and height of the plane carrying the ALS device. As the flying height in the ALS scan in 2010 (3800 m) was considerably higher than in the other years (2400 m), the relevant density of the point cloud was lower in 2010 and the scarp is evidently not properly reflected in the data. Therefore, the data at the beginning of the profiles (at a distance of 0–10 m in Fig. 7) are, at best, indicative. The end of the scanned profile depends on the instantaneous location of the waterline that may vary by 10–20 m depending on the water level during the scan.

Not surprisingly, the variation of the height of the beach surface along profile 3 measured by conventional means (Fig. 6) and using the ALS and TLS techniques (Fig. 7) largely coincide from the distance of 10–40 m from the beginning of the profile (reference point 106 in Fig. 4). This match *inter alia* once more confirms the reliability of the TLS and ALS data for changes to the subaerial beach.

The overall original shape of the beach in 2008 was moderately convex signaling a relatively healthy situation. The entire beach has undergone no substantial changes as noted also above. The volume of sand has increased at the waterline. The above discussion suggests that this may reflect either arriving of the underwater sand bar or local changes in the sediment volume caused by the small stream.

The ALS and TLS data for the other two profiles (3.1 and 3.2 in Fig. 5 and Fig. 7), however, indicate that substantial changes have occurred in the study area since 2008. These changes have clear structure along both profiles. As mentioned above, the changes at the distance of 0–10 m from their beginning may not be particularly reliable but still a certain loss of sand from the northern segment of the study areas characterized by this section of profile 3.1 is likely. Further down to the waterline, at a distance of 10–25 m from the beginning, the beach has kept its shape in 2008–2013 but has considerably lost sand in 2013. Its height has decreased by about 30 cm, which means the loss approximately 3 m³ per meter of the coastline during this year. Although a part of this difference may stem from inexact match of the ALS and TLS data, it is likely that this section of the beach had negative sand budget in 2013. This loss has been only partially compensated by an accumulation in the vicinity of waterline (25–30 m from the beginning). Similarly to profile 3, considerable volume of sand has accumulated in shallow water to the offshore of the waterline. This match of accumulation with the one for profile 3 and with Fig. 6 suggests that a sand bar is gradually moving into the study area.

The evolution of the beach height along profile 3.2 suggests that changes to the southern segment of the study area were quite different from the above-described course. This profile demonstrates rapid changes along its entire subaerial length. The beach rapidly gained sand (about 5–6 m³ per meter of coastline) in 2008–2010. This material was almost totally eroded in 2010–2013. A minor accumulating section in the TLS data in the immediate vicinity of the waterline may reflect the arrival of a sand bar (see the discussion above) but it may equally well reflect local and temporary wave-driven changes in the swash zone. The match of TLS and ALS for 2013 along this profile suggests that the differences between these data sets along profile 3.1 reflect changes to the beach and are not caused by uncertainties of the methods.

2. Spatial changes

As we are interested in the capacity of the ALS and TLS techniques to highlight and identify changes to beaches, we concentrate on the largest changes that occurred between the different measurement campaigns presented in Table I.

A comparison of the beach surface for 2008 and 2010 (both measured using the ALS technique) first demonstrates a rich spatial structure of changes superposed by substantial differences between the segments to the north and south of the stream mouth (Fig. 8). The entire study area gained sand with a total volume of about 500 m³/yr (Table III). Given the total scanned area of about 4500 m², the used technique is thus capable of clearly identifying average changes on the order of a few cm. Erosion was observed only in a few spots (about 5% of the area; mostly around the mouth of the small stream; see the right panel of Fig. 8) that lost a few tens of m³/yr altogether (less than 10% of the accumulation). Most likely, the related decrease in the height of the beach surface reflects

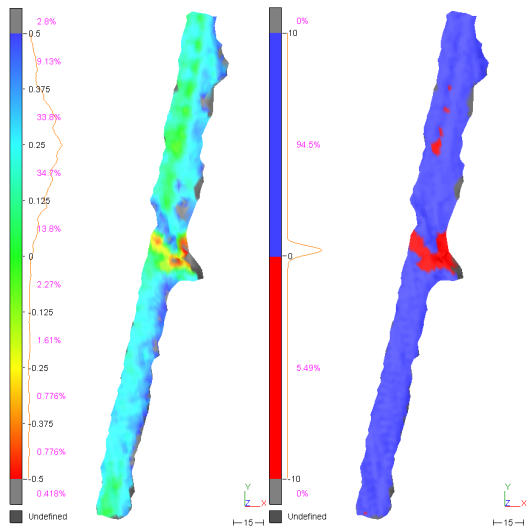


Figure 8. (left) Changes to the beach height from ALS in 2008 to 2010. The scale shows the extent of the differences (m) and the percentage of the scanned surface with a change rate within an interval of such rates; (right): the relevant erosion (red) and accumulation (blue) areas.

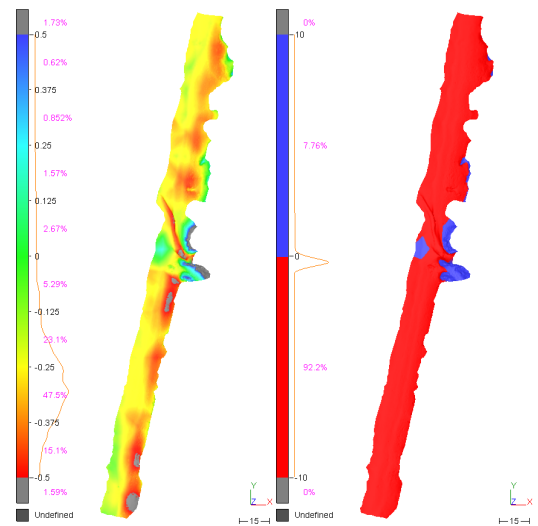


Figure 9. (left) Changes to the beach height from ALS in 2010 to TLS in 2013 (the scale shows the extent of the differences and the percentage falling between an interval); (right): the relevant erosion (red) and accumulation (blue) areas.

smoothing or relocation of local, small, temporary morphological features.

There were, however, considerable differences in the pattern of accumulation across the study area. The accumulation of sand was relatively rapid and homogeneous along and across the entire southern segment. The height of the beach typically increased by 20–30 cm (cf. profile 3.2 in Fig. 7). The accumulation in the northern segment, however, mostly occurred in the landward part of the beach. It is thus likely that most of the accumulation here was driven by aeolian transport. As mentioned above, a few areas of decrease in the height of the beach in the central part of the segment apparently reflect local smoothing of the beach surface.

Spatial changes in the beach height according to the above-discussed ALS survey in 2010 and a TLS survey in December 2013 (Fig. 9) revealed almost a totally opposite pattern. The entire study area lost sand. Only a small vicinity of the stream (8% of the entire surface) gained some sand. The total loss of sand over three years (2010–2013) was almost equal to the total gain in 2008–2010 (Table III). The amount of lost sand per meter of coastline was almost constant along the study area. Differently from the years 2008–2010, the changes to the beach height were distributed unevenly along the beach cross-section. The loss was largest in the landward part of the cross-section in the vicinity of the coastal scarp and somewhat smaller in the vicinity of the waterline. Although the ALS data may have relatively large uncertainty in the immediate vicinity of the coastal scarp near the forest, it is still likely that the loss of beach height was unevenly distributed across the beach.

The described radical difference of the sign and spatial pattern of changes within the two discussed time intervals suggests that the properties of driving forces were likely quite different in these intervals. In terms of visually observed wave heights, the years 2009–2010 were relatively mild and the year 2011 relatively stormy. The annual mean for these years at Ventspils and Liepaja was by about 20% lower and for 2011 by about 10% larger than the long-term average [29],[30]. It is therefore likely that in 2008–2010 relatively mild wave conditions with a comparatively large proportion of swells (generated by typical south-westerly storms in the open Baltic Sea and the western Gulf of Finland) dominated the coastal processes in Pirita Beach and were favourable for recovery of the beach.

The stormy seasons of autumn and winter 2011/2012 were different. The autumn was stormy and the ice period started later than usual. Several strong wave storms affected not only the open Baltic Sea [31] but also the Gulf of Finland [32]. The autumn and winter of 2012/2013 were also comparatively stormy. For example, in November 2012 the all-time highest single wave in the Gulf of Finland was recorded near Helsinki in a storm that repeated the all-time highest significant wave height in this bay [29]. Although the latter storm blew from the east, it is likely that Pirita Beach was frequently impacted by severe and destructive wave conditions in 2010–2013.

This conjecture is supported by the spatial structure of measured changes. This structure is characteristic to severe wave conditions superposed with high local water level. In such situations waves erode unprotected sediment relatively far from the coastline (here in the vicinity of the coastal scarp). As the Baltic Sea storms are usually short, this

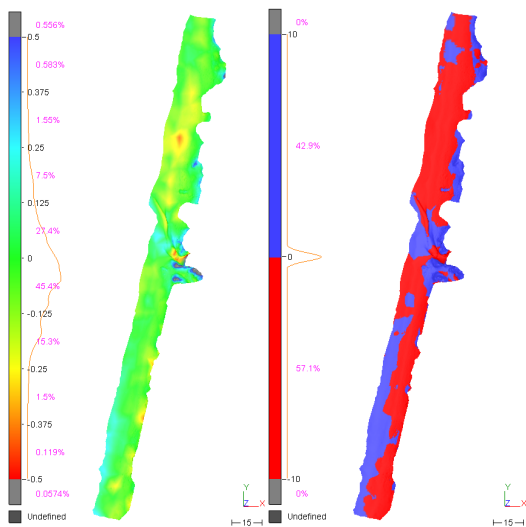


Figure 10. (left) Changes to the beach height from ALS in 2008 to TLS in 2013 (the scale shows the extent of the differences and the percentage falling between an interval); (right): the relevant erosion (red) and accumulation (blue) areas.

material is relocated to a relatively small distance along the coast and usually is deposited within the equilibrium beach profile for the particular storm and water level [33]. For the typical water levels and wave heights in storms that directly impact Pirita Beach [22][25], this means deposition mostly at depths from the waterline corresponding to the mean water level down to a depth of about 0.5 m. This material is often brought back to the seaward section of the subaerial beach by regular swells within a short period of time.

Based on the presented material and discussion, it is not unexpected that the changes to the study area during the five years 2008 (ALS)–December 2013 (TLS) are fairly minor (Table III) and have a variable spatial pattern (Fig. 10). The proportions of the eroding and accumulation regions are almost equal. The largest accumulation rates are in the vicinity of the mouth of the small stream but these apparently do not characterise properly the processes in other parts of the study area. These few small patches of accumulation around the stream are evidently connected with a relocation of the stream and filling the stream bed with sand from adjacent locations.

TABLE III
CHANGES IN THE SAND VOLUME IN THE 4567 M² TEST AREA

Interval	Accumulation [m ³]	Erosion [m ³]	Budget [m ³]
2008ALS–2009ALS	486	29	457
2009ALS–2010ALS	588	38	550
2008ALS–2010ALS	1046	38	1008
2008ALS–2013TLS	167	232	–65
2009ALS–2013TLS	63	653	–590
2010ALS–2013TLS	55	1164	–1109
2013ALS–2013TLS	139	258	119

An increase in the amount of sand is, however, noticeable in the vicinity of the waterline in the southernmost section of the experiment area while most of the northern part of the beach has lost sand. The local changes to the beach height are predominantly (73%) less than ± 12.5 cm. Only in a few locations in the middle of the northern segment has the beach lost almost 50 cm of height. As discussed above, areas of loss likely characterize local changes and are not representative of overall coastal processes.

The overall pattern of changes in the almost six years covered by the laser scanning data coincides with the common understanding of the nature of coastal processes and sand movement at Pirita Beach. As alongshore transport in the northern section of the beach is almost unidirectionally to the south [25] and sand sources in the north are quite limited, it is expected that the northern sections of the beach suffer more severely from sediment deficit and are more prone to erosion than the southern sections. Consistent with this conjecture, Fig. 10 reveals that in the northern segment of the test area the beach has mostly lost sand (predominantly from the central part of the strip, between the waterline and the scarp) while in the southern segment the losses are fairly minor and have occurred from the area relatively remote from the waterline and close to the scarp. This difference is also exemplified in profiles (Fig. 7).

VI. CONCLUSIONS AND DISCUSSION

The presented material suggests that the technology of repeated airborne and terrestrial laser scanning is accurate and reliable enough to recognize the internal structure of changes to the beach. Additional to the variations of the overall course of erosion and accumulation, the method in use is able to highlight changes in the beach profiles, local regions of accumulation and erosion and reveal relatively small changes in the shapes of the coastal profiles, and in this way better characterize the nature of the changes and to provide crucial information about whether the beach is losing sand or recovering.

The described major difference of the sign and spatial pattern of changes in 2008–2010 and 2010–2013 also vividly demonstrates one of the major shortcomings of classical coastal monitoring activities. As they largely rely on the observed changes along a few profiles, the credibility of the outcome crucially depends on the proper choice of the profiles. The presented material demonstrates that the beach height along profile No. 3 is governed by local processes, first of all by the impact of the small stream in the vicinity. Not only is this profile evidently able to replicate any essential changes to the adjacent segments of beach but in the discussed time intervals behaves almost oppositely to the real course of changes to the beach. The major advantage of both airborne and terrestrial laser scanning techniques is their ability to recognise a 'big picture' of the evolution of longer beach

sections and to avoid deceptive conclusions based on strongly localised data sets.

This feature suggests that the earlier estimates, both based on in situ observations [23] and on quite coarse modelling efforts [22] have led to valid conclusions about the spatial variations in the evolution of different parts of the beach. The numerical estimates in [22],[23], however, may reflect the intensity of sand loss in years when severe wave conditions directly impact Piritä Beach. As most of future climate projections suggest an increase in storminess and decrease in the length of the ice season, these estimates are evidently valid approximations of reality.

ACKNOWLEDGMENT

This study was a part of the projects ERMAS AR12052 and TERIKVANT, supported by the European Union (European Regional Development Fund, ERDF) and managed by the Estonian Research Council in the framework of the Environmental Technology R&D Programme KESTA. The ALS data used in this study was received from the Estonian Land Board under the license contract ST-A1-2422, 22/06/2012. The used Leica ScanStation C10 and licensed data processing software were acquired within frame of the Estonian Research Infrastructures Roadmap object Estonian Environmental Observatory (funding source 3.2.0304.11-0395, project No. AR12019). The research was partially supported by the targeted financing of the Estonian Ministry of Education and Research (grant SF0140007s11), by the Estonian Science Foundation (grant No. 9125) and through support of the ERDF to the Centre of Excellence in Non-linear Studies CENS.

REFERENCES

[1] J. Harff, S. Björck, and P. Hoth, Eds., *The Baltic Sea Basin*, Central and Eastern European Development Studies. Heidelberg Dordrecht London New York: Springer, 2011, 449 pp.

[2] M. Leppäranta and K. Myrberg, *The physical oceanography of the Baltic Sea*. Berlin Heidelberg: Springer, 2009.

[3] I. Didenkulova, E. Pelinovsky, and T. Soomere, "Long surface wave dynamics along a convex bottom," *J. Geophys. Res.-Oceans*, vol. 114, art. No. C07006, 2009.

[4] T. Soomere, K. Pindsoo, S.R. Bishop, A. Käard, and A. Valdmann, "Mapping wave set-up near a complex geometric urban coastline," *Nat. Hazards Earth Syst. Sci.*, vol. 13, pp. 3049-3061, 2013.

[5] K. Orviku, *Estonian coasts*. Tallinn, 1974, 112 pp. [in Russian].

[6] K. Orviku and O. Granö, "Contemporary coasts," in *Geology of the Gulf of Finland*, A. Raukas and H. Hyvärinen, Eds. Tallinn: Valgus, 1992, pp. 219-238 [in Russian].

[7] T. Kall, T. Oja, and K. Tänavsuu. "Postglacial land uplift in Estonia based on four precise levelings," *Tectonophysics*, vol. 610, pp. 25-38, 2014.

[8] T. Soomere and S. Keevallik, "Directional and extreme wind properties in the Gulf of Finland," *Proc. Estonian Acad. Sci. Eng.*, vol. 9, pp. 73-90, 2003.

[9] K. F. Nordstrom, "Bay beaches," in *Encyclopedia of Coastal Science*, M. L. Schwartz, Ed. Dordrecht, The Netherlands: Springer, 2005, pp. 129-130.

[10] T. Soomere and T. Healy, "On the dynamics of "almost equilibrium" beaches in semi-sheltered bays along the southern coast of the Gulf of Finland," in *The Baltic Sea Basin*, J. Harff, S. Björck, and P. Hoth, Eds.

Central and Eastern European Development Studies, Part 5, Heidelberg Dordrecht London New York: Springer, 2011, pp. 255-279.

[11] K. Orviku, J. Jaagus, A. Kont, U. Ratas, and R. Rivis, "Increasing activity of coastal processes associated with climate change in Estonia," *J. Coast. Res.*, vol. 19, pp. 364-375, 2003.

[12] D. Ryabchuk, A. Kolesov, B. Chubarenko, M. Spiridonov, D. Kurennoy, and T. Soomere, "Coastal erosion processes in the eastern Gulf of Finland and their links with geological and hydrometeorological factors," *Boreal Environ. Res.*, vol. 16 (Suppl. A), 117-137, 2011.

[13] D. P. Thoma, S.C. Gupta, M.E. Bauer, and C. Kirchoff, "Airborne laser scanning for riverbank erosion assessment," in *Remote Sensing of Environment*, vol. 95, pp. 493-501, 2005.

[14] M Bremer; O. Sass, "Combining airborne and terrestrial laser scanning for quantifying erosion and deposition by a debris flow event," *Geomorphology*, vol. 138, pp. 49-60, 2012.

[15] A. Gruno, A. Liibus, A. Ellmann, T. Oja, A. Vain, and H. Jürgenson, "Determining sea surface heights using small footprint airborne laser scanning," in *Remote Sensing of the Ocean, Sea Ice, Coastal Waters, and Large Water Regions 2013 (Conference 8888)*, Dresden, Germany, 2013, C. Bostater, S. Mertikas, and X. Neyt, Eds. SPIE - International Society For Optical Engineering, 2013, pp. 88880R-1-88880R-13.

[16] M. Viška, "Coastal erosion analysis using LiDAR data and field measurements in Zvejniekiems beach, east coast of the Gulf of Riga," in *5th International Student Conference [on] Biodiversity and Functioning of Aquatic Ecosystems in the Baltic Sea Region*: Conference Proceedings, October 6-8, 2010, Palanga, Lithuania, Klaipėda, 2010.

[17] E. Grünthal, A. Gruno, and A. Ellmann, "Monitoring of coastal processes by using airborne laser scanning data," in *Proceedings Cygas, D. (Ed): Selected papers of the 9th International Conference on Environmental Engineering*, Vilnius, Lithuania, 22-23, May, 2014. Vilnius: Vilnius Gediminas Technical University Press, "Technika" (in press).

[18] P. Dorninger, B. Szekely, A. Zamolyi, and A. Roncat, "Automated Detection and Interpretation of Geomorphic Features in LiDAR Point Clouds," *Vermessung & Geoinformation*, vol. 2, pp. 60-69, 2011.

[19] E.J. Huising and L.M. Gomes Pereira, "Errors and accuracy estimates of laser data acquired by various laser scanning systems for topographic applications," *ISPRS Journal of Photogrammetry and Remote Sensing*, vol. 53, No. 5, pp. 245-261, 2004.

[20] K. Julge and A. Ellmann, "Combining Airborne and Terrestrial Laser Scanning technologies for measuring complex structures," in *Selected papers of the 9th International Conference on Environmental Engineering*, Vilnius, Lithuania, 22-23, May, 2014. D. Cygas, Ed. Vilnius: Vilnius Gediminas Technical University Press "Technika" (in press).

[21] K. Orviku. "Seashore needs better protection," in *Year-book of the Estonian Geographical Society*, vol. 35, pp. 111-129, 2005, [In Estonian, with English summary].

[22] T. Soomere, A. Kask, J. Kask, and R. Nerman, "Transport and distribution of bottom sediments at Piritä Beach," *Estonian J. Earth Sci.*, vol. 56, pp. 233-254, 2007.

[23] K. Orviku, and M. Veisson. Lithodynamical investigations on the most important resort areas of Estonia and in the area of the Olympic Yachting Centre in Tallinn. Research report. Tallinn, Institute of Geology, 1979, 105 pp. [In Russian].

[24] H. Alexandersson, T. Schmith, K. Iden, and H. Tuomenvirta, "Long-term variations of the storm climate over NW Europe," *Global Atmos. Ocean Syst.*, vol. 6, pp. 97-120, 1998.

[25] T. Soomere, A. Kask, J. Kask, and T. Healy, "Modelling of wave climate and sediment transport patterns at a tideless embayed beach, Piritä Beach, Estonia," *J. Marine Syst.*, vol. 74, Suppl., pp. S133-S146, 2008.

[26] W. A. Birkemeier, "Field data on seaward limit of profile change," *J. Waterw. Port Coastal Ocean Eng. - ASCE*, vol. 111, pp. 598-602, 1985.

[27] A. Kask, T. Soomere, T. Healy, and N. Delpeche, "Sediment transport patterns and rapid estimates of net loss of sediments for "almost equilibrium" beaches," *J. Coast. Res.*, Special Issue 56, pp. 971-975, 2009.

[28] S. Suuroja, A. Talpas, and K. Suuroja. 2004. *Mererannikute seire*. Report on activities on the subprogram "Monitoring of sea coasts of the state environmental monitoring in 2003. Part II: graphical attachments". Manuscript, Estonian Geological Survey, Tallinn [in Estonian]; see also http://seire.keskkonnainfo.ee/index.php?option=com_content&view=article&id=2096&Itemid=409

- [29] I. Zaitseva-Pärnaste, *Wave climate and its decadal changes in the Baltic Sea derived from visual observations*. PhD thesis. Tallinn University of Technology, 173 pp., 2013.
- [30] B. Hünicke, T. Soomere, K.S Madsen, M. Johansson, Ü. Suursaar, and E. Zorita, Sea level and wind waves. Chapter 3.4.3 in The BACC Author Team. *Assessment of climate change for the Baltic Sea basin*. Springer, 2014, in press.
- [31] H. Tõnisson, Ü. Suursaar, R. Ravis, A. Kont, and K. Orviku, "Observation and analysis of coastal changes in the West Estonian Archipelago caused by storm Ulli (Emil) in January 2012," *J. Coast. Res.*, Special Issue 65, pp. 832-837, 2013.
- [32] H. Tõnisson, Ü. Suursaar, S. Suuroja, D. Ryabchuk, K. Orviku, A. Kont, Y. Sergeev, and R. Ravis, "Changes on coasts of western Estonia and Russian Gulf of Finland, caused by extreme storm Berit in November 2011," in *IEEE/OES Baltic 2012 International Symposium : May 8-11, 2012, Klaipeda, Lithuania, Proceedings: IEEE*, 2012, 1-7.
- [33] R.G. Dean and R.A. Dalrymple, *Coastal Processes with Engineering Applications*. Cambridge: Cambridge University Press, 2002.

CURRICULUM VITAE

1. Personal data

Name: Kalev Julge
Date and place of birth: 24.09.1987, Haapsalu
Nationality: Estonian
E-mail: kalev.julge@ttu.ee

2. Education

Educational Institution	Graduation year	Field of study, degree
Tallinn University of Technology	2013	Transport Engineering specializing in Construction Geodesy, Master of Science

3. Language skills

Language	Level
Estonian	Native language
English	Proficient
Russian	Basic

4. Professional Employment

Period	Organization	Position
2013 - ...	Tallinn University of Technology	Early stage researcher
2012-2013	Geo S.T. OÜ	Surveyor

5. Field of research

Remote sensing by methods of airborne, mobile and terrestrial laser scanning.

6. Honours and awards

2012, Kalev Julge, Helga Minnus and Elmar Minnus scholarship

Received financial support from the European Geosciences Union (EGU) to present research at the EGU General Assembly 2014.

7. Additional information

Short term research missions to:

Finnish Geodetic Institute (FGI), November 2013

Center of Excellence in Laser Scanning Research (CoELaSR), January 2017

Teacher for Photogrammetry (ETG0113).

8. MSc theses supervised

Aidi Sula, Master's Degree, 2015, (sup) Artu Ellmann; Kalev Julge, UAV mõõdistuse kõrgusliku ja plaanilise täpsuse evalveerimine (Evaluating the vertical and horizontal accuracy of UAV photogrammetry), Tallinn University of Technology Faculty of Civil Engineering, Department of Road Engineering.

Silver Aule, Master's Degree, 2014, (sup) Artu Ellmann; Kalev Julge, Mittestandardse kujuga ehitiste laserskaneerimine ja punkt pilve põhjal modelleerimine TTÜ veetorni näitel (Laser scanning and point-cloud based modelling of non-standard structures with application to a historic water tower), Tallinn University of Technology Faculty of Civil Engineering, Department of Road Engineering, Chair of Geodesy.

9. Publications

Peer-reviewed journal articles:

Julge, K., Vajakas, T., Ellmann, A., (2017). Performance analysis of a compact and low-cost mapping-grade mobile laser scanning system. *Journal of Applied Remote Sensing*, 11(4), 044003, 10.1117/1.JRS.11.044003.

Eelsalu, M., Soomere, T., Julge, K. (2015). Quantification of changes in the beach volume by the application of an inverse of the Bruun Rule and laser scanning technology. *Proceedings of the Estonian Academy of Sciences*, 64 (3), 240–248.10.3176/proc.2015.3.06.

Julge, K., Ellmann, A., Gruno, A. (2014). Performance analysis of freeware filtering algorithms for determining ground surface from airborne laser scanning data. *Journal of Applied Remote Sensing*, 8 (1), 083573-1–083573-15.10.1117/1.JRS.8.083573.

Peer-reviewed conference proceedings:

Julge, K., Ellmann, A., Vajakas, T., Kolka, R. (2016). Initial tests and accuracy assessment of a compact mobile laser scanning system. In: *The International Archives of the Photogrammetry, Remote Sensing and Spatial Information Sciences* (633–638). XXIII ISPRS Congress, 12–19 July 2016, Prague, Czech Republic: Copernicus publications. (ISPRS Commission I, ICWG I/Va).10.5194/isprsarchives-XLI-B1-633-2016.

- Julge, K., Gruno, A., Ellmann, A., Liibus, A., Oja, T. (2014). Exploring sea surface heights by using Airborne Laser Scanning. IEEE/OES Baltic 2014 International Symposium: 2014 IEEE/OES Baltic International Symposium "Measuring and Modeling of Multi-Scale Interactions in the Marine Environment": Tallinn, Estonia, May 26-29, 2014. IEEE, 1-7. (IEEE Conference Proceedings).10.1109/BALTIC.2014.6887853.
- Julge, K., Eelsalu, M., Grünthal, E., Talvik, S., Ellmann, A., Soomere, T., Tõnisson, H. (2014). Combining airborne and terrestrial laser scanning to monitor coastal processes. 2014 IEEE/OES Baltic International Symposium, May 26.-29.2014, Tallinn, Estonia: 2014 IEEE/OES Baltic International Symposium "Measuring and Modeling of Multi-Scale Interactions in the Marine Environment": Tallinn, Estonia, May 26-29, 2014. IEEE, 1-10. (IEEE Conference Proceedings).10.1109/BALTIC.2014.6887874.
- Julge, K., Ellmann, A. (2014). Combining Airborne and Terrestrial Laser Scanning technologies for measuring complex structures. Cygas, D. Selected papers of the 9th International Conference on Environmental Engineering, Vilnius, Lithuania, 22-23, May, 2014. (1-7). Vilnius: Vilnius Gediminas Technical University Press "Technika".10.3846/enviro.2014.213.

Conference presentations:

- Ellmann, A., Julge, K., Gruno, A., Liibus, A. (2016). Airborne laser scanning validation of marine geoid models. Electronical programme of GGHS2016 "Gravity, Geoid and Height Systems 2016" Meeting: Thessaloniki, 18-23.09.2016. Aristotle University of Thessaloniki, 1-1.
- Julge, K., Ellmann, A., Vajakas, T., Kolka, R. (2016). Initial tests and accuracy assessment of a compact mobile laser scanning system. Electronical programme of the the XXIII International Society for Photogrammetry and Remote Sensing Congress: July 12-19, 2016 - Prague, CZECH REPUBLIC. Copernicus publications, 1-1. (IS 18/7: Interactive session).
- Ellmann, A., Julge, K., Gruno, A., Liibus, A. (2015). Airborne laser scanning determination of sea surface heights. Electronical programme of 26th IUGG General Assembly (IUGG2015): 26th International Union of Geodesy and Geophysics (IUGG) General Assembly, June 22- July 02, 2015, Prague, Czech Republic. International Union of Geodesy and Geophysics (IUGG).
- Julge, K., Ellmann, A. (2015). Enhancement of Unmanned Aerial Vehicle photogrammetry by high-resolution airborne laser scanning data. Electronical programme of 26th IUGG General Assembly (IUGG2015): 26th International Union of Geodesy and Geophysics (IUGG) General Assembly, June 22- July 02, 2015, Prague, Czech Republic. International Union of Geodesy and Geophysics (IUGG).

- Eelsalu, M., Soomere, T., Julge, K., Grünthal, E. (2015). Quantification of the changes in sediment volume in a small beach applying laser scanning technology. 10th Baltic Sea Science Congress: Science and innovation for future of the Baltic and the European regional seas, 15-19 June 2015, Riga, Latvia, Abstract Book. 197.
- Eelsalu, M., Soomere, T., Julge, K. (2015). Quantification of changes in the beach volume by applying an inverse Bruun's Rule and laser scanning technology in Pirita Beach, Tallinn Bay. Climate modelling and impacts from the global to the regional to the urban scale: An international scientific seminar at HafenCity University Hamburg, 10 March 2015, Poster Abstracts. Baltic Earth, HCU, 8.
- Julge, K., Ellmann, A. (2015). Evaluating the accuracy of orthophotos and 3D models from UAV photogrammetry. Geophysical Research Abstracts, 17: EGU General Assembly 2015. European Geophysical Society.
- Julge, K., Ellmann, A. (2014). Combining Airborne and Terrestrial Laser Scanning technologies for measuring complex structures. Abstract. 9th International Conference "Environmental Engineering", Vilnius, May 22-23, 2014.
- Julge, K., Gruno, A., Ellmann, A., Liibus, A., Oja, T. (2014). Using airborne laser scanning profiles to validate marine geoid models. Geophysical Research Abstracts, 16.
- Eelsalu, M., Julge, K., Grünthal, E., Ellmann, A., Soomere, T. (2014). Laser scanning reveals detailed spatial structure of sandy beaches. IUTAM Symposium on Complexity of Nonlinear Waves: 8-12 September, Tallinn 2014, Book of Abstracts. Ed. Salupere, Andrus, Maugin, Gérard A. Tallinn: Institute of Cybernetics at Tallinn University of Technology, 45.
- Eelsalu, M., Julge, K., Soomere, T., Grünthal, E. (2014). Quantification of the evolution of a small beach applying laser scanning technology. Baltic Earth - Gulf of Finland Year 2014 Modelling Workshop "Modelling as a tool to ensure sustainable development of the Gulf of Finland-Baltic Sea ecosystem", Finnish Environment Institute, Helsinki 24-25 November 2014, Programme, Abstracts, Participants. Geesthacht, Germany: Helmholtz-Zentrum Geesthacht, 10. (International Baltic Earth Secretariat Publication, 4).
- Eelsalu, M., Julge, K., Grünthal, E., Talvik, S., Ellmann, A., Soomere, T., Tõnisson, H. (2014). Combined laser scanning to monitor coastal processes. MEME'2014: Mathematics and Engineering in Marine and Earth Problems, 22-25 July 2014, Aveiro, Portugal, Book of Abstracts. 106–108.
- Julge, K., Eelsalu, M., Grünthal, E., Talvik, S., Ellmann, A., Tõnisson, H. (2014). Combining airborne and terrestrial laser scanning to monitor coastal processes. Measuring and Modeling of Multi-Scale Interactions in the Marine Environment: IEEE/OES Baltic Symposium 2014, May

26.-29.2014, Tallinn, Estonia, Book of Abstracts. Tallinn: Tallinn University of Technology, 49–49.

Julge, K., Gruno, A., Ellmann, A., Liibus, A., Oja, T. (2014). Exploring sea surface heights by using airborne laser scanning. Book of abstracts: 2014 IEEE/OES Baltic International Symposium "Measuring and Modeling of Multi-Scale Interactions in the Marine Environment": Tallinn, Estonia, May 26-29, 2014. Tallinn: Tallinn University of Technology, 50–50.

Other:

Eelsalu, M., Ellmann, A., Julge, K., Märdla, S., Soomere, T. (2014). Rannaprotsesside anatoomia laserskaneerimise skalpelliga. Aan, Anne, Narusk, Kirke (Toim.). Kaugseire Eestis 2014 (47–58).. Tallinn: Keskkonnaagentuur.

Julge, K., Gruno, A., Ellmann, A. (2013). Aerolaserskaneerimise andmetest maapinna tuvastamine erinevate filtreerimisalgoritmidega. Geodeet, 32–36.

ELULOOKIRJELDUS

1. Isikuandmed

Nimi: Kalev Julge
Sünniaeg ja -koht: 24.09.1987, Haapsalu
Kodakondsus: Eesti
E-post: kalev.julge@ttu.ee

2. Hariduskäik

Õppeasutus	Lõpetamise aeg	Haridus (eriala/kraad)
Tallinna Tehnikaülikool	2013	Transpordiehitus spetsialiseerumisega ehitusgeodeesia, Tehnikateaduste magister

3. Keelteoskus

Keel	Tase
Eesti	Emakeel
Inglise	Kõrgtase
Vene	Algtase

4. Teenistuskäik

Periood	Tööandja	Ametikoht
2013 - ...	Tallinna Tehnikaülikool	Nooremteadur
2012-2013	Geo S.T. OÜ	Geodeet

5. Teadustöö põhisuunad

Kaugseire s.h. aero-, terestriiline ja mobiilne laserskaneerimine.

6. Teaduspreemiad ja -tunnustused

2012, Kalev Julge, Helga Minnuse ja Elmar Minnuse stipendium.

Toetati Euroopa Geoteaduste Ühingu (EGU) poolt teadustöö tulemuste tutvustamist EGU Üldassambleel 2014.

7. Lisainfo

Lühiajalised teadusvisiidid:

Soome Geodeesia Instituut (FGI), november 2013

Center of Excellence in Laser Scanning Research (CoELaSR), jaanuar 2017

Õppejõud aines Fotogramm-meetria (ETG0113).

8. Juhendatud väitekirjad

Aidi Sula, magistrikraad, 2015, (juh) Artu Ellmann; Kalev Julge, UAV mõõdistuse kõrgusliku ja plaanilise täpsuse evalveerimine, Tallinna Tehnikaülikool, Ehitusteaduskond, Teedeinstituut.

Silver Aule, magistrikraad, 2014, (juh) Artu Ellmann; Kalev Julge, Mittestandardse kujuga ehitiste laserskaneerimine ja punktipilve põhjal modelleerimine TTÜ veetorni näitel, Tallinna Tehnikaülikool, Ehitusteaduskond, Teedeinstituut, Geodeesia õppetool.

9. Publikatsioonid

Avaldatud teadusartiklite ja ettekannete loetelu on toodud inglise keelse CV juures.

